Technical White Paper

Aging Master Curve (FP 10) and Aging Rate Model (FP 11)

Fundamental Properties of Asphalts and Modified Asphalts III Product: FP 10 and 11

March 2015

Prepared for
Federal Highway Administration
Contract No. DTFH61-07-D-00005

By
Ronald R. Glaser, Thomas F. Turner, Jenny L. Loveridge,
Stephen L. Salmans, and Jean-Pascal Planche
Western Research Institute
3474 North 3rd Street
Laramie, WY 82072
www.westernresearch.org

WesternResearch
INSTITUTE

TABLE OF CONTENTS

TABLE OF CONTENTS (continued)

LIST OF FIGURES

LIST OF FIGURES (continued)

LIST OF FIGURES (continued)

LIST OF FIGURES (continued)

LIST OF FIGURES (continued)

LIST OF FIGURES (continued)

LIST OF FIGURES (continued)

LIST OF TABLES

LIST OF TABLES (continued)

LIST OF TABLES (continued)

INTRODUCTION

OBJECTIVES

The primary goal of this work is to develop an understanding of asphalt binder oxidation to the extent that materials can be tested for susceptibility to oxidation in quantitative terms that can be used in rational pavement performance computations. A secondary, but very important additional goal is to understand how the products of oxidation affect the changes in mechanical (rheological) properties of the asphalt binder. With this knowledge, the prediction of stresses in pavements over long time periods becomes possible. In addition, if relationships between oxidation extent and failure stress can be known, then predictions of cracking behavior over long time periods can be made as well.

Asphalt is subject to chemical oxidation by reaction with dissolved oxygen originating from the atmosphere. Asphalt oxidation results in the hardening of the asphalt and a reduction in its ability to relax stresses. Consequently, oxidized asphalt will retain stress for a longer time under loading, and that stress will be larger than for fresh asphalt. During a cooling event, oxidized asphalt will build stress faster, and fail at a higher temperature. Ultimately, oxidation will lead to cracking and failure of asphalt concretes through a combination of thermal stresses and loading. The philosophy in this work has been to use physical and chemical fundamentals as much as possible to provide robust methods that will survive a changing technology, tempered by a realization that practical use of such a complex material as asphalt may require empiricism as well.

This report describes work performed under FHWA contract (Contract No. DTFH61-07-D-00005) aimed at describing the oxidation kinetics of asphalt binders at ambient pressure and correlating the changes in the extent of oxidation with the changes in rheological properties and failure. The primary questions are:

1) How fast will an asphalt binder oxidize under a given set of conditions?
2) How do the mechanical properties of the binder change after a given extent of oxidation?

Our primary focus is furthering the understanding of asphalt oxidation to enable the development of design procedures for asphalt concrete pavements that allow rational consideration of the important role of mechanical property changes that occur during oxidation. Rational design procedures require mathematical descriptions of the phenomena of interest. Robust descriptions are founded in scientific fundamentals as much as possible.

BACKGROUND

General

The oxidative aging of asphalt binders in pavements causes a stiffening of the material, a loss in ductility, and a reduction in its ability to relieve stress (relaxation). Consequently, the pavement is more susceptible to stress accumulation, generally associated with thermally induced stress

caused by cooling. In order evaluate the long term performance of a pavement, the changes in the binder rheological properties, and the effect of the binder chemical changes on the pavement mechanical properties, must be understood. Hubbard and Reeve (1913) examined the effects of outdoor weathering on the physical and chemical properties of paving grade asphalt cements, finding that oxidation, and not volatilization alone, is responsible for the changes in asphalt binder properties over time. Subsequent studies have confirmed the Hubbard and Reeve finding (Thurston and Knowle 1936; Van Oort 1956).

The oxidative aging of asphalt binder has been studied for almost a century. It is beyond the scope of this work to describe this long history in detail. Information in the literature ranges from observations of actual pavements to detailed studies of the chemistry of the reactions in the asphalt binder itself. At the inception of this study, the state of art was sufficiently mature to imagine a procedure to generate the information required for modern mathematical simulation studies, but these methods were time consuming and expensive. The time required to complete a proper oxidation rate study sufficiently detailed for pavement performance estimation purposes was excessive (several months) and not likely to be used routinely by the paving industry. Conventional wisdom dictated that the complex process of asphalt oxidation was highly binder source dependant, requiring testing of each binder.

For practical reasons, binder testing procedures commonly used to oxidize the material were conducted at elevated pressures and temperatures to shorten the test time to an acceptable level. However, detailed rate expressions which would be required for pavement performance estimates, were of little value when obtained under accelerated conditions as it was believed that the pressure dependency of the reaction rate was also dependant on the binder source. It was also not well understood at what elevated temperature the oxidation mechanism changes significantly from conditions in a pavement. Consequently, the advantage of accelerated rate was offset by the disadvantage that is would be impossible to confidently use that information for ambient pressure and temperature rational design without further testing to include the long time ambient pressure test requirements to discover the pressure dependency. Furthermore, many studies concluded that the temperature dependency (usually described using the activation energy in the Arrhenius equation) was also significantly different from one binder source to another.

The investigators in this work speculated that a consistent study over a wide range of asphalts at atmospheric pressure might point to easily obtained chemical and/or physical measurements that would correlate with either the chemical rate and/or the change in physical properties with aging. One possible explanation is that of the wide variation in conclusions arising from previous studies is variability in the study methods and goals themselves. A description of the complex processes that lead to pavement degradation is helpful in understanding the wide variation in research methods and goals that this rich history contains. With this overview, the literature can be more easily appreciated and utilized. The important points to consider in the oxidation of the pavement are that a number of physical and chemical processes occur as a pavement oxidizes. How fast it oxidizes depends upon how the air enters the pavement, how the air becomes dissolved in the binder hydrocarbon, and how the chemistry responds to the amount of air dissolved. All of these processes depend on temperature, mix design, and the asphalt binder source. The temperature of the pavement itself varies with depth and time and depends upon its response to climate, primarily driven by solar insolation. An understanding of the complex

processes occurring in the pavement is critical, and consistent research methods must carefully separate these processes to understand them correctly in experimental design.

Pavement Oxidation Processes

Oxidation is a chemical reaction. For a chemical reaction to occur, the chemical species must come into molecular contact with each other. The molecules must be able to collide. Oxygen occurs in the air as a gas, and the asphalt binder is a visco-elastic material with solid and liquid like properties existing in a separate phase coating the mineral components of the pavement, cementing it together. Asphalts cements are porous and permeable to some extent, some mix designs more permeable than others. For oxidation to occur, the air must enter into the pavement through the pore structure via a number of processes and then become dissolved into the asphalt binder through the process of molecular diffusion. Coons and Wright (1967) found that the level of oxidation was greatest at the top of the pavement, and less with depth. Vallerga, White and Rostler (1970) collected data that showed that more porous (more permeable) pavements age more severely and with less variation with depth than pavements with low air void contents. These observations can be explained by considering that the oxygen in the air is being consumed as the air moves down into the pavement. In addition, the variation in the pavement temperature with depth affects the rate.

The variable temperature with time profiles of soils and pavements have been studied extensively, and it is well documented that surface temperatures for pavements vary much more than temperatures deeper in the pavement (Rumney and Jimenez 1969; Dempsey 1970; Lytton et al. 1989; Solaimanian and Kennedy 1993; Hermansson 2000, 2004; Gui et al. 2007; Herb et al. 2009). The data presented in Herb 2009 is particularly interesting in that the average temperatures at any depth do not vary significantly, but the daily excursions are much greater at the surface. This clearly illustrates that the temperature effect cannot be captured using mean air temperature information. Reaction rates are exponential in temperature, so the highest temperatures experienced have large effects on the amount of aging. Simple arithmetic averaging will not account for this dependency. The temperature effect alone would not produce the observation of Vallerga and coworkers (1970) in that above a certain void volume level, the amount of oxidation would not depend upon void volume at all if temperature alone was controlling the rate. So, we are inclined to believe that both movement of air in and out of the pavement, and thermal gradients, contribute to the degree of oxidation differences in a pavement from top to bottom.

One might be tempted to think that identifying the slowest step of this process of air movement into the pavement, diffusion into the asphalt binder, and finally reaction, would be sufficient to estimate the oxidation aging of the pavement. However, both the diffusion into the asphalt binder, and the chemical reaction rate once dissolved determine how much of the original oxygen in the air still remains after traveling down from the top. These processes are coupled and to properly compute one, the other must be computed as you advance in time and depth. At the surface the rate is controlled by reaction rate. As this is, on average, the most reactive zone, the greatest reduction in oxygen concentration in the air occurs here as the binder consumes the oxygen. In order to map the changes in a pavement over many years time, the relative rates of all three processes(movement of air into the pavement, diffusion of oxygen into the asphalt binder,

and reaction inside the binder) must understood well enough to be described mathematically in terms of mix design, climate, and binder selection. Under some conditions, the mathematics might be made simpler if one process dominates the overall rate. Once the rate, and subsequently the degree of oxidation have been accurately estimated, the effect of this state of oxidation on the binder in question must be known. Then, knowledge of the relationship of the extent of oxidation to the mechanical property changes of the binder would allow an estimate of the mechanical properties of the binder. Finally, application of the appropriate mix model that accounts for the mechanical properties of the binder and other mix variables allows an estimate of the properties history of the mix itself at each depth. The net result of the oxidation state calculation that is of value to pavement designers and road maintenance decision makers is the resulting property gradient in the pavement, particularly the modulus. An averaged pavement section modulus is not sufficient to compute stresses, as the stiffness gradient concentrates more of the stress near the top of the pavement where modulus values are highest. This situation results in higher stresses in the top of the pavement than would be estimated if the pavement mechanical properties were homogenous. Using average pavement section values will result in overly optimistic pavement life predictions.

In summary, the climate, the mix design, and the characteristics of the selected binder are all important considerations when predicting pavement performance over long periods of time. This work focuses on the binder alone in an attempt to provide mathematical descriptions of the rate of chemical reaction and also mathematical descriptions of the effect of oxidation on the mechanical properties of the binder once the extent of oxidation is known. Rational prediction of pavement oxidation and the resulting mechanical properties will require combining the results of this work with thermal and mass transfer models that account for all processes that affect oxidation rate.

Oxidation Rates and Rates of Physical Property Change

In this section we focus upon what happens at the binder level ignoring the transport of air into the pavement. A complete fundamental understanding requires that these phenomena be studied separately, but this has not always been done historically. Consequently, a good deal of confusion has resulted in just how to interpret much of the historical data. Recent reviews of asphalt binder oxidation studies in the literature illustrate that considerable study has addressed this topic, with an emphasis on chemical interpretation (Petersen 2009; Petersen and Glaser 2011). It is important to mention that some studies focus on actual reaction rates that result in the production of chemical products or the consumption of reactants, while others track the changes in mechanical properties over time. These differences can lead to some confusion as the chemical process of reaction with oxygen, and the chemo-physical process of how these new products affect the mechanical properties are two distinctly different research topics. Add to that a third process of diffusion of air into the asphalt sample to supply oxygen, and we can see that great care must be exercised in sorting experimental results found in the literature and which combinations of the three are involved in the data under examination. It is very unlikely for a simple explanation to any of these phenomena to be found in data subject to more than one of them.

Oxidation of very thick samples will be diffusion controlled and the underlying chemistry is difficult or impossible to observe. When measuring mechanical properties such as viscosity or moduli as time progresses, it is not likely to easily understand the role of reaction and the effect of those reaction products within a complex system. In order to mathematically describe the time dependency of the asphalt oxidation itself (commonly referred to as intrinsic reaction kinetics), the course of the reaction itself must be tracked through some kind of measurement, preferably the reactants and/or the products of the reaction. Furthermore, the experimental process of oxidizing the asphalt binder must be designed to prevent diffusion control of the rate. Asphalt is a complex mixture of hydrocarbons, and oxidation of this material undoubtedly involves many different reactions all proceeding at the same time, and having some effect on each other. Over the many decades of asphalt research, a number of approaches have been used to track the reaction. The three most common are listed below:

1) Consumption of oxygen (King and Corbett 1969; Knotnerus 1972a and b)
2) Changes in spectral response, primarily mid-infrared (Petersen et al. 1974; Epps et al. 1986; Martin et al. 1990; Lau et al. 1992; Petersen et al. 1993; Lee and Huang 1973)
3) Changes in solvent defined fractions (Rostler and White 1959; Nellenstyn 1924)

Of these three methods, infrared spectroscopy (IR) has proven to be the most widely accepted method for tracking asphalt oxidation response. Infrared analysis of asphalt is, however, not without difficulties in interpretation. Petersen states in his 2009 TRB circular:

> *"Infrared spectrometry has been a rewarding technique in this research because it can be applied to the whole asphalt or complex mixtures without prior separation into molecular components. Early research to explore infrared spectrometry for the characterization of asphalts showed the technique to be useful in identifying general chemical structural types present (41); however, the strongly associating polar functionalities present were never adequately identified and characterized. Attempts to use standard infrared spectral scans to characterize these polar functionalities were frustrated by such inherent problems as overlapping and ill-defined absorption bands, and shifting and broadening of absorption bands from association such as hydrogen bonding."*

In addition to examining the whole asphalt IR spectrum, Petersen created the functional group analysis method (FGA) that, though a series of sequential chemical reactions, chemically removes some of the band overlap and assists in proper peak assignments (Petersen 1986). The FGA method is quite powerful, but also difficult and time consuming to perform on a routine basis. Using FGA, Petersen found that sulfoxide and carbonyl functional groups are the major functional groups formed during asphalt oxidation, with carboxylic acids and anhydrides being produced in minor amounts. His determinations were not able to clearly identify alcohol and phenolic product amounts. Dorrence et al. (1974) found evidence that carbonyl products are formed at the benzyl carbon, and Mill and Tse (1990) found large amounts of benzyl hydrogen in the asphalts they studied, amounting to 6% to 11% in the four asphalts tested. Petersen (1981) also found that sulfoxides are formed by oxidation organic sulfides, most likely dialkyl or alkylaromatic types. Obviously, proper use of infrared determinations to track oxidation may require combinations of a variety of wave number absorbencies, properly weighted, to be

meaningful. This problem is addressed in this study through multivariable regression analysis techniques using a new algorithm designed to handle the large number of independent variables present in spectra, particularly infrared spectra. This algorithm and software implementation is another product from this contract, and is described in detail in a separate technical white paper (FP 06). The results of using this tool as it applies to our oxidation studies are presented here.

Addition difficulties exist when using infrared as the reaction tracking tool of choice. Correlations of oxidation that include sulfoxide production are plagued by the possibility of sulfoxide decomposition interfering with the measure of oxide formation. When examining Boscan crude, a material particularly sensitive to sulfoxide decomposition, Petersen (2009) found that significant decomposition occurred within one hour at temperatures above 70°C under vacuum. Petersen also noted modest decreases in the dynamic viscosity after decomposition. From these observations came the idea that perhaps sulfoxide was of minor importance in the oxidative hardening of asphalts and that for most purposes, so it is sufficient to track only carbonyl (Liu et al. 1996). Herrington (1995) found similar results. However, Herrington interpreted this phenomenon as indicating the products of decomposition contribute in a similar way to asphalt stiffening, and one of his samples showed an increase in stiffening after sulfoxide decomposition. The work presented here show that understanding the oxidation process requires tracking sulfur oxidation as well as carbonyl formation. A low temperature solvent removal technique was developed to minimize sulfoxide decomposition in this study. Oxidation temperatures in the sample preparation were also kept below 70°C for the same reason.

Infrared Quantification

How does one best quantify the mid-infrared (IR) spectra to insure that readings are indeed proportional to molar concentration and to also insure that these readings are comparable across a range of asphaltic materials? A number of IR methods exist, with traditional transmission through a cell of known thickness and concentration of dissolved asphalt often being replaced by the more convenient attenuated reflectance method (ATR), which can produce a reading on the whole asphalt without the use of solvents. The major drawback to ATR is the fact that it does not produce a Beer's law spectra. In addition, the ATR method suffers from lower signal-to-noise ratios, often approaching two orders of magnitude less, than measurements taken with traditional transmission methods. There is no known universal correction of ATR to match a transmission obtained spectra. This unfortunate situation can be understood if we consider how the ATR works. In a simple one-bounce system, the infrared beam strikes a prism made of a high index of refraction, η_0, material (in the wave lengths of interest) at an angle θ to the specimen resting on another face of the prism. A portion of the beam is absorbed at each wave length depending on its molecular structure, diminishing the intensity of the beam leaving the third face of the prism. The depth of penetration into the sample, on the order of microns, depends upon the wavelength, and also the index of refraction of the sample at that wave length. This depth is essentially equivalent to the path length found in Beer's law and is described by equation 1 (Nunn and Nishikida 2008):

$$d = \frac{\lambda}{2\pi\eta_1\sqrt{\sin^2(\theta) - (\frac{\eta_2}{\eta_1})^2}} \quad (1)$$

where:

η_2 = $f(\lambda)$

λ = wave length

η_i = index of refraction of the material and the prism

θ = incident angle of the IR beam

While most ATR manufacturers provide "correction" algorithms which address the wavelength correction in equation 1, they do not address the index of refraction correction because that would have to measured at each and every wave number of interest. As a binder oxidizes, the index of refraction changes, and the index of refraction is different for different asphalt sources, making comparisons of IR measurements on oxidized materials semi-qualitative at best, and comparison of the behavior of asphalts from different sources nearly impossible in any quantitative way. ATR was determined to be unsuitable for this kinetic study of asphalt oxidation because fundamental Beer's law proportional measurements across a range of materials cannot be obtained from ATR.

Some investigators have used normalization against non-reactive peaks in an attempt to overcome, at least partially, the limits of ATR and transmission of thin films of whole asphalt with variable thickness. For studies of a single asphalt source, there are some advantages to normalization, but aliphatic peaks are not consistent across all binder sources, so these ratios are of little value when comparing the behavior of several binders from a variety of sources. No experiment was performed evaluating normalization as it was rejected for the reasons mentioned.

The arguments for using transmission measurements as compared to ATR are fairly straight forward and compelling, but investigators using transmission measurements (and ATR) also use a variety of methods to reduce the spectra to numerical representations of an absorbance. In addition to fundamentally defined readings of peak height, the existence of overlap of unrelated peaks, and the existence of the same functional groups on different molecular types at slightly different wave numbers, has led to a variety of approaches to actually assigning a numerical value to the IR response. The reason for many of these variations is rooted in the fact that infrared spectra of asphalts consist of thousands of spectra of individual molecules added together. These molecules are a quite large and individual functional groups attached to different molecular types will not present themselves at exactly the same wave number. Furthermore, these various molecular types will have different absorbtivities (Petersen 1986). Beer's law, equation 2, tells us that the molar concentration of a given function group on a specific molecule in a cell with a specific path length and solvent is proportional to the absorbtivity as measured from zero.

$$A = -\log(I / I_0)$$
$$A = \varepsilon \ell c \leftarrow Beer's\ Law \quad (2)$$

where:
c = molar concentration
A = Absorbance
ε = extinction coefficient (molar absorbtivity)
ℓ = beam path length

No alternatives exist to validate the asphalt IR measurements. Prior to this study, little or no effort has gone into assessing these quantization methods to determine which more closely represents the true value in terms of both precision and accuracy. Examination of actual spectra, particularly the second derivative, provides some indication of the peak width changes over the course of oxidation, and how variable these are from asphalt to asphalt. A good deal of effort by others (Pelikán et al. 1993) and during this study was also applied to the mathematical separation of overlapping peaks with limited success using simultaneous fitting of a range of aged materials and requiring the fit quality to judged by the spectra, and its first and second derivatives. Ultimately, the idea of separating the complex spectra into fundamental peaks was abandoned. This is because any fit solution is not unique.

Infrared spectral analysis is commonly used to study asphalts and quantify concentrations of functional groups of interest, usually, but not limited to, wave number region near 1700, and the region around 1037. These two are assigned to the carbonyl and sulfoxide functional groups respectively, which are quite important in oxidation studies. Although Beer's law indicates that the height of the peak is proportional to the concentration, areas of the peak are often employed to generate calibrations or estimations. The peak width does not vary with concentration, so this approach should yield the same linear proportionality if the width used to compute the area is constant. Asphalt, however, is a mixture of many compounds, and the spectra are the sum of the spectra of hundreds, perhaps thousands, of individual chemical species. It is well known that many functional group adsorbtivities depend upon the molecule they are attached to. For example, the Beer's Law proportionality constant (adsorbtivity) for aliphatic alcohols is different than aromatic alcohols, and phenol hydroxyl groups are also different. In addition, peak locations are similar, but slightly shifted depending on the molecule the group occurs in. Consequently, areas of peaks as a metric are often employed to "gather up" all of these similar responses and an average adsorbtivity is applied for quantization. Additional difficulties exist with complex mixtures like asphalts because overlap of neighboring peaks always occurs, so the peaks of interest may be lifted up. This concern is often mitigated by drawing a "tangent" line below the peaks of interest in the hopes that this line approximates the overlap (figures 1 and 2). While this is indeed a good approximation in simple systems, with highly complex spectra having multiple overlap, the value of the method can only be evaluated in terms of precision and not accuracy. Many of these difficulties are reduced by the application of chemical derivatization methods wherein a function group of interest is reacted with a reagent, removing the peaks, and the before and after differences provide the proper peak shape. These methods, such as the functional group analysis method developed by Petersen (Petersen 1986; Western Research Institute 2005), are perhaps the best available methods of quantization available. In asphalt studies, particularly

oxidation kinetics, the method is not routinely used because it is time consuming and requires expert laboratory skills.

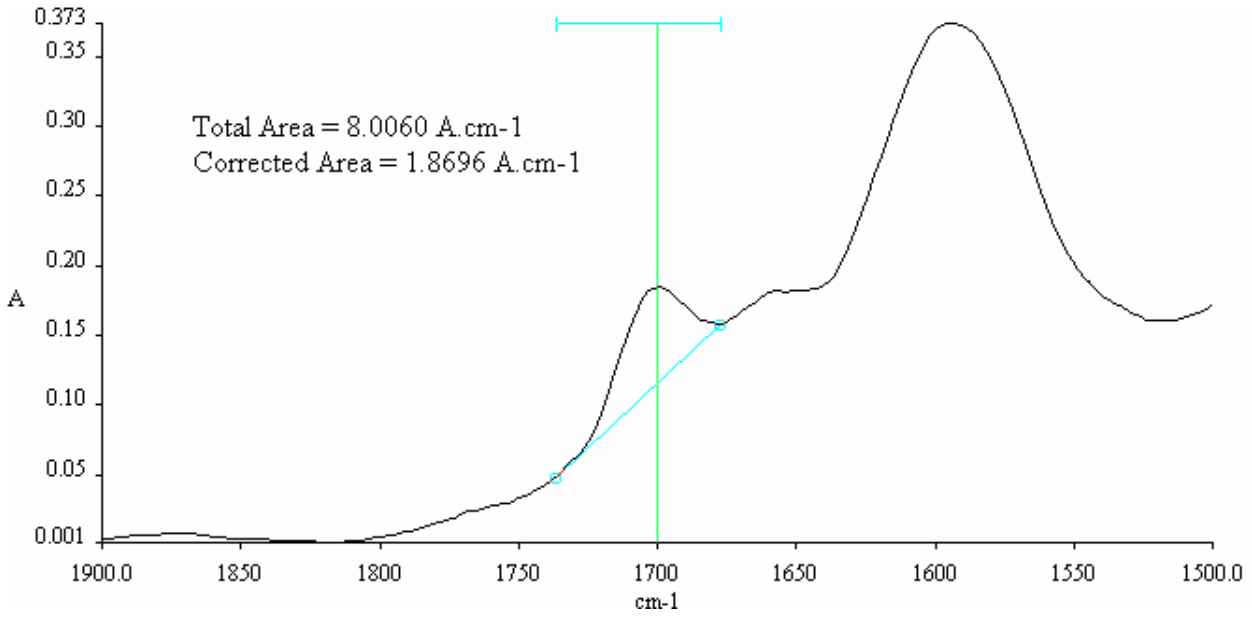

Figure 1. Screenshot. The clipped area technique illustration (Western Research Institute 2005).

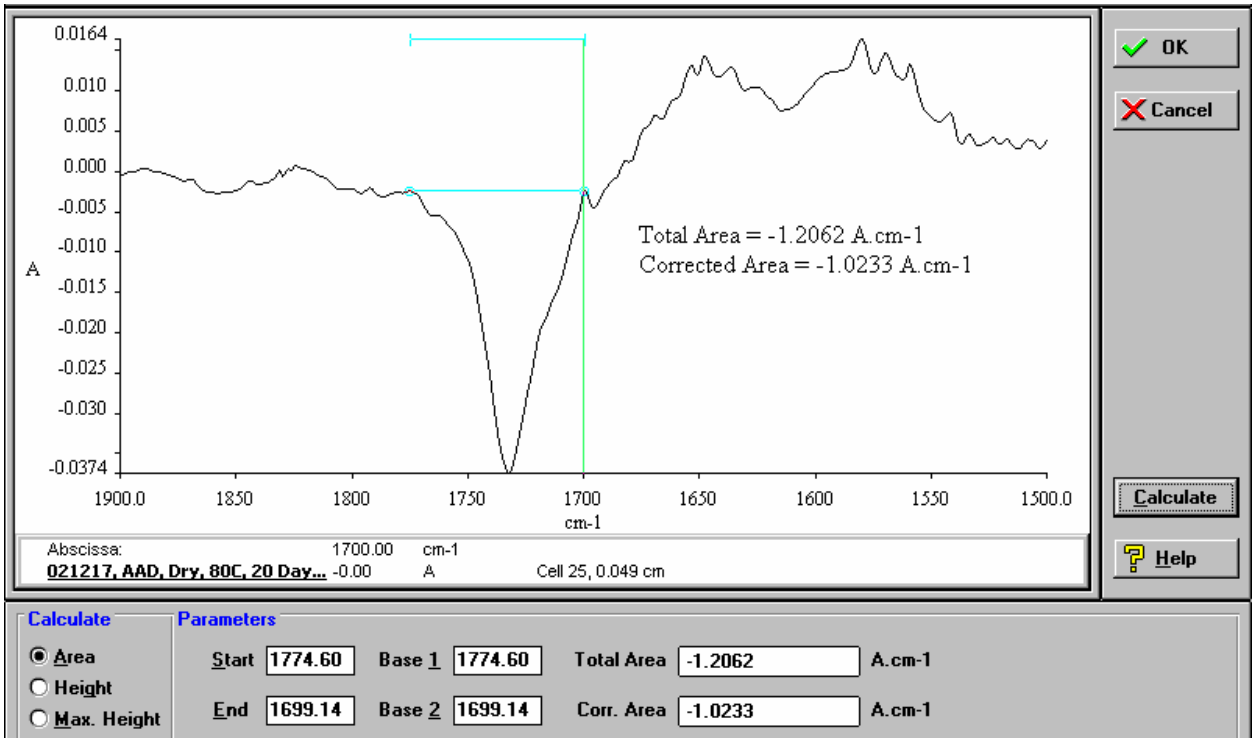

Figure 2. Screenshot. The base clip for Carboxylic Acids applied to derivitation difference spectra (Western Research Institute 2005).

The actual absorbtivities of functional groups in asphalts are not well known and quite approximate values are applied to obtain molar concentration estimates (table 1).

Table 1. Model compounds used to estimate absorbtivities (Western Research Institute 2005).

Functional Group	Model Compound	Peak Location, cm-1	Absorptivity Coefficient (B)
Phenol	2,4,6-Trimethylphenol 4-tert-Butylphenol	3393 3317	25958 30983 $\overline{x}$ = 28471, δ = 3553
Pyrrole	3-Indolepropionic acid Indole	3306 3304	13218 21034 $\overline{x}$ = 17126, δ = 5527
Ketone	1-Phenyl-2-butanone 4-Phenylcyclohexanone Acetophenone Dodecanophenone Valerophenone	1716 1719 1689 1690 1689	6046 8687 7256 6471 5002 $\overline{x}$ = 6693, δ = 1380
Carboxylic Acid	3-Indolepropionic acid 9-Anthracenecarboxylic acid Benzoic acid Cholic acid Lauric acid Phenyl octanoic acid Stearic acid Undecanoic acid	1735 1721 1722 1734 1736 1735 1736 1736	12239 12397 11906 13051 13731 13209 12966 13354 $\overline{x}$ = 12857, δ = 619
2-Quinolone	2-Hydroxy-4-methylquinoline 2-Hydroxyquinoline n-Methyl-2-quinolone	1678 1681 1666	32015 31626 19294 $\overline{x}$ = 27645, δ = 7235
Anhydride	1,8-Napthalic anhydride Benzoic anhydride	1780 1793	26278 23948 $\overline{x}$ = 25113, δ = 1647
Sulfoxide	Benzyl sulfoxide Butyl sulfoxide Didecyl sulfoxide Dimethyl sulfoxide Pentyl sulfoxide	1056 1037 1055 1070 1043	2446 4498 7439 4633 2939 $\overline{x}$ = 4066, δ = 1920

What is the best way to quantize these peaks? There are no accepted standards to calibrate against for asphalt spectra. However, these methods can be tested against synthetic spectra where the value of the changing peak is known because it is artificially created. In other words, study the competing methods as a mathematical problem, not a chemical problem. This paper study approach was applied, and our decision for quantization method is largely based upon this study. Provided the dilution factor and cell path length are reported, the absorbtivity will be proportional to the molar concentration. Kinetic analysis based upon absorbtivity alone (with path length and dilution noted) amounts to rate constants with those units that can be converted to molar concentration if a good absorbtivity can be estimated. We ignore the absorbtivity issue entirely, preferring to report measurements that can be repeated easily without concern over the validity of the absorbtivity assumed. Determining the best way to quantize the spectra still leaves open the question of which wave numbers (functional groups) to select to track the extent of reaction through time to obtain the proper kinetic equation(s). Chemometric methods, which allow the correlation of spectra to other measurements, were employed to discover which areas of the spectra affect the rheology the strongest in the hope that this information may also provide clues to the underlying chemistry and from that, the correct functional groups could be measured to track the extent of oxidation as determined by the rate limiting step.

Chemometric Methods-Multivariable Correlations of Chemical Change with Rheological Changes

After reviewing the available methods for multivariate studies of spectral data, we found that understanding the important wave numbers was very difficult with methods utilizing latent variable concepts. The time honored linear multivariable method does produce closed form correlations, but is only useful if intelligent selection of possible significant wave numbers is known apriori, because a typical spectra contains thousands of possibilities to test against a much smaller number of observations. The number of independent variables to use in the correlations is also limited based upon the number of actual observations used. Monte Carlo approaches would likely work, but the adaptation of the ideas to reduce variable counts in a logical manner, along with a defendable method for expanding the observation matrix is the strategy we chose to employ. The core strategy we employ involves reducing the number of independent variables into groups that grow proportionally as binders oxidize and increasing observations artificially if needed based upon known instrument precision. In short, we use multivariable linear regression to examine the entire spectra at one time. This is possible by preconditioning the data set by combining independent variable single measurements (that is, a single wave-number) that represent the same information to reduce the independent variable list and by increasing the observation matrix size by generating synthetic replicates from a knowledge of measurement precision. This method is a separate product and discussed in detail in the Chemo-mechanical Software (FP 06) technical white paper.

Oxidation Kinetics

The primary product of this work is a fundamentally derived asphalt oxidation mathematical model in differential and isothermal-isobaric integral form (the non-isothermal form is not analytic and requires numerical integration to account for temperature and partial pressure oxygen variations in time and is needed to couple to pavement performance models). A number

of mathematical and/or kinetic expressions and/or chemical mechanisms have been proposed in the past (Liu et al. 1996; Petersen 1998; Herrington et al. 1994; Mill 1996; Knotnerus 1972a; Van Gooswilligen et al. 1985; King 1993; Mushrush 1992; Herrington 1998). The dual sequential mechanism for oxidation of asphalts proposed by Petersen (1998) provides a simplified conceptual view of oxidation chemistry in asphalts. Reducing this chemical path concept to a mathematical form is the approach we used in the hope of creating a robust model based upon fundamental chemistry. The resulting equations should appear to be a combination of first order in some reactive material in the binder for the fast parallel reaction path, and zero order for the slow, long term reaction path as observed by numerous investigators.

Petersen's concept consists of two parallel paths, a fast one and a slow one that likely share free radical species (figure 3).

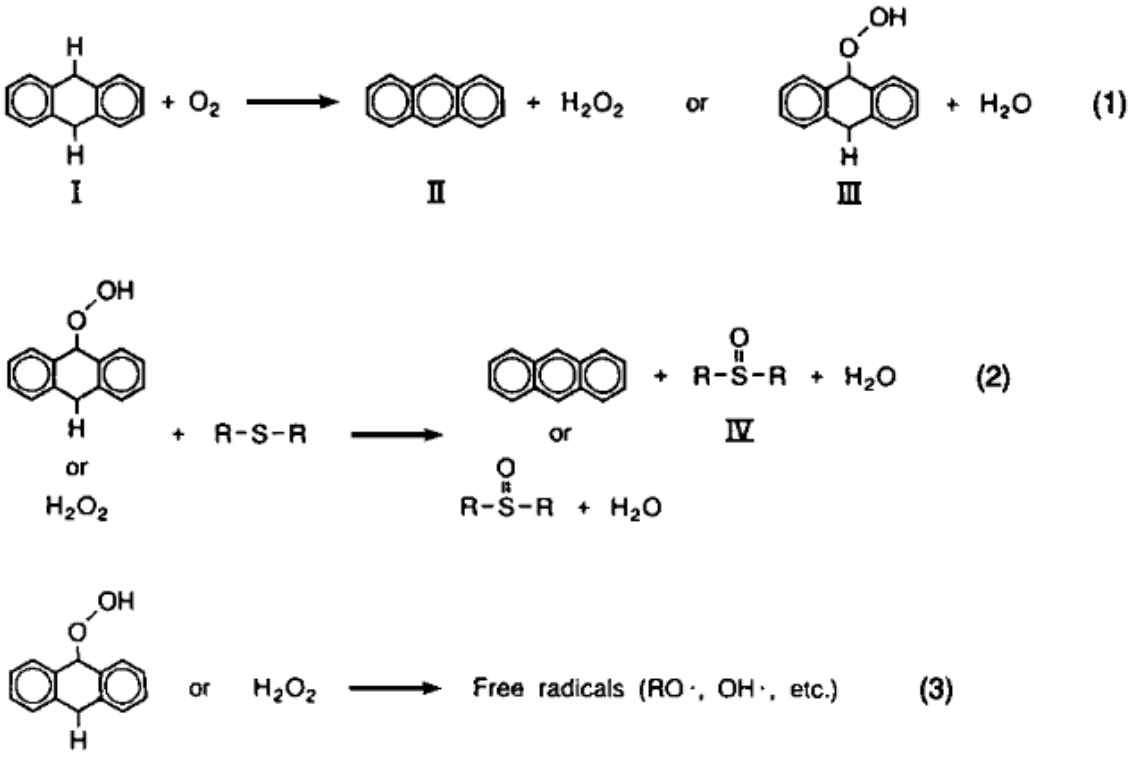

Figure 3. Illustration. Reaction sequence for the fast reaction assuming polycyclic hydroaromatics are the reactive material (Petersen 1998).

The important feature of the fast reaction is that this sequence generates a free radical population. Other reactants could be responsible for uninitiated or rapid initiation, but for the purpose of mathematical formulation the exact identity of the chemical type responsible does not need to be known. In parallel with the fast reaction that eventually consumes all of the very reactive material; we have the slow reaction that appears to continue throughout the useful life of a pavement (figure 4).

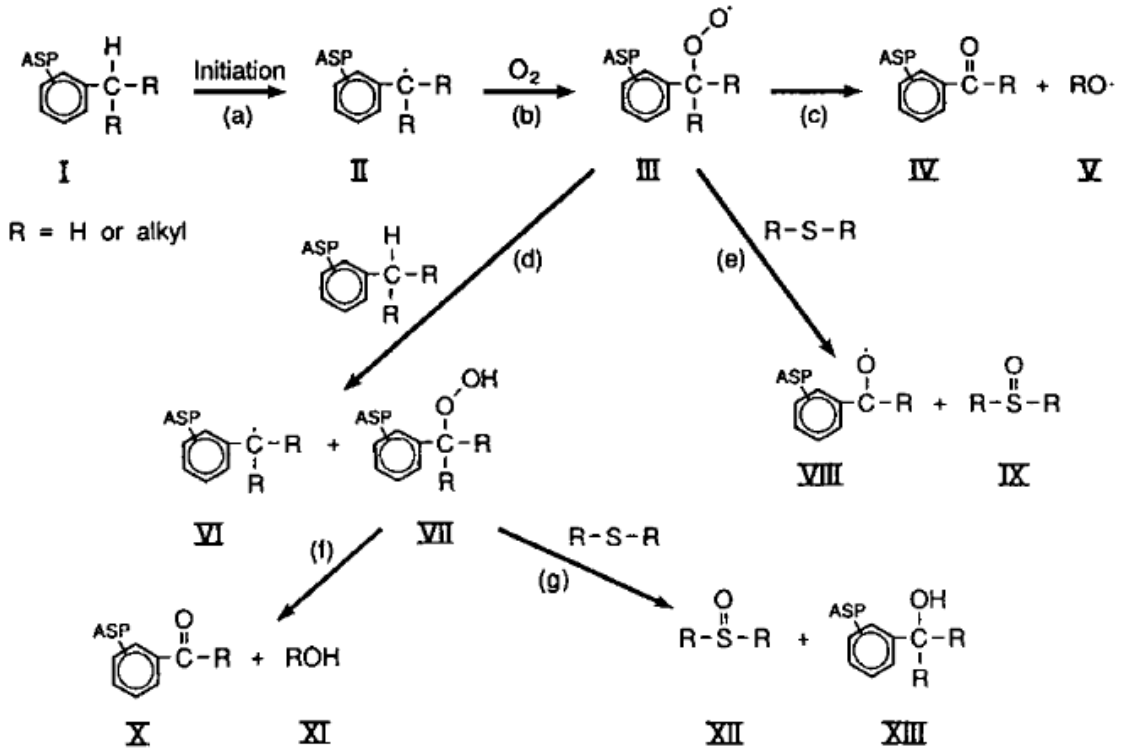

Figure 4. Illustration. The slow reaction path driven by benzyl carbon (Petersen 1998).

A plausible explanation of why the isothermal rate of asphalt oxidation appears to follow parallel first and zero order paths can be provided if one assumes the rate limiting step occurs very near reaction with oxygen. For both paths, conducting the experiment with thin films to insure the rate of oxygen diffusion into the sample is much greater than the intrinsic chemical kinetics insures that the oxygen concentration for both paths is constant in time (a small spatial gradient will still exist). In the fast reaction, which appears first order, the depletion of the reactant in step I of the fast reactant will produce the first order curve because the true second order nature of the reaction is obscured since the dissolved oxygen concentration does not change. Similarly, the slow reaction appears to be zero order because there is a huge excess of reactant in the form of benzyl carbon (Jennings et al. 1993) such that both species concentrations participating in the bimolecular reaction are not significantly changed (oxygen and benzyl carbon radical). The dissolved oxygen continues to be replaced through diffusion, and only a tiny fraction of available benzyl carbons react during the time frame of observation. The other important detail to note when studying Petersen's mechanism is the initiation step where benzyl carbon is converted to a benzyl carbon radical via hydrogen abstraction from a radical not shown in the diagram. Glaser and Loveridge (2012 and Glaser et al. 2013) derived a set of differential and isothermal integrated rate expressions assuming the rate limiting step in the fast reactions to occur in or near the oxygen attack step, and hydrogen abstraction in the slow reaction.

The important point to note is that the proposed fast reaction is assumed to produce a free radical in addition to the final reaction products, and this radical, or some descendant of it in a more complex chain, is responsible for the hydrogen abstraction in the slow pathway. Furthermore, the

slow pathway regenerates a new radical for the one used in abstraction. The net result is the fast reaction continues to produce free radicals until its reactive material is consumed. The slow reaction rate rises as the concentration of radicals from the fast reaction increases to its final value, resulting in the nearly constant rate observed at long times after the fast reaction goes to completion. If the hydrogen abstraction step is quite fast relative to the benzyl carbon radical and oxygen step, then the rate of the slow reaction is controlled by the extent of completion of the fast reaction. This is because the concentration of free radicals, which in turn determine the concentration of benzyl carbon radicals, set the rate of the slow reaction rate limiting step. Once the fast reaction is finished, the slow reaction continues at a constant rate for a very long time since both oxygen and benzyl carbons are available in great abundance and the benzyl carbon radical concentration remains nearly constant as these are regenerated through hydrogen abstraction from radicals produced during the slow reaction. Mathematically, this interaction is actually quite simple. The two reaction pathways can be simplified to

Reaction 1: $C_{fast} + O_2 \xrightarrow{\text{rate limiting}} several\ rapid\ steps \longrightarrow P_{fast} + F^*$

Reaction 2a: $C_{slow} + F^* \xrightarrow[rapid]{} C^*_{slow}$

Reaction 2b: $C^*_{slow} + O_2 \xrightarrow{\text{rate limiting}} several\ rapid\ steps \longrightarrow P_{slow} + F^*$

C_{fast} represents the reactive material for the fast reaction, C_{slow} represents the reactive material for the slow reaction, generally assumed to be benzyl carbons, and F^* is a generic symbol for any species of effective radicals produced. P_{fast} and P_{slow} represent the products produced, which we assume to be proportional to the sum of the carbonyl and sulfoxide concentration as determined from infrared analysis. To do the mathematics properly, the distinction between the product origins must be kept in mind, but once the isothermal integration is completed, these terms can be combined to obtain the values we can measure.

The basic rate equations can be written as:

$$\frac{dP_1}{dt} = k_1'\left[C_{fast}\right][O_2] = k_1\left[C_{fast}\right] = k_1\left[C_{fast,0} - P_1\right] \tag{3}$$

$$\frac{dP_2}{dt} = k_2'\left[C^*_{slow}\right][O_2] = k_2\left[P_1\right] \tag{4}$$

Here $C_{fast,0}$ represents the fast reaction reactive material at the beginning of the aging experiment. The slow reaction reactive material is assumed to be a benzyl radical produced in proportion to the products of the fast reaction. During the course of the slow reaction, additional radicals are produced to replace the radical consumed in the hydrogen abstraction of benzyl carbons. Integration of the rate equations above produces the isothermal equation used to fit the data:

$$P = C_{fast,0}\left(1-\frac{k_2}{k_1}\right)\left(1-e^{-k_1 t}\right)+k_2 C_{fast,0} t + P_o \tag{5}$$

Equation 5 is used to fit the isothermal data to determine the rate constants and amount of reactive material for each binder studied.

Equation 5 above assumes isobaric conditions. Expanding the apparent rate constants to include the dissolved oxygen concentration results in the more general equations, which also corrects for the oxygen order not being restricted to 1.

$$\frac{dP_1}{dt} = A_1 e^{\frac{-E_{a,1}}{RT}}\left[O_2\right]^n\left[C_{fast,0}-P_1\right] \tag{6}$$

$$\frac{dP_2}{dt} = A_2 e^{\frac{-E_{a,2}}{RT}}\left[P_1\right]\left[O_2\right]^m \tag{7}$$

$$P_T = [S=O]+[C=O] = P_1 + P_2 \tag{8}$$

The isothermal kinetic model can be written:

$$P = C_{fast,0}\left(1-\frac{k_2 P_{O_2}^n}{k_1 P_{O_2}^m}\right)\left(1-e^{-k_1 P_{O_2}^m t}\right)+k_2 P_{O_2}^n C_{fast,0} t + P_o \tag{9}$$

where:

P = the extent of oxidation metric, usually s=o and c=o absorbance sums

P_o = the RTFO time zero value of P

$C_{fast,0}$ = the reactive material concentration for the fast reaction

k_2, k_1 = the slow and fast reaction rate constants for isothermal aging, temperature dependent according to the Arrhenius equation

$P_{O_2}^n$ = the partial pressure oxygen, n is the pressure exponent for the slow reaction

$P_{O_2}^m$ = the partial pressure oxygen, m is the pressure exponent for the fast reaction

In the above equations, sulfoxide and carbonyl concentrations are assumed to be proportional to oxygen incorporation into the binder as oxidation proceeds. The above model is applied to data generated in the ambient pressure oxidation study, and also tested against a limited set of 20 atmospheric air pressure legacy data.

IR to Master Curve Changes

The extents of the oxidation reactions that have occurred in an asphalt binder are of little interest to the pavement designer apart from how the binder oxidation changes pavement mechanical properties. Rutting and cracking are the two major areas of interest, although effects on adhesion and moisture susceptibility are important as well. Rutting failures generally occur in young pavements that are too soft at high service temperatures under high loading. Oxidation stiffens the asphalt, resulting in a more brittle material, and is generally thought to be a root cause of many cracking failure modes. Oxidation increases the complex modulus at a given comparative temperature and lengthens the relaxation time, producing greater stress accumulation (Bell et al. 1994). Less is known concerning how oxidation affects failure stress levels. It is generally believed that continuum damage accumulation is faster in oxidized asphalts, perhaps not because failure stress levels are lower, but because healing is diminished (Zou et al. 2012). Ruan, Davison and Glover (2003) have developed a parameter based upon rheological measurements of the binder alone that correlates well with ductile failure. Consequently, a correlation of oxidation extent that can be used to obtain a complex modulus master curve could also be used to estimate ductile failure. The Christensen-Anderson (CA) (1992) model has proven to be a good mathematical description of asphalt binder master curves for all but the most exotic modified materials. This work fits the CA parameters to the extent of aging based upon ambient pressure aged binders. The details of this fitting procedure are described in detail in the experimental section. The relationship between the CA model and the extent of oxidation provides a complete master curve under any extent of aging, and all derivative information as well, including relaxation for pavement performance model inputs (described in FP 23).

Application to Pavements

Fundamental pavement performance models that account for asphalt binder oxidation require estimates the amount of oxidation at the various levels in the pavement, along with the rheological and failure properties of the asphalt concrete. The calculation must account for the thermal history of the pavement based upon the climatic factors and the thermal properties of the asphalt concrete. The differential form of the kinetic model derived in this work can be integrated over time if the temperature history is known, but the reaction rate is also dependent upon the partial pressure oxygen inside the pavement, which decreases with depth. The computation must therefore perform a differential material balance on oxygen in time and with depth, which balances the consumption of oxygen in the air moving downward through the pavement with the amount of oxygen consumed by oxidation. Once temperature and oxygen pressure are known, the rate of oxidation at that point in time and space may be computed. These complications of mass transfer are beyond the scope of this work (examined in some detail in FP 05), but calculations of the extent of oxidation assuming unimpeded oxygen flow can easily be made if knowledge of the temperature history with depth is known. These can then be compared to oxidation levels found in field core slices and a mass transfer correction applied. One could imagine a simplification to the modeling effort if correlations of the mass transfer correction based upon climatic zones and mix designs were generated, enabling sufficient precision for comparative life cycle cost analysis for rational design. Once the rheological properties have been estimated with depth for an age of interest, a finite element model that considers expected loading from traffic and thermal effects can compute the stress field in the pavement, which

would then be compared to failure stress levels or used to accumulate damage in a continuum damage approach. A complete model would consider damage accumulation in order to have an accurate assessment of failure stress at that age, and to credit the material for healing. A simple comparison is made comparing measured oxidation extents from ALF core slices with model predictions assuming no oxygen depletion.

EXPERIMENTAL

This work spans several years of effort and as such, a variety of individual experimental and computational designs were performed, often using the results of previous efforts as guidance, along with feedback from many meetings and conferences. Visits with the client (Federal Highway Administration) and Expert Task Group meetings were particularly useful. The following topics are approximately sequential in the order they were addressed, but often include additional work and refinement as the project progressed.

INFRARED QUANTIFICATION

For reasons outlined in the background section, transmission IR was selected as the method of choice for the study of asphalt oxidation since only this method strictly obeys Beer's law and allows direct comparison of binders from different source crudes. Transmission IR also has good signal-to-noise ratios. The issue of transmission IR quantification was studied in two ways, first by attempting to resolve individual peaks responses mathematically and second by evaluating typical approximate methods used against artificially created complex spectra where true values are known. Thin film transmission could also be used if an internal standard was added to enable the determination of path length, but this approach was not investigated.

Peak Extraction

Using legacy data of aged asphalt spectra (RITA 2010), some initial studies were conducted to see how spectral peaks change as aging progresses. The second derivatives of mid infrared spectra of SHRP asphalts AAM-1, AAD-1, AAC-1, and AAB-1 after 480 hours of aging at 80°C in the PAV at 20 atmospheres air were examined. The zero crossings of the second derivative are an indicator of peak width, and we were interested to see how much variability existed in asphalts from different sources. This provided some information useful in later efforts to arrive at the best quantization approach to use in aging studies.

A simple examination of existing spectra and how they change was followed by attempts to mathematically separate the overlapping peaks to arrive at good Beer's law numbers. Untangling or decomposing a single spectrum is usually not possible without some ambiguity in the results, as series expansions to peak shapes often do not possess guaranteed unique solutions (not to be confused with deconvolution, which does not separate overlaps). This is easy to understand when one considers a set of wave shapes that are very narrow with minimal overlap fitting the data as well as a wide peak with several small ones riding on top of it. WRI has several data sets of reaction series spectra (oxidation) where the shape of the spectra change over time; hence, fitting of a series of spectra as a regression may remove the ambiguity from peak series decomposition of a single spectrum. The non-linear deterministic fit now is converted to a regression problem, hopefully removing ambiguity. This study is aimed at evaluating the possibility of providing complete functional group information from asphalt spectra using a decomposition method that may include peak series decomposition.

Peaks series decomposition involves the determination of the individual peak parameters in a series of peaks that add to the observed spectra:

$$Abs(x) = \sum_{0}^{n} f(A_i, \mu_i, \sigma_i, x) \tag{10}$$

where:
Abs = IR absorbance
f = peak shape function, usually assumed to be Gaussian or Lorentzian
A = peak function height
μ = peak location
σ = peak width parameter
x = wavenumber of interest

Although the true peak shape in IR is generally believed to be the convolution of the Lorentz shape forcing function with a Gaussian transfer function, the computational cost of repeated convolutions is usually avoided by assuming either one or the other shape, or, some linear combination of them. In any case, the summation can be re-written for either Gauss or Lorentz peaks as:

$$Abs(x) = \sum_{0}^{n} A_i f(\mu_i, \sigma_i, x) \tag{11}$$

Equation 11 illustrates that knowledge of peak locations and peak widths prior to fitting a spectrum reduces the non-linear problem into a simple linear algebra problem, where established matrix methods could be employed rapidly to fit the peak height. However, we have tried Gauss-Jordan and LU decomposition routines of initial data in a fitting routine and found the results unsatisfactory, with the solution usually returning several negative peak heights.

Non-linear regression techniques were employed taking some advantage of special properties of peak shaped functions. The effect of an individual peak is minor on the rest of the spectra several peak widths distant. Fitting small regions, and then moving back and forth across the spectra to get refinements due to peak tails from adjacent peaks, provides a reasonable algorithm for attacking this highly dimensional non-linear problem with several hundred unknowns. The program fit to residuals based upon the spectrum error, or the spectrum first derivative error, or the spectrum second derivative error, or weighted combinations of all of them at once.

Approximate Methods Compared

Not satisfied with our attempts at mathematical peak extraction, a study was done comparing commonly used approximation methods, with special attention to which method produced the best rendering of the true rate, even if absolute accuracy was less than desired. Our ultimate goal is to produce the best possible data and interpretation of that data to study reaction rate (chemical kinetics) and therefore, good rate measurements are essential.

Beer's law tells us that the molar concentration of a particular functional group is proportional to the absorbance. This is only strictly true if there is only one peak in the vicinity of the resonant wave number. In the case of a nearby peak interfering or overlapping, the response to the IR beam will be a combination of the two peaks. In the simplest of cases, only two overlapping peaks, a very good correction can be obtained by "clipping" the peak of interest using a correction "tangent" line (figure 5).

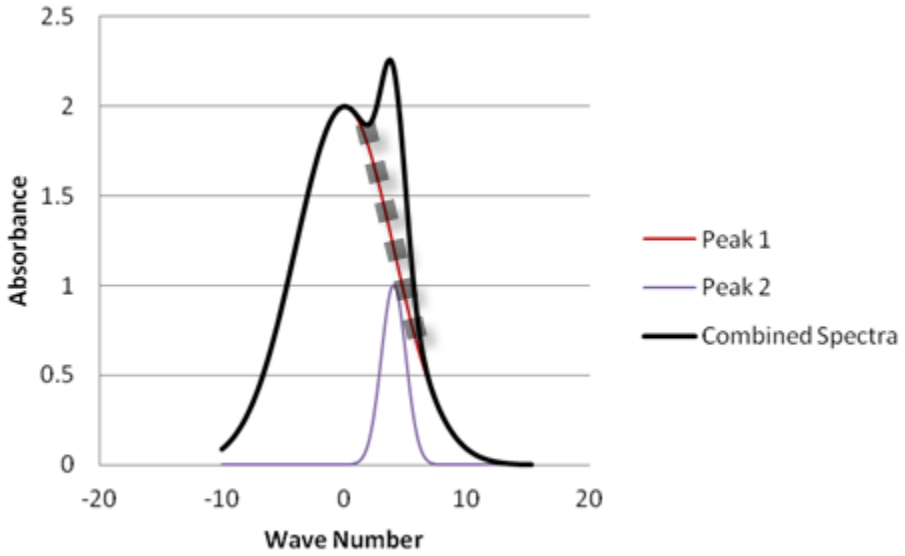

Figure 5. Graph. A simple two peak overlap with tangent correction.

The square dotted line indicates the location of the correction "tangent". The corrected height would be obtained by obtaining the length from the peak to its intersection with the "tangent" line. Alternatively, the area of the peak above the tangent is sometimes used instead of the corrected height. There are two variations of this procedure. One variation maintains the position of the end points of the correction "tangent" (fixed tangent end points) while another allows these end points to move as a peak from a reaction such as oxidation grows over time (emergent tangent end points). In reality, peaks extend from negative to positive infinity, so both peaks contribute to the observed spectrum across the entire spectrum, although at some point this contribution is less than the instrument precision.

Figure 6 shows a situation where the tangent line approach fails miserably. In very complex spectra, like we have with asphalt, multiple peaks may interfere. Even only two peaks make the tangent method unreliable; in the example the error would exceed 50%.

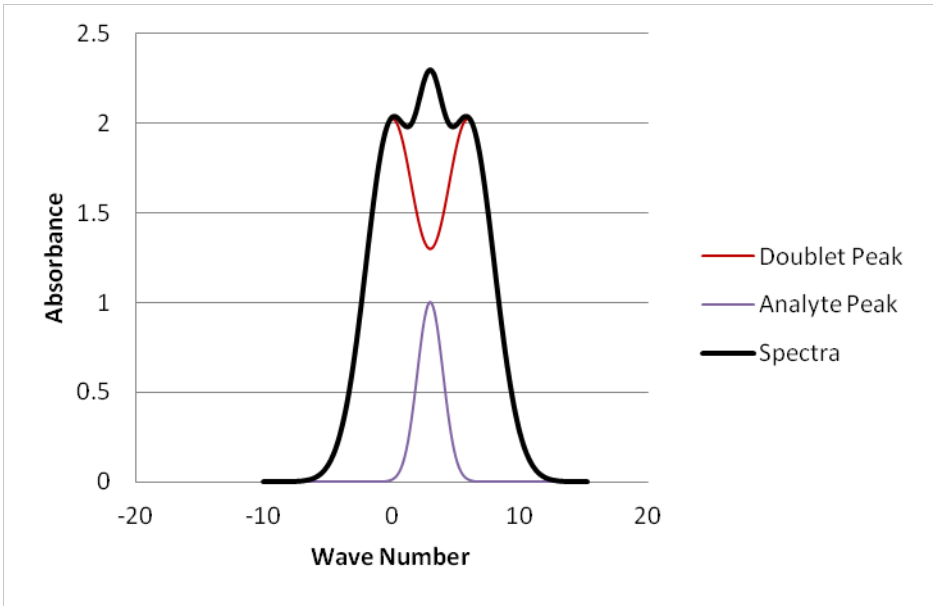

Figure 6. Graph. An example of a simple three peak overlap situation where tangent correction does not work well.

A variety of quantization methods were tested against a synthetic spectra of 9 peaks with peak 4 growing over time to assess the possible errors associated with a range of methods commonly used. Since the spectra are synthetic, we know exactly what the answer should be, and comparison with the approximation methods is straight forward. Figure 7 depicts the various metrics often employed.

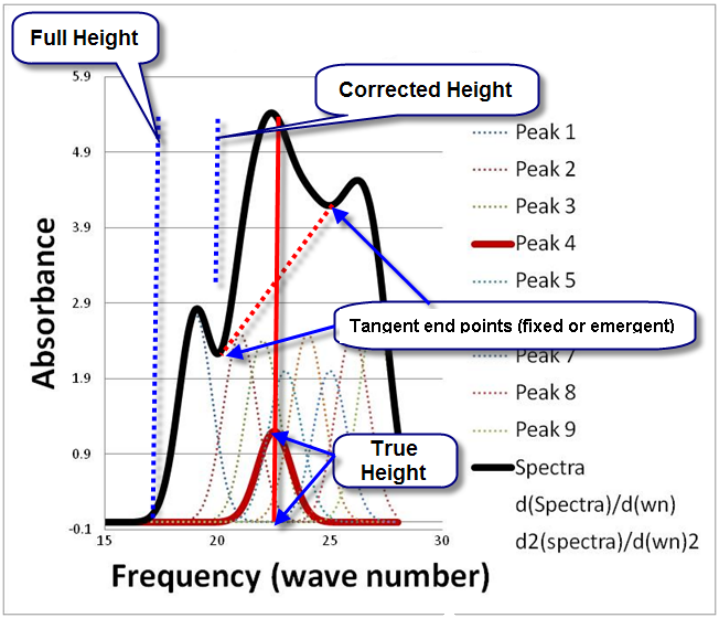

Figure 7. Illustration. The types of quantization approximations investigated.

The spectral response for complex overlap situations can be quantized by simply measuring the total peak height, or, alternatively, by attempting some kind of “tangent correction.” If the peak of interest is clearly a shoulder, then the tangent seems fairly obvious, and this is usually the case with the wave number 1700 response (assigned to carbonyl). However, the response at 1034 wave number (assigned to sulfoxide) is not clearly resting on the side of the underlying spectra, and selection of “tangent’ end points is less clear and somewhat subjective (similar to the situation in figure 6). Once satisfied we have the best practical quantization method to quantify the spectral response, correlation studies could begin. The literature contains many examples of correlations of IR spectra for oxidation reaction kinetic purposes and/or to track the time dependence of the rheological changes directly, or to correlate the degree of oxidation with the degree of rheological change. Most of these studies do not investigate multivariate methods. We investigated available multivariable techniques, and then developed our own described in FP 06.

CHEMOMETRIC METHODS-MULTIVARIABLE CORRELATIONS OF CHEMICAL CHANGE WITH RHEOLOGICAL CHANGES

A large collection of data analysis tools is considered to fall into the general description of chemometric methods. Our focus has been to use chemical measurements, particularly infrared spectra, to determine rheological properties. After reviewing available methods, a software package was developed to search IR spectra for the most significant combinations of wave numbers that correlate with rheological measurements. The details of the algorithms used are described in the FP 06 technical white paper. The software combines the spectra into groups of wave numbers that describe the same response, and rank these according to significance when correlated against some other measured property in a data set, such as a sequence of measurements obtained from asphalts oxidized over a range of conditions, usually different time spans under isothermal and isobaric testing. The software also provides the option of single wave number correlations over the entire spectra, producing a regression scan. Once developed, this tool was applied to legacy data on several asphalts aged at 20 atmospheres air and correlated to changes in complex modulus, loss and storage moduli, and phase angle at 10 radians per second. This legacy data did not include sufficient DSR data to produce master curves, so changes in master curve model parameters could not be investigated. Additional work was later performed on the data from the ambient pressure aging testing where master curves were generated and Christensen-Andersen model fit parameters could be correlated against the extent of oxidation. The most valuable outcome from the multivariable correlations of the infrared spectra against rheological changes was to discover which functional groups most strongly affect the rheology. The question still remained open as to which functional groups best quantize the rate of reaction, and if secondary reactions govern the relationship between reaction extent and rheological change.

DIFFUSION FILM THICKNESS STUDY

The oxidation process of asphalt binders is a heterogeneous reaction. The rate of oxidation observed depends upon the system geometry. In very thick films or layers, the overall rate is controlled by the ability of the oxygen to diffuse into the asphalt. In very thin layers, the rate is

limited by the reaction itself. The slowest step is the reaction mechanism, since oxygen can quickly diffuse into the sample as it is consumed. To properly study the actual chemical mechanism, it is critical that the film thickness is sufficiently small so that diffusion rates are very fast and can be neglected. Diffusion rates and reaction rates are both influenced by temperature and pressure. Typically, both increase with temperature, but usually the reaction rate accelerates more than the diffusion rate. Diffusivities of gases in ordinary liquids are nearly independent of pressure, but the diffusion rate is accelerated during unsteady saturation of the liquid because the gas solubility is higher. Higher gas solubility also increases the reaction rate if the rate limiting step is controlled by reaction with oxygen or direct products of oxygen. For gases, pressure increases result in a decrease in diffusivity. Asphalts can have rather large voids at the molecular scale, so the pressure dependency of asphalts could possibly appear to behave in unexpected ways intermediate to liquid and porous solids. All of these potential complexities can be resolved by designing the experiments in such a way that the rate of diffusion is much faster than the rate of reaction. This is usually accomplished by using a characteristic diffusion length (film thickness in films, radius in particles) that is sufficiently small to insure that diffusion rates are much faster than the reaction. A mathematical model could suggest this thickness, but experimental work is preferred and simple to execute. If a series of films over a range of thickness are oxidized at the highest temperature used in the study, the extent of reaction observed in the entire sample will increase as film thickness decreases, up to a point where there is no change within the error of available measurements. This thickness is the maximum thickness to use. Lower temperature testing could, in theory use a slightly thicker film, but selecting the film for the most extreme temperature assures that diffusion can be neglected for the lower temperature tests.

The maximum film thickness to use was studied during two testing periods. Several films were prepared over a range of thickness, and the resulting mid infrared response for carbonyl and sulfoxide compared. Within the variance of this study, caused by temperature differences inside the oven chamber, a film thickness of 100 microns was selected for the ambient pressure oxidation and rheology study.

The maximum film thickness was later repeated using SHRP asphalts AAC-1 and AAK-1 to verify our previous determination at higher precision and check the possibility of using thicker films. The results confirmed the earlier work.

AMBIENT PRESSURE ASPHALT OXIDATION AND RHEOLOGICAL CHANGE KINETIC STUDY

The laboratory oxidation study followed the usual course of isothermal kinetic studies. Prior to beginning the aging tests, all of the binders were aged in a rolling thin film oven (RTFO) to simulate oxidation occurring in the mix plant and during pavement placement. All of the materials were aged at four different temperatures, 40, 50, 60, and 70°C for a total period of 12 weeks in Salvas^{tm} precision forced convection ovens to simulate long term aging in the field. Our laboratory is located in Laramie, Wyoming, at 2200 m elevation, so the aging pressure was nominally 0.75 atmospheres. Intermediate time samples were obtained at the start of aging, 3 days later, then 2 weeks, 4 weeks, 8 weeks, and finally 12 weeks. The samples used are

100 micron thick solvent cast films of binder. A description of the binders used is provided in table 2.

Table 2. Asphalt binders used in oxidation study.

Binder	Grade	Type	Source
AAB-1	PG 58-22	Straight run	Strategic Highway Research Program Asphalt
AAC-1	PG 58-16	Straight run	Strategic Highway Research Program Asphalt
AAD-1	PG 58-28	Straight run	Strategic Highway Research Program Asphalt
AAM-1	PG 64-16	Straight run	Strategic Highway Research Program Asphalt
ABD-1	PG 58-22	Straight run	Strategic Highway Research Program Asphalt
ALF (base)	PG 70-22	Straight run	Accelerated Loading Facility Asphalt
ARC-1	PG 67-22	Straight run	Asphalt Research Consortium Asphalt
ARC-2	PG 64-16	Straight run	Asphalt Research Consortium Asphalt
AZ1-1	PG 76-16	Air Blown	WRI/FHWA Arizona Test Strip Asphalt
MCR	PG 54-34	Straight run	WRI/FHWA Manitoba Test Strip Asphalt
MN1-3	PG 58-28	Straight run	WRI/FHWA Minnesota Test Strip Asphalt
MN1-4	PG 58-28	Straight run	WRI/FHWA Minnesota Test Strip Asphalt

The films were prepared in aluminum pans. Toluene was used as the casting solvent with enough asphalt to produce 100 micron films. Removal of the solvent involves 4 hours at room temperature in an argon sweep followed by vacuum oven treatment for 4 hours at 70°C. Solvent removal was verified by mid-infrared analysis. Higher temperatures were avoided to prevent sulfoxide decomposition. The pans used to cast the films are commercially available aluminum weighing pans. A separate pan was used for each time point. After aging for the prescribed time, the changes in composition were monitored by fast Fourier transform infrared spectroscopy (FTIR) using a Perkin-Elmer Spectrum One instrument. The infrared readings were obtained in transmission mode through sodium chloride window material with a 1 mm beam path length. The aged binder was prepared for measurement by dilution with carbon tetrachloride at a concentration of 50 mg binder per ml of solvent. All absorbance measurements are reported as actual peak height absorbencies, with no area calculations or attempts to convert to molar concentration.

Rheological changes were obtained by running isotherms on each 60 and 70°C aging time sample on a Malvern dynamic shear rheometer (DSR) fitted with 4 mm plates, using the method developed by Sui et al. (2010). The isotherms typically ranged from -30 to 30 °C, with a few more highly aged samples including a 45 °C isotherm. Machine compliance corrections were employed, as they become more significant with the small plates and low temperatures used. Master curves were fit with the Christensen-Anderson (CA) (1992) model assuming a constant glassy modulus of 1.5 GPa, consistent with the average value obtained from our compliance corrected rheology. Although the glassy modulus is generally taken to be 1.0 GPa, we found, on average that an assumed value of 1.5 GPa gives slightly better fits to the CA model. This may be because of the use of compliance corrections. Fortunately, a sensitivity study indicates very little

difference in the remaining parameters in the model when results using the two assumed glassy moduli (1 GPa or 1.5 GPa) are compared.

$$G^*(\omega) = G^*_g \left[1 + \left(\frac{\omega}{\omega_c} \right)^{\frac{-\log 2}{\log\left(G^*_g / G^*_c \right)}} \right]^{\frac{-\log\left(G^*_g / G^*_c \right)}{\log 2}} \tag{12}$$

where:

G^* = complex modulus

G^*_g = glassy modulus

G^*_c = crossover modulus

ω = frequency

ω_c = crossover frequency

The remaining CA model parameters, crossover modulus and crossover frequency were then correlated against the extent of aging as quantified by the sum of wave number 1700 cm^{-1} and 1034 cm^{-1} absorbencies, generally considered to be primarily carbonyl and sulfoxide absorbencies, respectively, although other functional groups in asphalt contribute to these peak groups. The two absorbance measurements were not weighted based upon the coefficients for these peaks determined by correlations to complex modulus changes in the multivariate work. The shift function employed is a quadratic fit on an Arrhenius plot, but regular Arrhenius fits and WLF fits are also done automatically using WRI master curve software.

SARA SEPARATIONS

A subset of the binders oxidized in the ambient pressure oxidation study were divided into solubility defined fractions at time zero (RTFO treated) and after 12 weeks of oxidation at 70°C. The seven binders investigated are:

ALF (base)
AZ1-1
MCR
MN1-3
MN1-4
ARC1
ARC2

The separation used is a heptane asphaltene precipitation, followed by a chromatographic separation of the maltenes using a silica gel packed column. The details of this method are proprietary and were developed by John Schabron and Joe Rovani at WRI.

Once the oxidation kinetics were fit, and the relationship of oxidation extent to CA model parameters changes determined, these kinetic parameters were tested against the SARA fraction recoveries.

PRESSURE DEPENDENCY

The RITA (2010) data set, previously used in our initial chemometric multivariable studies, was re-examined using the results obtained from our ambient pressure kinetic work to assess the pressure dependency on the reaction kinetics. This legacy data set consists of four SHRP binders, AAB-1, AAC-1, AAD-1 and AAM-1 aged at three temperatures (60, 80 and 100°C) for up to 480 hours in a 20 atmosphere air environment (PAV vessel). Since these same binders were also examined at 0.75 atmospheres, only the pressure ratio exponent was varied to obtain the fits.

RAP BLEND OXIDATION

Two recycled asphalts pavements (RAP) extracted binders, one from Manitoba and a second from South Carolina were aged under ambient pressure conditions as thin films for 12 weeks at 60°C in ambient pressure air. Infrared analysis was done at 0,2,14,28,56,and 84 days. These data were fit using the activation energies determined from our aging studies by adjusting only the reactive material parameter. Blends of these same materials with AAC-1 at 15% and 50% RAP content were also aged in an identical manner. The oxidation rates of the blends were compared to predictions on the rates using a simple Kay's rule mixing law for reactive material contents in the virgin binders and RAPs.

ALF CORE ANALYSIS

An extensive study of sliced cores from the Turner Fairbanks Accelerated Aging Facility (ALF) was performed under a separate task (FP 19, FP 20, FP 21). Using temperature history profile data supplied by FHWA, the kinetic model was used to predict the extent of aging for these slices assuming no mass transfer limitations or pore oxygen depletion considerations. Equivalent average dissolved oxygen concentrations required to match the predictions with the observed extents of aging were calculated.

RESULTS AND DISCUSSION

INFRARED QUANTIFICATION

Peak Extraction

A comparison of the second derivative zero crossings of aged SHRP asphalts AAD-1, AAB-1, AAC-1 and AAM-1 indicates that chemical functional groups in these materials are very similar. The peak locations and peak widths are nearly identical and are depicted in figure 8 from a curve fitting program we developed and used for this purpose:

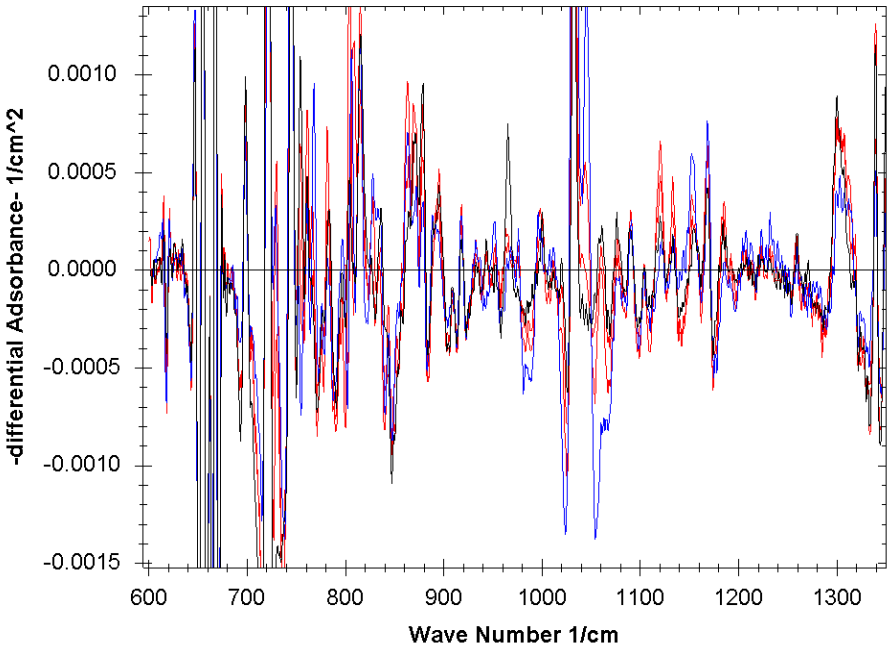

Figure 8. Screenshot. Second derivatives of infrared spectra of SHRP asphalts AAM-1, AAD-1, AAC-1 and AAB-1.

These observations suggest that if a library of spectra peak locations and widths found in asphalts was assembled, rapid decomposition could be done routinely. However, there is also considerable evidence that extensive overlap exists and that the fundamental peaks are quite narrow, perhaps 5 to 10 wave numbers. One might imagine that locations and peak width information can be extracted from first and second derivatives, but a careful study of over lapped peaks reveals that this is not as straight forward as hoped. Peak locations can be fairly reliably approximated when one realizes that with overlapped peaks, second derivative maxima or minima might define a location, along with concavity-up areas. Widths cannot be directly obtained from second derivatives of overlapped peaks, as the inflection is no longer defined at zero. Consequently, peak widths can only be roughly estimated to obtain a starting point for a

search. We use spacing to nearest neighbor as an estimating parameter, divided by 4. Early calculations (fitted to simple absolute value error between the calculated spectra and the measured spectra) illustrate the sensitivity of the search and what appears to be a uniqueness problem. Using the estimated peak widths as describe above, fitting AAM-1, AAD-1, AAC-1, and AAB-1 simultaneously after 480 hours of aging at 80°C in the PAV at 20 atmospheres air, the following result (figure 9) is obtained ($r^2 = 0.9942$):

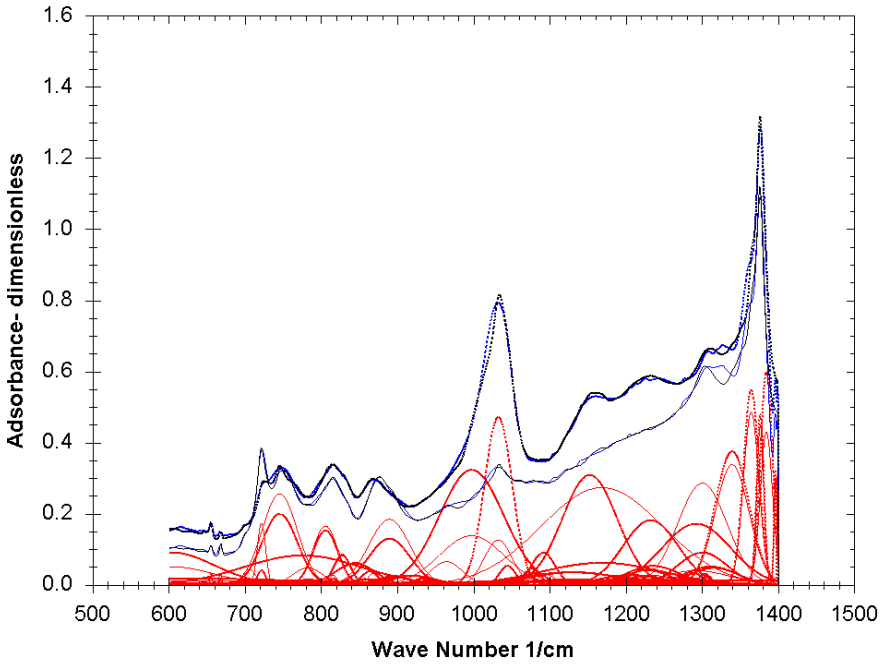

Figure 9. Screenshot. Peak separation of AAD-1 and AAM-1 spectra using detector routine widths as initial guess.

A much different result, but similar quality of fit ($r^2 = 0.9987$), is obtained if we start with constant widths of 5 cm^{-1}, demonstrating the lack of uniqueness when fits are attempted using only the spectra itself, and not the differential forms (figure 10):

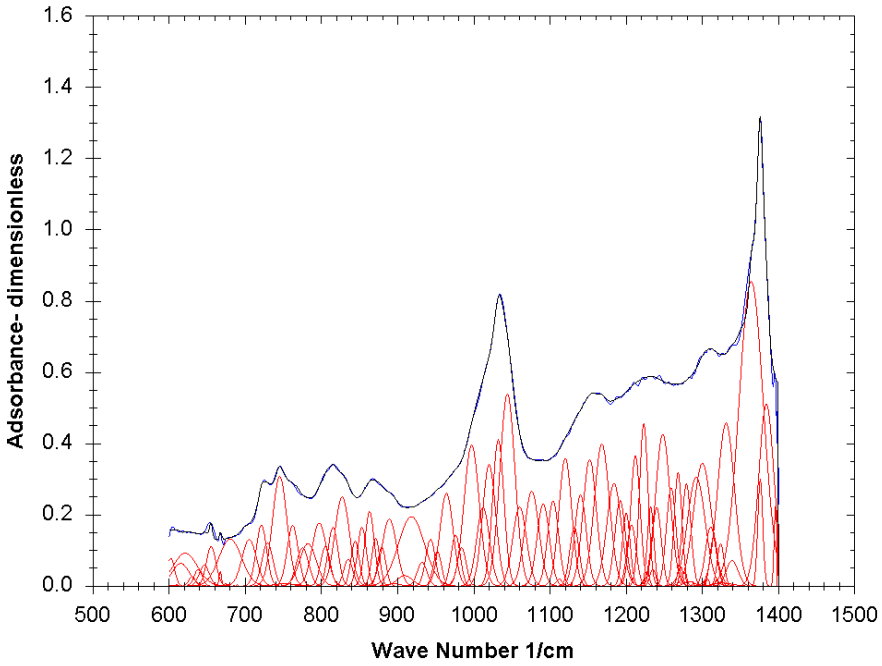

Figure 10. Screenshot. Best fit of AAD-1 and AAM-1 spectra with a narrower peak width starting guesses.

A comparison of the second derivatives in the two examples shown above indicates that the narrower collection of peaks is a better approximation of reality, however, second derivative peak heights cannot be resolved to match experimental data second derivative peak heights, and the computed heights in the second derivative are higher. For the mathematics to produce the correct height in the second derivative, hidden peaks must exist. The region between 1100 and 1300 cm-1 wave numbers is particularly plagued with hidden peaks. Our conclusion is that additional information concerning peak locations from model compound studies, requiring extensive experimental work, would be required to obtain an accurate extraction of the peaks involved in asphalt and heavy oil mid infrared spectra. Such an effort was beyond the current scope of work and this approach was abandoned.

Approximate Methods Compared

Approximate quantization methods applied to asphalt IR spectra in the literature are quite varied, but typically fall into either peak height measurements or peak area measurements. These can be as simple as a direct reading from the instrument, to localized truncations in an effort to correct for overlap, to analysis after subtraction of a reference or a time-zero spectrum. A more detailed discussion of the methods examined is described in the experimental section above.

Figure 11 shows a plot of total and corrected height measurements for our simulated spectra plotted against the true value. A linear regression fit with a slope of 1 represents a perfect measurement of the rate, while an intercept of zero would represent a perfect Beer's law

measurement. In this example, the “tangent” end points are all always at the same location, that is, they do not grow wider as the peak grows taller.

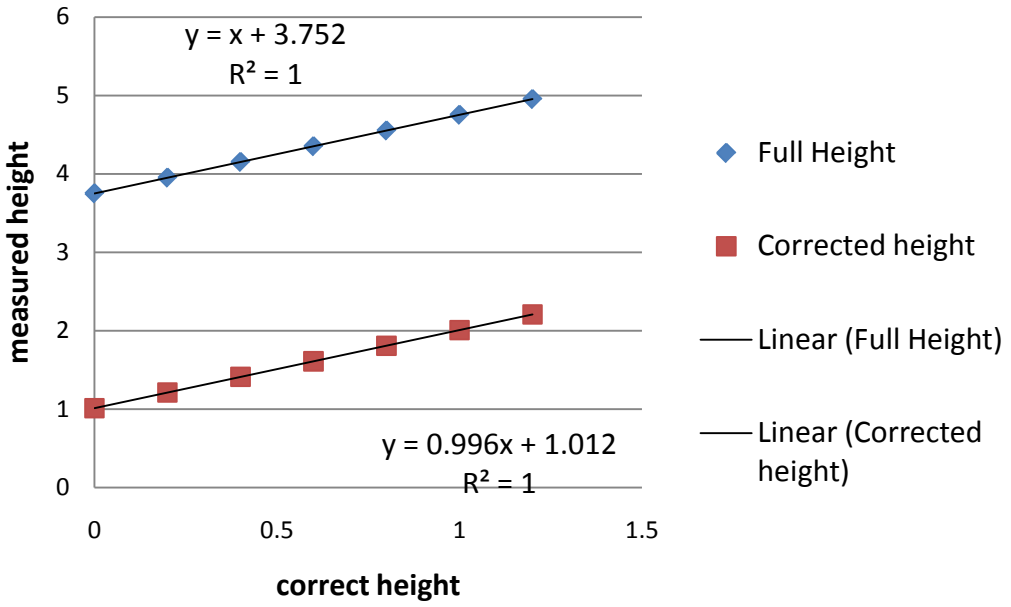

Figure 11. Graph. A comparison of tangent corrected and total peak height measurement value against known correct values.

Both methods produce very good representations of the rate. Both methods also produce a positive bias for the actual value, however, subtraction of the intercept removes this bias. If there is a finite amount of material responsible for the peaks of interest at time zero, this subtraction would not correctly describe the concentration. However, the net result does accurately describe the change in concentration. For kinetic work, this is important, particularly when measuring reactants. When measuring products that do not appear in the rate limiting rate equation, it is the net accumulation that matters. The preceding figure assumes that the true peak location is known. Usually, this is not the case as the peak is geometrically shifted “uphill” when added to an underlying spectrum with a slope. Using the apparent peak height, instead of the true peak location for height determinations, produces less desirable results with an 8% error in rate for a total height measurement, and a 23% rate error when using corrected heights. Using areas, with the end point held constant, produces rate errors of 1% for the total area to the zero absorbance line, and 7.5% if the corrected area is used. Allowing the length of the tangent to grow over time as the peak becomes more pronounced has terrible effects on the rate and accuracy as values are too low early on and much too large as the peak becomes more pronounced. This produces a non-linear response and adds curvature to the rate measurement which could lead to misinterpretation of the actual form of the kinetic expression. We use full peak height in our studies. When kinetics fits are tested, the rate equation subtracts the time zero value. For correlations with rheological change, the infrared change of the full peak height is employed, which is the time-zero spectra subtracted from the time of interest to eliminate overlap effects as much as possible.

CHEMOMETRIC METHODS-MULTIVARIABLE CORRELATIONS OF CHEMICAL CHANGE WITH RHEOLOGICAL CHANGES

The existing RITA (2010) data set was examined to search for possible correlations of rheological changes with changes in the mid infrared spectra. It was found that difference spectra using simple peak heights produced the best correlations, consistent with our studies of IR quantization methods.

Single Wave Number Studies

Prior to multivariate studies, single wave number correlations were performed across the entire spectrum for all four asphalts in the RITA (2010) data set, SHRP asphalts AAB-1, AAC-1, AAD-1 and AAM-1. These binders were aged up to 480 hours in 20 atmosphere air at 60, 80 and 100°C in standard PAV pans (3175 microns thick). The following figures (12-15) are regression scans of IR spectra when correlated against the change in the logarithm of the complex modulus at 10 radians per second. If was found that for a given binder, many wave number absorbance changes correlate well with changes in the complex modulus. When several binders are correlated together, only a few wave numbers produced reasonably good correlations (figure 16). However, the limited data examined here suggests other wave numbers besides 1700 might be useful, particularly for remote sensing applications.

The examination of correlations across the spectra is depicted here by screen shots from the software as “regression spectra”. Each regression spectrum represents a correlation of an individual wave number change against the change in the log of the complex modulus. As such, these regression spectra represent several thousand individual correlations. The x axis is the wave number used in each correlation, and the y axis is the correlation coefficient (r-squared) obtained from that linear fit. Values near 1 are nearly perfect linear correlations. Figures 12 through 15 are regression scans for individual SHRP binders AAB-1, AAC-1, AAD-1 and AAM-1.

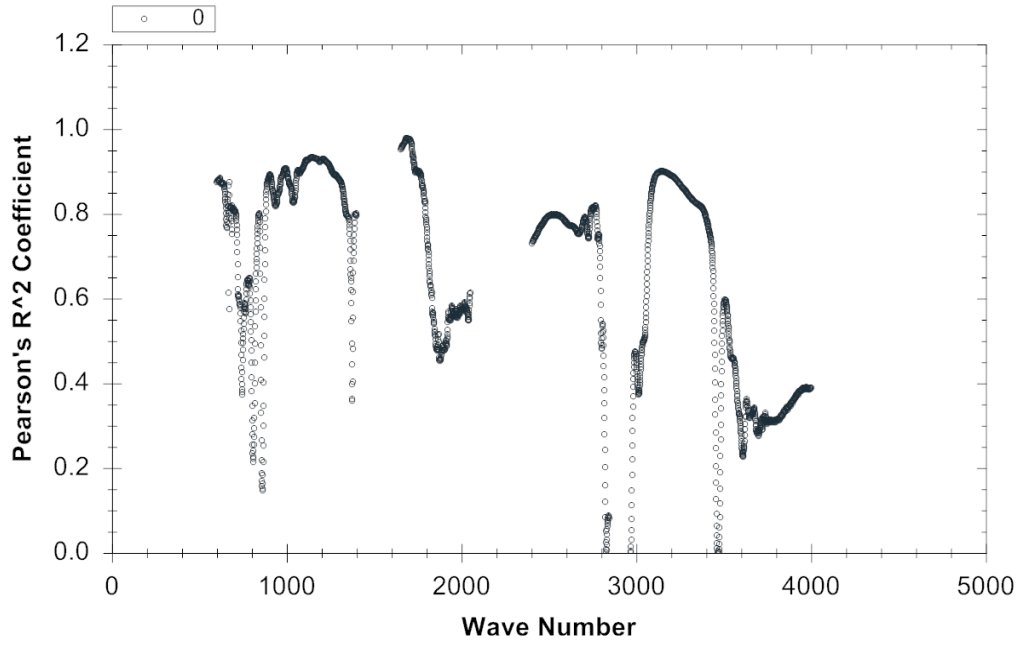

Figure 12. Screenshot. AAB-1 regression scan against log change in G* at 10 radians/s.

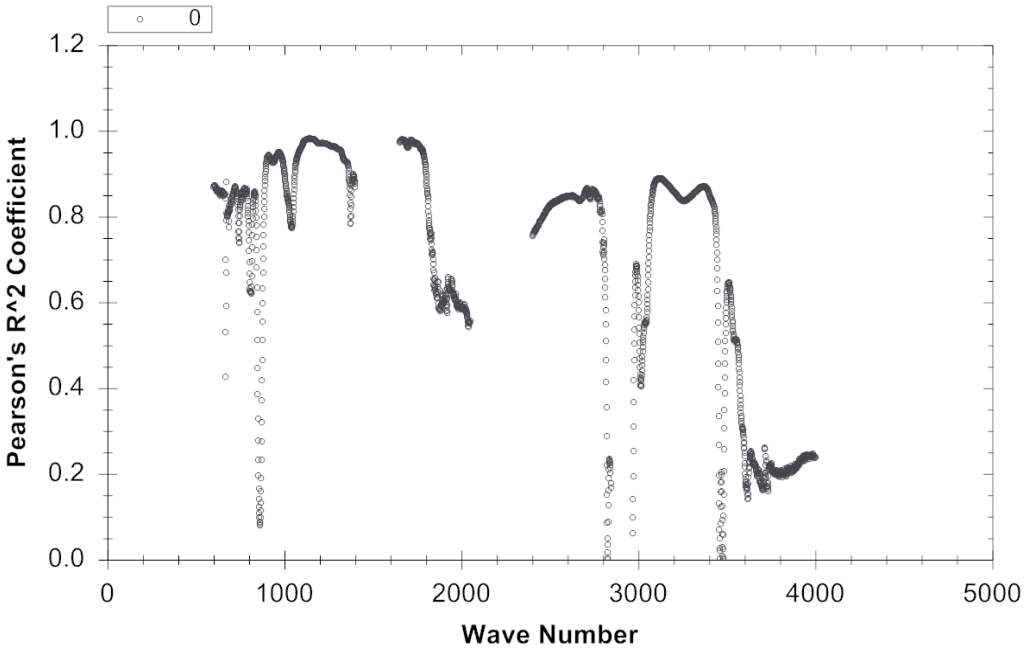

Figure 13. Screenshot. AAC-1 regression scan against log change in G* at 10 radians/s.

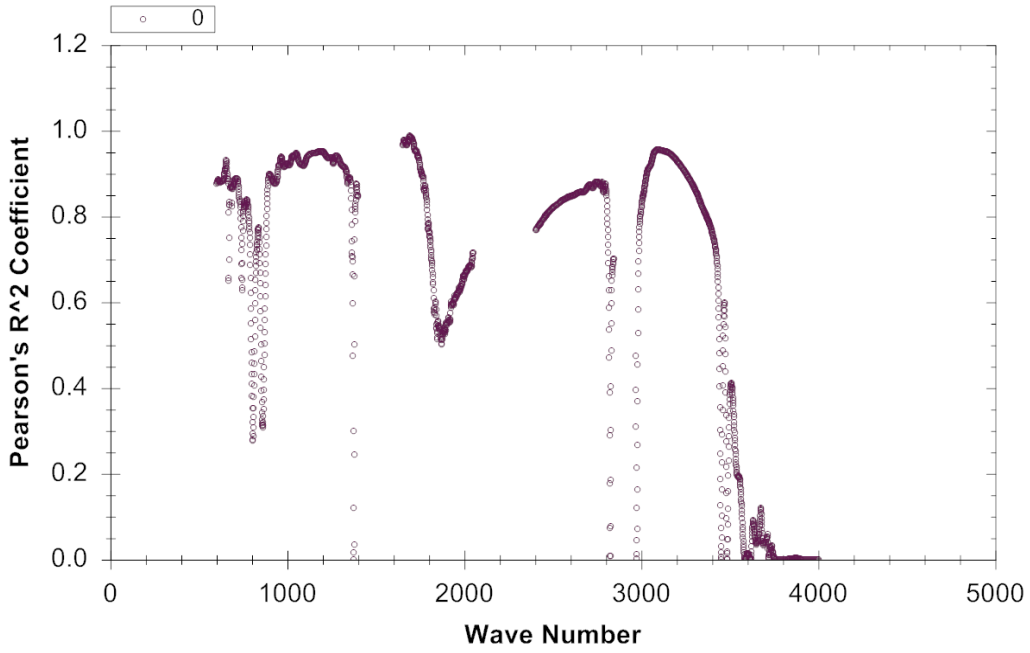

Figure 14. Screenshot. AAD-1 regression scan against log change in G* at 10 radians/s.

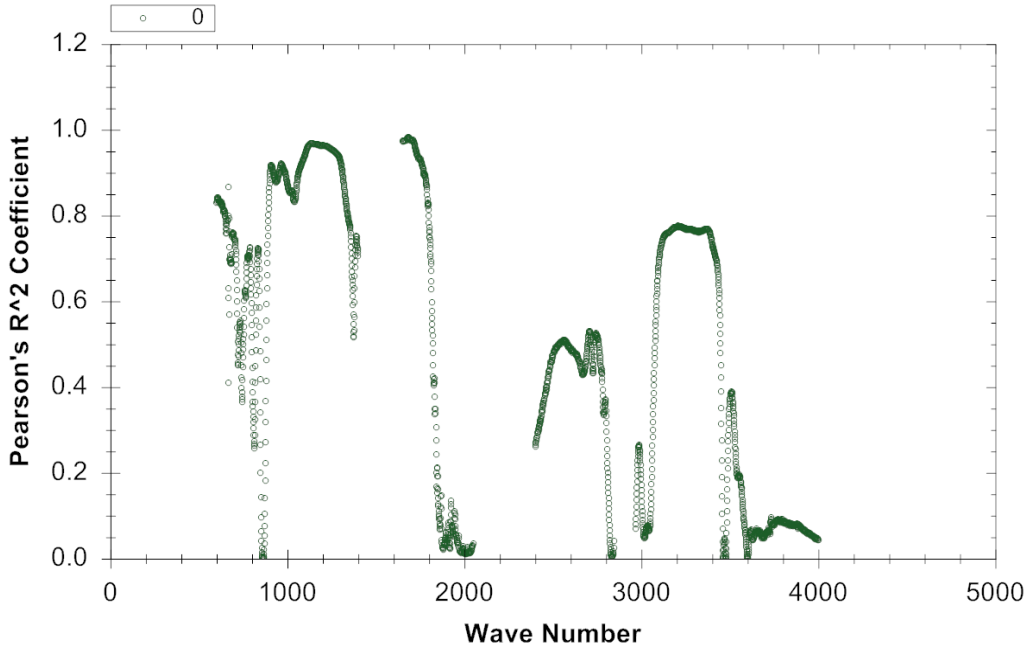

Figure 15. Screenshot. AAM-1 regression scan against log change in G* at 10 radians/s.

All four binders fit at the same time (figure 16) produce just a few single wave numbers that correlate well with complex modulus changes.

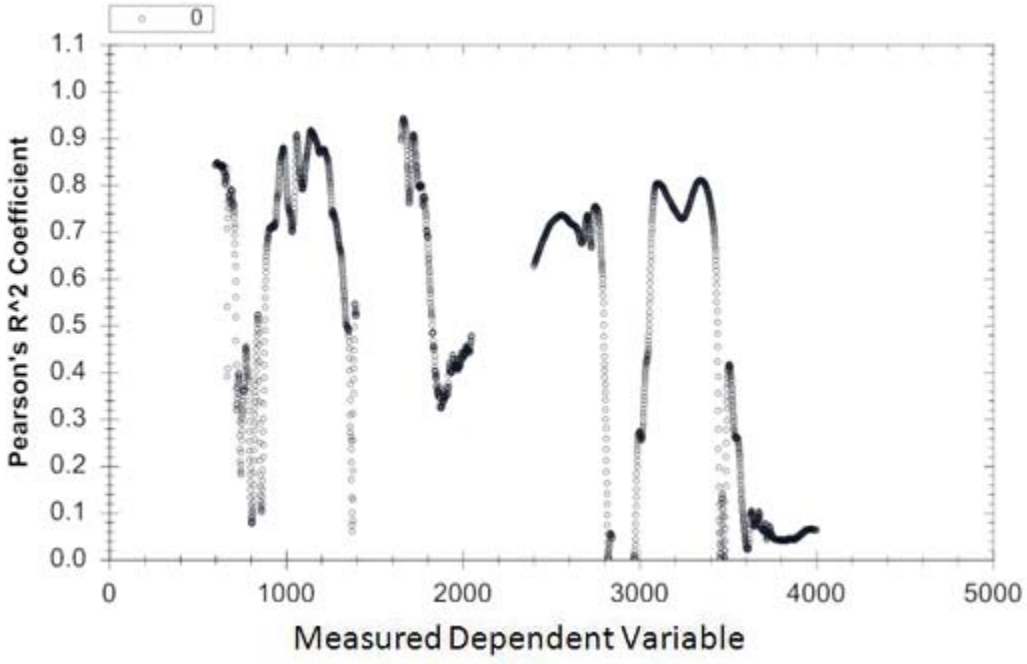

Figure 16. Screenshot. All four binders (AAB-1, AAC-1, AAD-1, and AAM-1) regression scan against log change in G* at 10 radians/s.

It is interesting that for these four binders, correlation coefficients exceeding 0.9 can be obtained correlating wave numbers 1060, 1140, 1664, and 1721. Plots for these correlations are shown in figures 17-20.

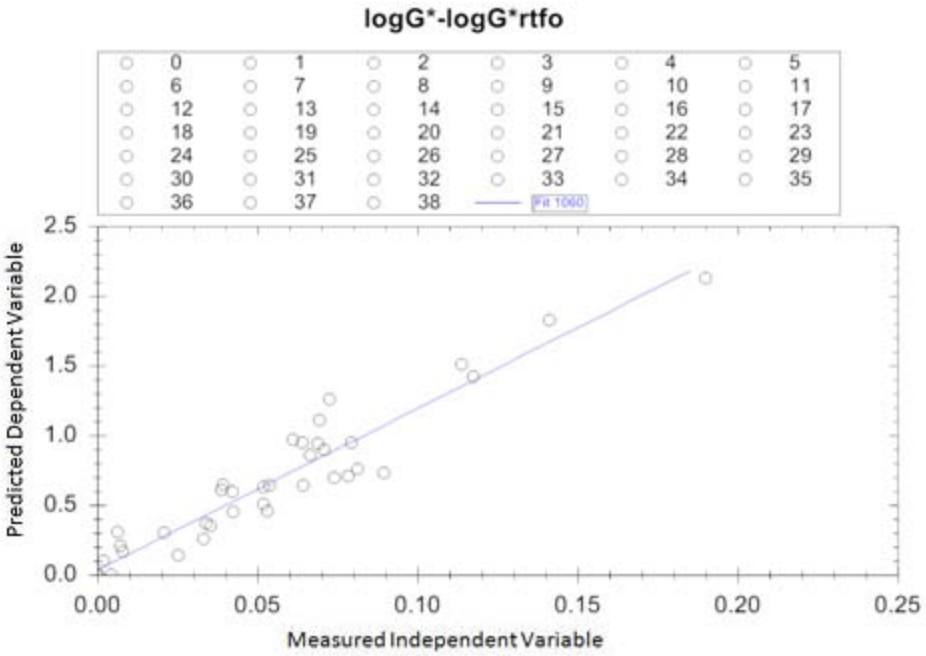

Figure 17. Screenshot. Wave number 1060 correlated to G* at 10 rad/s for 4 asphalts.

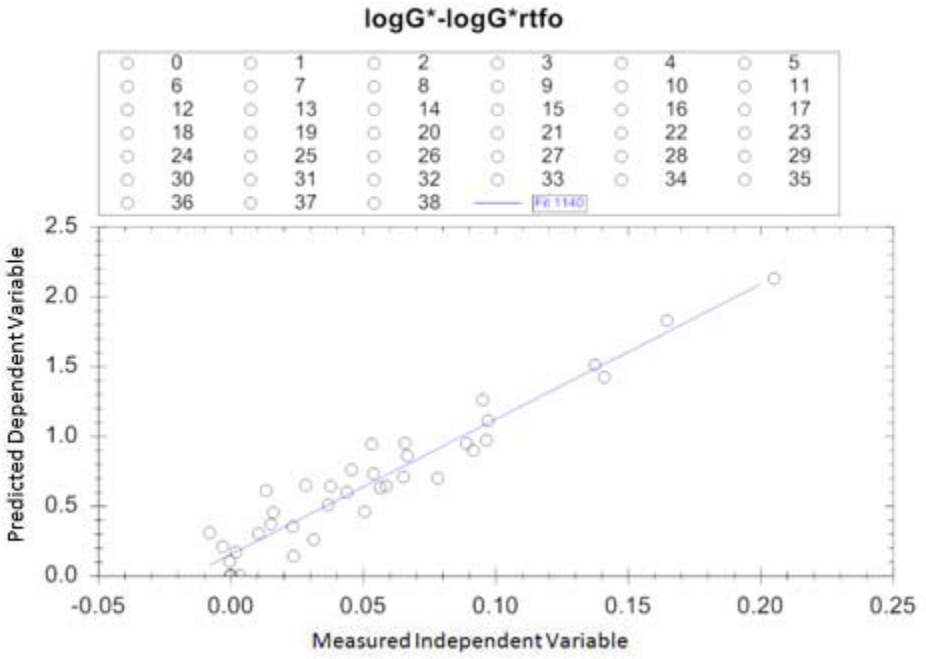

Figure 18. Screenshot. Wave number 1140 correlated to G* at 10 rad/s for 4 asphalts.

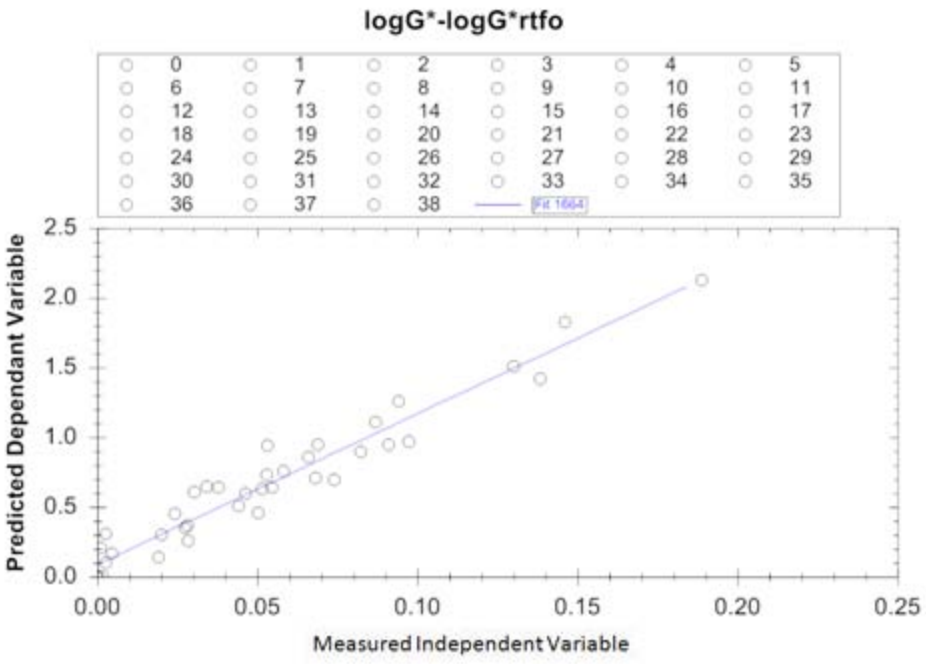

Figure 19. Screenshot. Wave number 1664 correlated to G* at 10 rad/s for 4 asphalts.

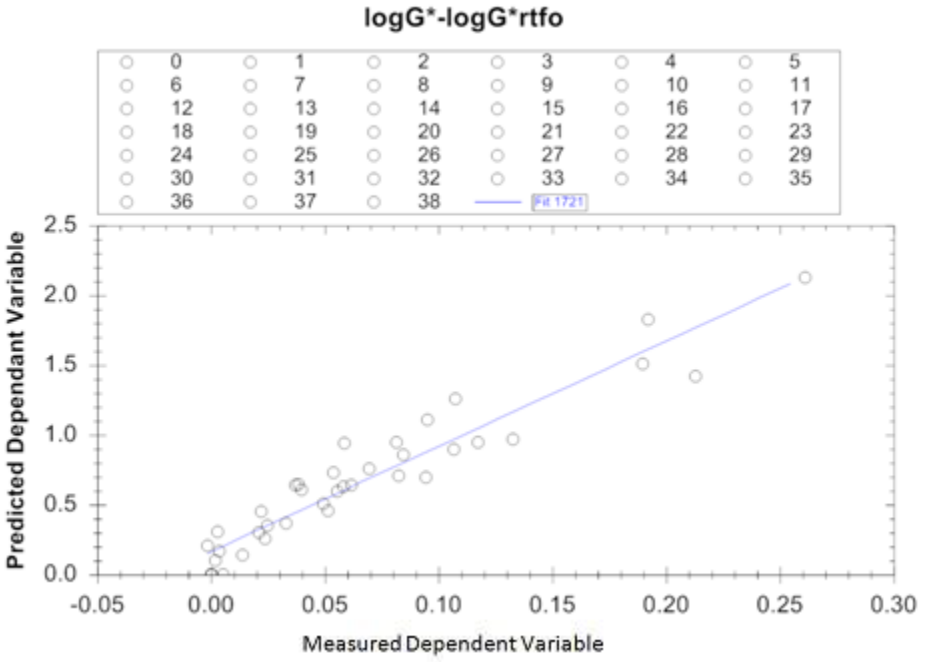

Figure 20. Screenshot. Wave number 1721 correlated to G* at 10 rad/s for 4 asphalts.

Carbonyl (wave number 1700) is often used as a metric for degree of oxidation. Figure 21 shows these correlations for each binder, which are quite good, but combined the correlation is poor.

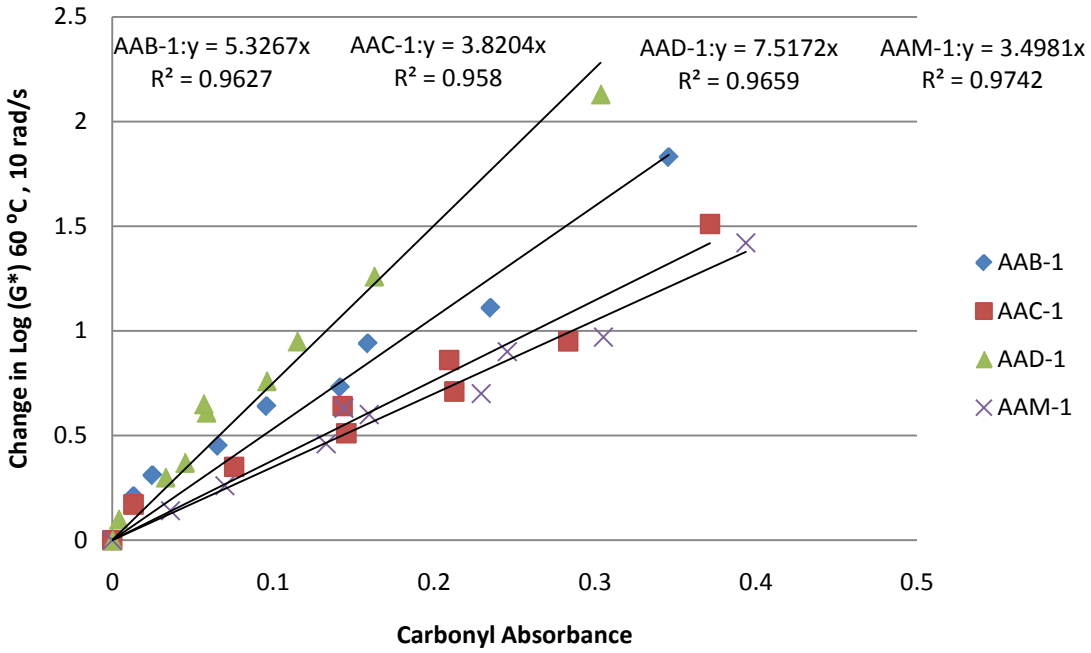

Figure 21. Graph. Source dependent relationship between carbonyl growth and complex modulus increase.

Carbonyl correlates extremely well for individual asphalts, but the slope is source dependant:

The slopes of the carbonyl absorbance change and Log(G*) change correlate quite well (figure 22) with elemental sulfur contents reported during SHRP.

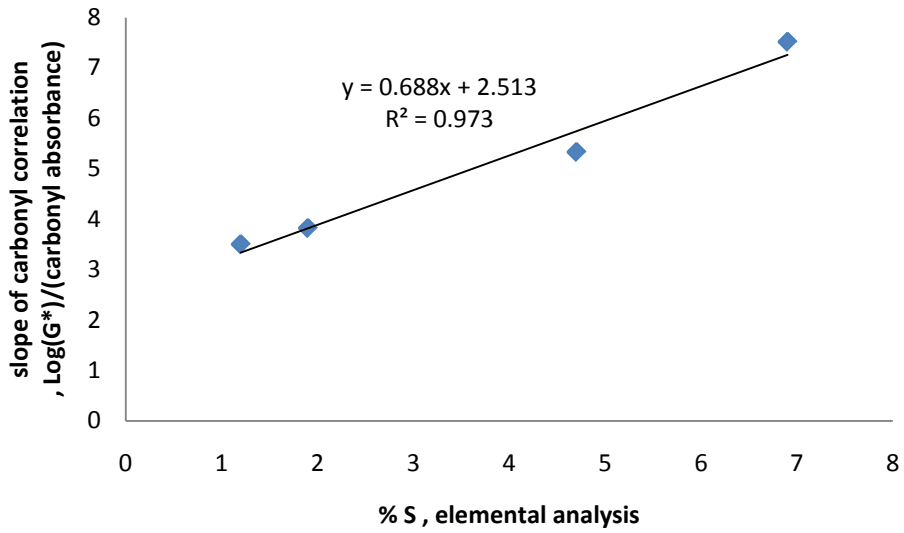

Figure 22. Screenshot. Carbonyl growth and complex modulus change slope relationship to total binder sulfur content.

The results with this rather limited collection of asphalts (although they have a wide range of properties and compositions) suggest that a simple direct correlation between the extent of oxidation and the rheological change might be possible if multivariate methods were employed.

Multivariate Correlations of IR and Complex Modulus for Four Asphalts

Multivariable correlation methods were next employed in the hopes of discovering this potentially quite useful correlation. The RITA (2010) data set was again employed in this study. The wave numbers were grouped using a cross correlation threshold of 0.9. This produces 36 groups identified as independent variables. The groups were quantized using the highest peak absorbance, since this value has the best signal to noise ratio. Areas of the spectra with non-linear response (above 3 for this instrument, validated by a dilution study) were not included in the correlation. Sufficient synthetic replicates were generated to ensure an observation to parameter ratio exceeding 7. (For this data set, 7 replicates are needed for each of the 36 groups.) More details on how this software works can be found in technical white paper FP 06. The regression run on the entire 36 groups produced the following results (table 3).

Table 3. First run program correlation results.

Coefficient of determination = 0.94866				
regression data				
IV x	Coefficient	Group no.	F	Good
x(0)	3.414E-002			
x1	5.021E-001	1056.0000	00003.575	YES
x2	3.661E-001	3101.0000	00001.893	NO
x3	3.051E-001	0666.0000	00001.454	NO
x4	6.555E-001	0667.0000	00008.074	YES
x5	5.503E-001	0668.0000	00005.375	YES
x6	-5.887E-001	0669.0000	00006.317	YES
x7	3.786E-001	0670.0000	00002.074	YES
x8	1.098E000	1108.0000	00017.486	YES
x9	-3.430E-001	1380.0000	00001.852	NO
x10	1.796E-001	1379.0000	00000.499	NO
x11	2.881E-001	0881.0000	00001.343	NO
x12	7.287E-002	0874.0000	00000.083	NO
x13	-3.103E-001	0867.0000	00001.404	NO
x14	1.081E000	1025.0000	00023.967	YES
x15	8.932E-001	1035.0000	00026.280	YES
x16	2.155E000	1701.0000	00287.300	YES
x17	8.553E-001	1318.0000	00010.205	YES
x18	-1.059E-001	1376.0000	00000.253	NO
x19	-1.205E-001	1801.0000	00000.191	NO
x20	-5.802E-001	1835.0000	00004.911	YES
x21	-2.777E-001	2441.0000	00001.256	NO
x22	-5.073E-001	2628.0000	00003.446	YES
x23	8.098E-002	3065.0000	00000.095	NO
x24	3.436E-001	2819.0000	00001.705	NO
x25	-8.611E-001	2971.0000	00020.626	YES
x26	-5.515E-002	3000.0000	00000.048	NO
x27	2.180E-001	3067.0000	00000.827	NO
x28	2.374E-001	3428.0000	00000.833	NO
x29	-5.194E-001	3443.0000	00003.745	YES
x30	2.180E-001	3450.0000	00000.628	NO
x31	-2.766E-001	3456.0000	00001.116	NO
x32	1.442E-001	3463.0000	00000.304	NO
x33	-2.527E-001	3579.0000	00001.059	NO
x34	-2.178E-001	3594.0000	00000.692	NO
x35	-4.149E-001	3874.0000	00002.421	YES
x36	4.405E-001	3990.0000	00002.853	YES

The group number represents the wave number of the largest absorbance (tallest peak) in the group. Significance is judged when the F-test exceeds 2. Removal of the insignificant groups produces 16 significant variables. Running the regression again after removing insignificant variables identifies several more insignificant wave numbers (table 4):

Table 4. Second run independent variable reduction program correlation results.

Coefficient of determination = 0.93050				
Regression data				
IV x	Coefficient	Group no.	F	Good
x(0)	6.098E-002			
x1	2.893E-001	1056.0000	00001.344	NO
x4	6.739E-001	0667.0000	00006.359	YES
x5	3.815E-002	0668.0000	00000.024	NO
x6	3.861E-001	0669.0000	00002.368	YES
x7	3.881E-001	0670.0000	00002.110	YES
x8	9.755E-001	1108.0000	00014.801	YES
x14	1.161E000	1025.0000	00026.810	YES
x15	9.490E-001	1035.0000	00024.280	YES
x16	2.051E000	1701.0000	00197.007	YES
x17	6.737E-001	1318.0000	00007.418	YES
x20	-1.070E-001	1835.0000	00000.166	NO
x22	7.623E-001	2628.0000	00007.345	YES
x25	-7.210E-001	2971.0000	00023.302	YES
x29	-4.447E-001	3443.0000	00003.003	YES
x35	-8.562E-002	3874.0000	00000.077	NO
x36	-6.673E-001	3990.0000	00005.498	YES

Rerunning with the remaining 12 significant wave numbers produces a regression coefficient for the data of 0.9678 (table 5):

Table 5. Independent variable reduction program correlation results with 13 parameters.

Coefficient of determination = 0.9678				
Regression data				
IV x	Coefficient	Group no.	F	Good
x(0)	3.245E-002			
x4	1.895E-001	0667.0000	00000.473	NO
x6	-4.315E-002	0669.0000	00000.032	NO
x7	-2.508E-001	0670.0000	00000.833	NO
x8	6.228E-001	1108.0000	00005.671	YES
x14	1.238E000	1025.0000	00026.493	YES
x15	1.336E000	1035.0000	00049.093	YES
x16	2.306E000	1701.0000	00283.431	YES
x17	3.767E-001	1318.0000	00002.095	YES
x22	2.256E-001	2628.0000	00000.585	NO
x25	-5.910E-001	2971.0000	00015.955	YES
x29	-2.986E-001	3443.0000	00001.130	NO
x36	-2.930E-001	3990.0000	00001.092	NO

At this point, it may be instructive to examine where these groups are in the spectra. Group 1108 is depicted in the following screen shot (figures 23-28):

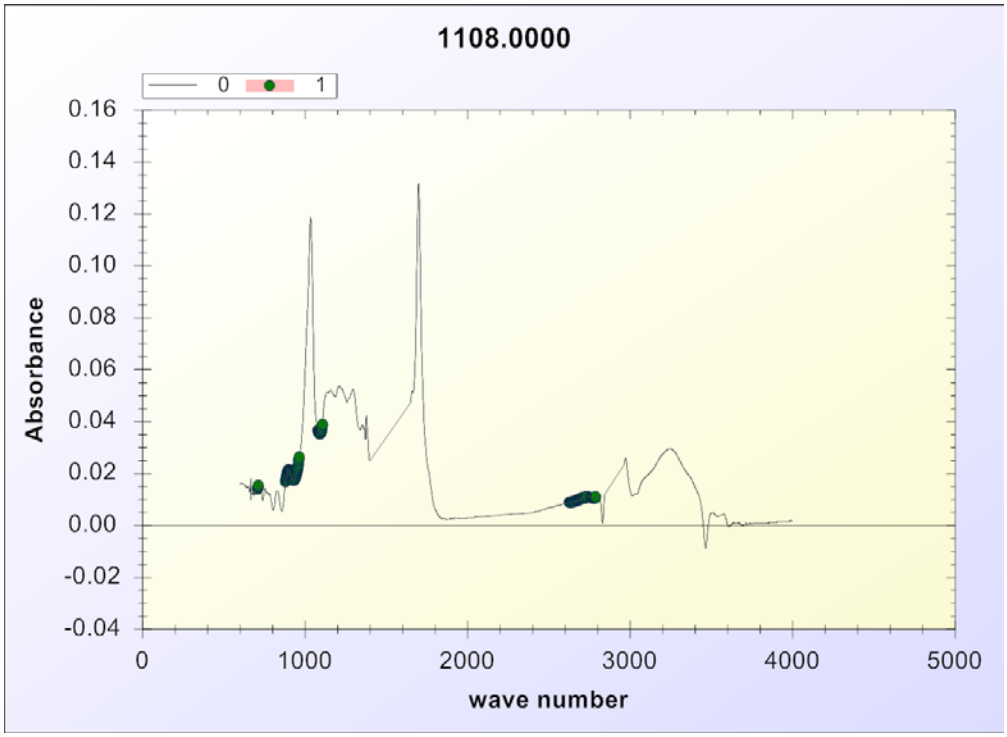

Figure 23. Screenshot. Group 1108 members shown on change spectra relative to time zero (RTFO sample).

Group 1025 contains the wave number depicted in figure 24.

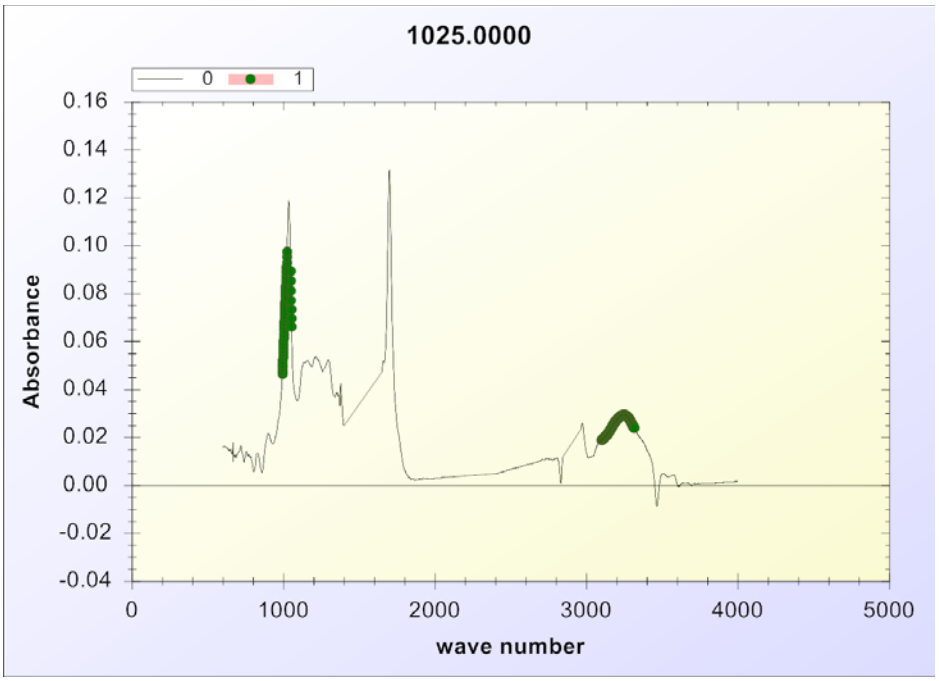

Figure 24. Screenshot. Group 1025 members shown on change spectra relative to time zero (RTFO sample).

Group 1035 is shown next (figure 25).

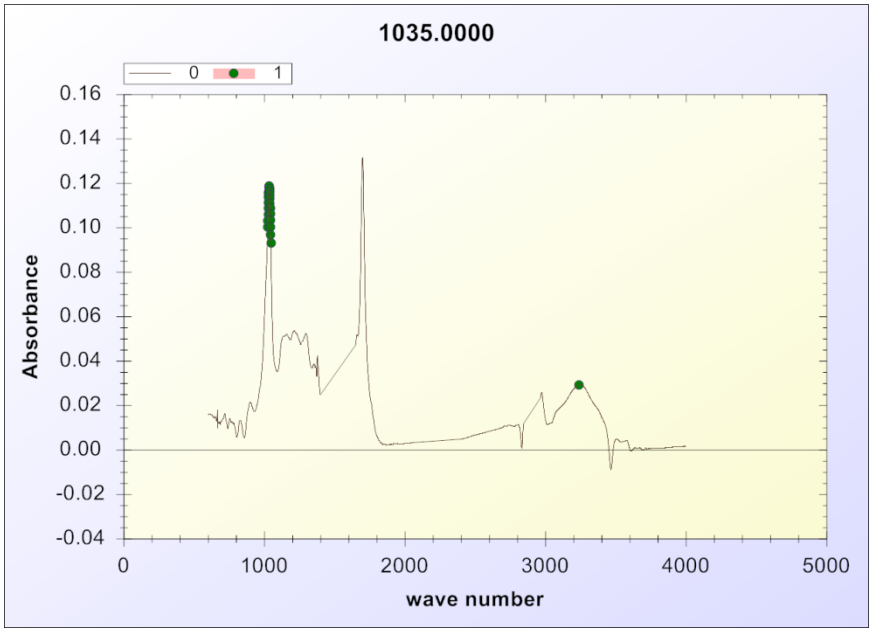

Figure 25. Screenshot. Group 1035 members shown on change spectra relative to time zero (RTFO sample).

The two previous groups indicate a strong relationship exists between the evolution of the sulfoxide peak at 1035, and the hydrogen bonding peak at 3240.

The 1701 Group, usually assigned to carbonyl, also appears to have a relationship to responses in the 1100-1300 range, most likely single bonded oxygen acid (figure 26).

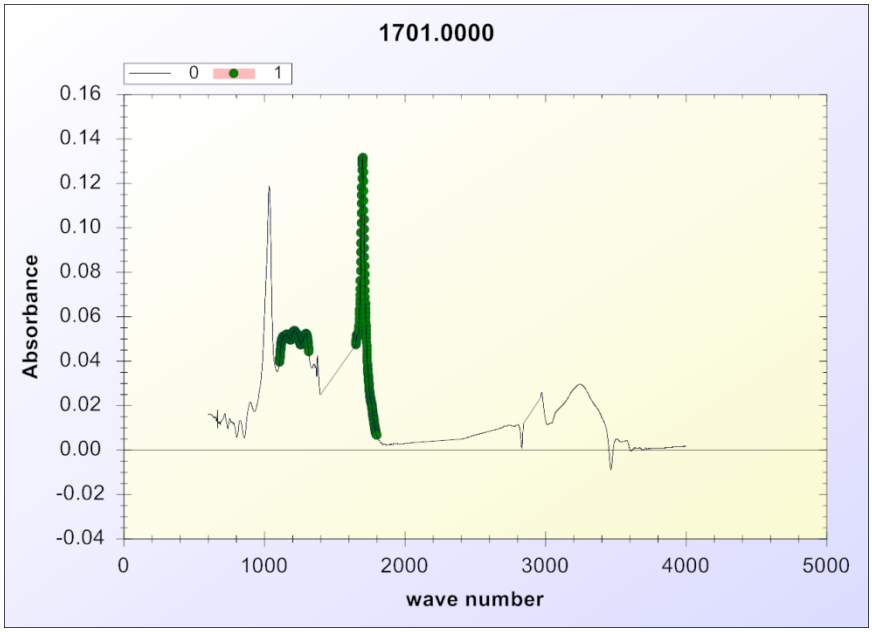

Figure 26. Screenshot of group 1701 members shown on change spectra relative to time zero (RTFO sample).

The small grouping at 1318 may represent sulfones and/or sulfonic acid (figure 27).

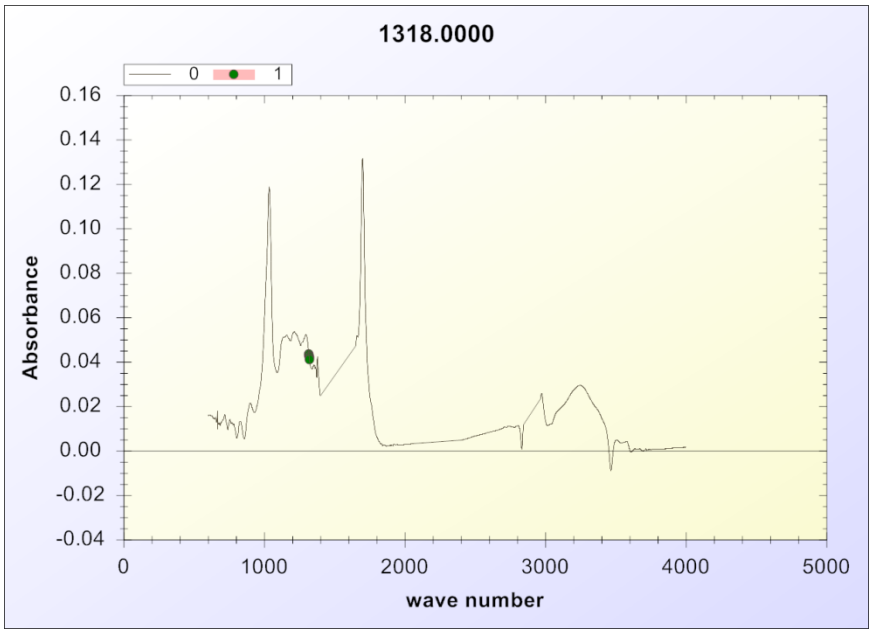

Figure 27. Screenshot. of group 1318 members shown on change spectra relative to time zero (RTFO sample).

The group at 2971 (figure 28) appears to represent a material being consumed, as these are difference spectra with time zero values removed. It should be noted that there is no such thing as a baseline for asphalt and/or oxidized asphalt spectra. There are so many functional group responses in asphalt that the response tails all add to significant values. When oxidized, there is even more diversity in chemical species, hence more tails, and a general lifting of the spectra. So, even though the 2971 group is not negative, it may still represent a consumed material.

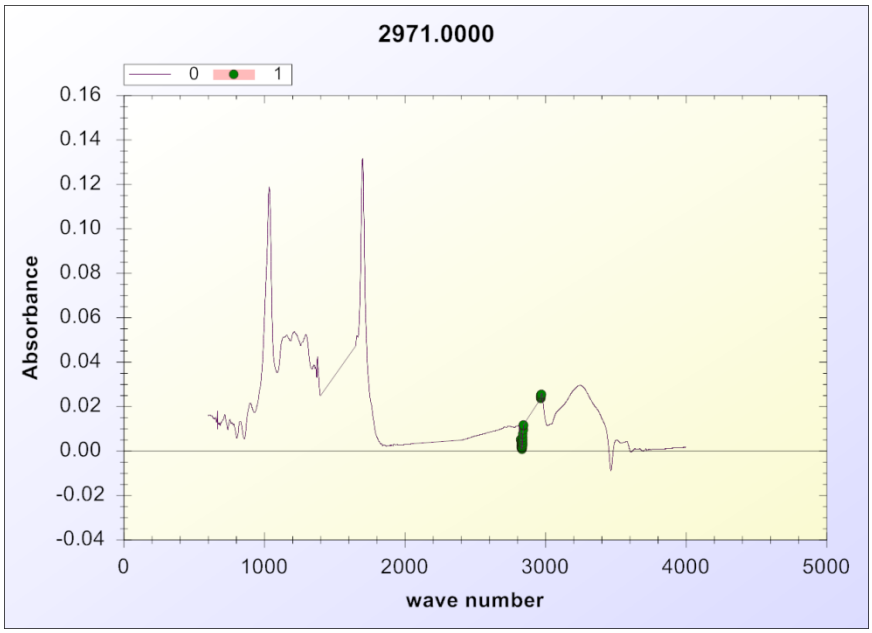

Figure 28. Screenshot. of group 2971 members shown on change spectra relative to time zero (RTFO sample).

Running the regression again after removing insignificant wave numbers yields only six wave numbers of significance with a regression coefficient of 0.969 (table 6):

Table 6. Independent variable reduction program correlation results with 9 parameters.

Coefficient of determination = 0.969				
Regression data				
IV x	Coefficient	Group no.	F	Good
x(0)	2.603E-002			
x4	2.497E-001	0667.0000	00001.094	NO
x8	1.019E000	1108.0000	00018.597	YES
x14	1.253E000	1025.0000	00037.948	YES
x15	1.120E000	1035.0000	00038.241	YES
x16	2.176E000	1701.0000	00281.235	YES
x17	8.742E-001	1318.0000	00011.910	YES
x22	1.074E-001	2628.0000	00000.146	NO
x25	-7.553E-001	2971.0000	00027.565	YES

Overall regression is SIGNIFICANT.

Clearly carbonyl is the most significant wave number, followed by sulfoxide. The least significant is 1108. Its removal from consideration produces a correlation coefficient of 0.968, essentially no change with one less variable. Next we remove 1318 (table 7).

Table 7. Independent variable reduction program correlation results with 4 parameters.

Coefficient of determination = 0.9644				
Regression data				
IV x	Coefficient	Group no.	F	Good
x(0)	1.915E-002			
x14	1.727E000	1025.0000	00047.293	YES
x15	1.015E000	1035.0000	00023.387	YES
x16	2.567E000	1701.0000	00542.356	YES
x25	-2.395E-001	2971.0000	00002.257	YES

With only four wave numbers in the correlation we see a minor reduction in the correlation coefficient to a value of 0.964. Removal of 2971 produces a correlation coefficient of 0.961. The three remaining wave numbers represent the carbonyl peak, the sulfoxide peak, and the shoulders of the sulfoxide peak. Removal of the 1025 group produces a regression coefficient of 0.961 again. Notice that the fit coefficients are nearly identical, suggesting that a simple sum of these oxides may produce a reasonable estimate of stiffness change (table 8).

Table 8. Independent variable reduction program correlation results with 3 parameters.

Coefficient of determination = 0.9610				
Regression data				
IV x	Coefficient	Group no.	F	Good
x(0)	2.557E-002			
x15	2.329E000	1035.0000	00522.777	YES
x16	2.573E000	1701.0000	00773.112	YES

A comparison of the measured and predicted values for the change in Log(G*) is shown in figure 29.

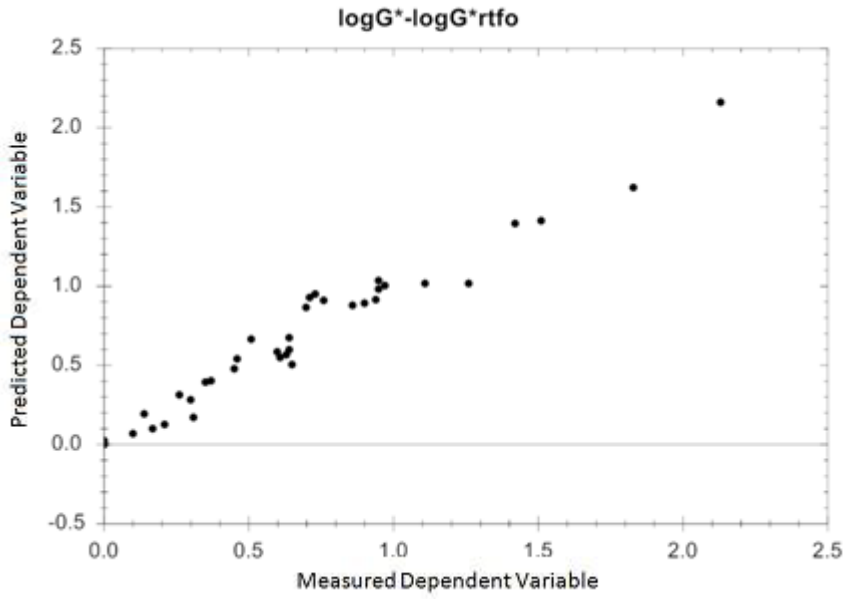

Figure 29. Screenshot. Predicted and observed complex modulus using carbonyl and sulfoxide IR measurements for four SHRP asphalts.

A plot of the change in the Log(G*) vs. the change in carbonyl + sulfoxide absorbance for this data set is show in figure 30.

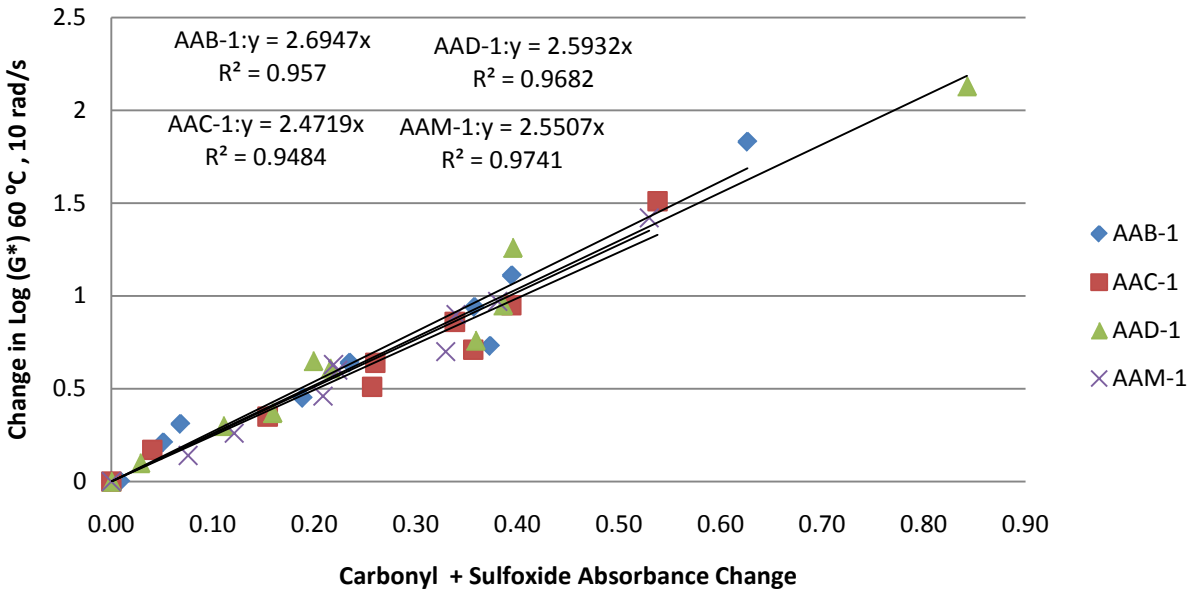

Figure 30. Graph. Carbonyl and sulfoxide absorbance change correlated to the change in complex modulus.

Compare this to previous views about oxidation susceptibility as interpreted from a carbonyl alone correlation (figure 31).

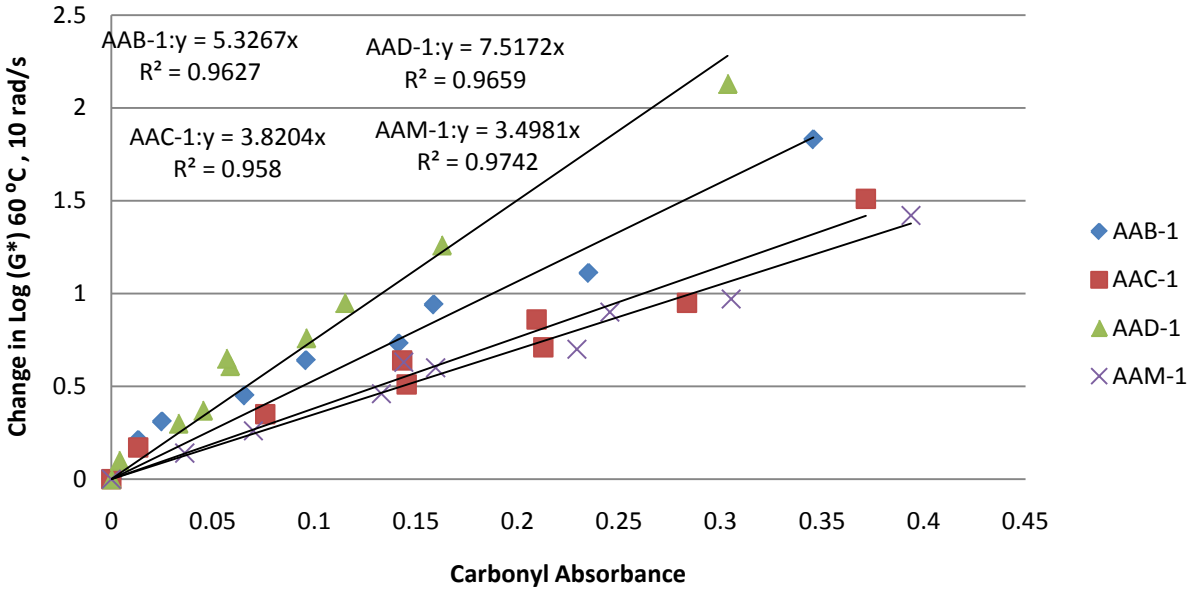

Figure 31. Graph. Carbonyl alone absorbance change correlated to the change in complex modulus.

These results suggest that the phenomenon of stiffening with oxidation is more uniform than previously believed and also indicates that carbonyl alone is insufficient to properly capture the extent of the oxidation. Clearly, oxidation of sulfur reactions in the binder plays an important role in the changes in complex modulus.

Similar correlations with the loss modulus for this data set produce the same list of significant wave numbers (table 9).

Table 9. Independent variable reduction program correlation results with loss modulus.

Coefficient of determination = 0.9707				
Regression data				
IV x	Coefficient	Group no.	F	Good
x(0)	1.304E-001			
x14	2.264E000	1025.0000	00023.369	YES
x15	2.810E000	1035.0000	00051.195	YES
x16	5.415E000	1701.0000	00501.286	YES
x17	2.042E000	1318.0000	00014.601	YES
x25	-1.974E000	2971.0000	00032.681	YES

Correlations against the storage modulus also give the same wave numbers as being significant (table 10).

Table 10. Independent variable reduction program correlation results with storage modulus.

Coefficient of determination = 0.9694				
Regression data				
IV x	Coefficient	Group no.	F	Good
x(0)	2.901E-001			
x14	1.293E000	1025.0000	00002.742	YES
x15	4.558E000	1035.0000	00038.975	YES
x16	8.642E000	1701.0000	00509.318	YES
x17	5.086E000	1318.0000	00035.325	YES
x25	-3.035E000	2971.0000	00032.801	YES

The results from this limited study suggest that chemical changes on oxidation and corresponding rheological changes may not be source dependant. However, a test on only four binders is a perhaps insufficient to verify the idea of a universal correlation between chemical changes on oxidation and the resulting change in rheology. In addition, there is some concern that the thick films (3175 microns) may exhibit some diffusion control, minimizing the differences in the source dependant chemistry. These preliminary studies led to a more detailed oxidation study with 12 binders at ambient pressure, with sufficient rheological characterization to attempt correlations between IR changes and master curve changes, along with a study of the reaction kinetics of many binders with consistent methods employed for tracking the extent of reaction.

DIFFUSION FILM THICKNESS STUDIES

Two asphalts, SHRP AAC-1 and AAK-1 were aged at 70°C for two weeks (the highest rate period) to determine the maximum film thickness to use in oxidation studies where the effect of diffusion rate can be neglected. A variety of film thicknesses from 25 to 1000 micron was tested to determine at what thickness a smaller film produces the same conversion. For both binders, 100 microns appears to be the thickest films usable at 70°C, based on carbonyl and sulfoxide responses. An anomalous measurement occurred at the 25 micron thickness for carbonyl in the AAC-1 sample that was ignored as a spurious measurement, probably caused by an error in sample handling. Figures 32 and 33 summarize these results.

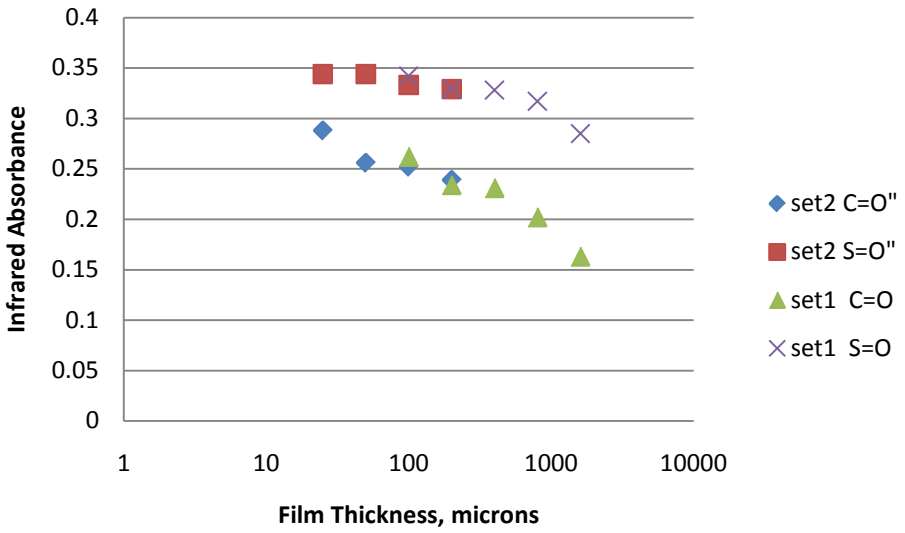

Figure 32. Graph. Net oxide production for asphalt AAC-1 as a function of film thickness after 2 weeks at 70°C.

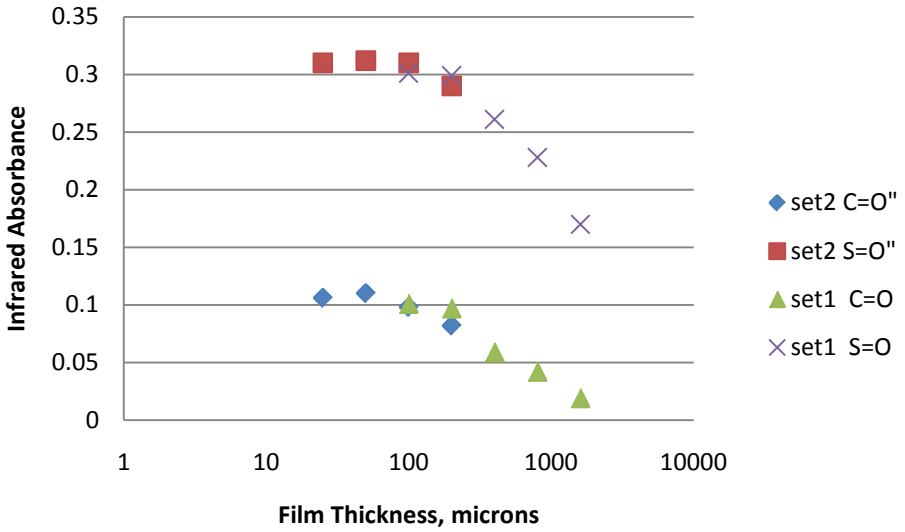

Figure 33. Graph. Net oxide production for asphalt AAK-1 as a function of film thickness after 2 weeks at 70°C.

AMBIENT PRESSURE ASPHALT OXIDATION

The extent of the oxidation reaction is probably best tracked by using oxygen uptake, although there has been little work done to verify if fugitive reaction products, like water, need to be accounted for. Over the course of this study it was discovered that the two major infrared responses, the peak in the vicinity of wave number 1034 cm-1 and the peak at 1700 cm-1 (these

peak locations vary slightly with technique and solvent used) correlate well with oxygen uptake as measure by direct oxygen determination. Figure 34 shows a plot of change in direct oxygen content plotted against the change in the IR oxides for four binders used in the WRI/FHWA Arizona test strip. There does appear to be some exceptions as is apparent in the AZ1-1 sample, which is an air blown asphalt.

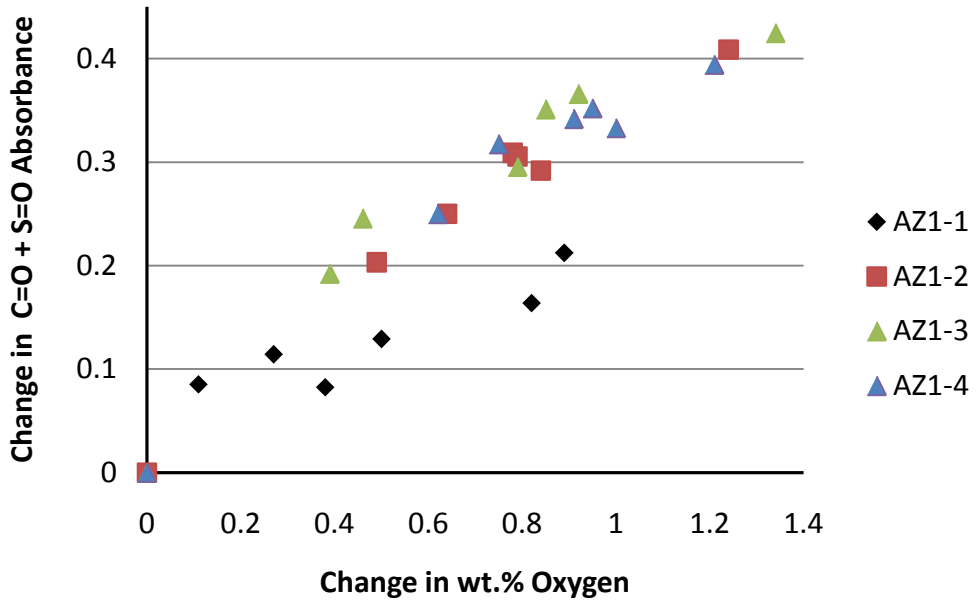

Figure 34. Graph. Relationship between IR oxides and direct oxygen measurements for four asphalt binders.

The Arrhenius fits below in table 11 were prepared using the dual reaction isothermal rate expression that models an apparent first and an apparent zero order reaction occurring in parallel.

$$[C=O] = RM\,(1-e^{-k_1 t}) + k_2 t \qquad (13)$$

where:
$[C=O]$ represents the carbonyl absorbtion measured from the infrared
RM represents the concentration of a first order reactant in the fast reaction
k_1, k_2 represent the isothermal rate constants for the fast and slow reactions, respectively.

$$k = Ae^{\frac{-E}{RT}} \qquad (14)$$

where:
A is the pre-exponential factor
E is the activation energy
R is the universal gas constant
T is the absolute temperature.

The materials were aged at 4 temperatures (40, 50, 60, and 70°C) and equation 13 was fit to each one, producing rate constants (k_1 and k_2) at each of the four temperatures to obtain the activation energy and pre-exponential factors that describe the rate dependence upon temperature. These are fit by linearizing the equation and plotting ln(k) vs. 1/T.

When carbonyl alone is used to track oxidation, the measured activation energies vary depending upon the binder source. Table 11 show the huge variation obtained when individual wave numbers are used to track the extent of oxidation.

Table 11. Arrhenius fit of rate constants based upon isothermal carbonyl formation alone.

Asphalt	E1/R	lnA1	E2/R	lnA2
AAB-1 C=O	-8405	22.01	-9932	22.43
AAC-1 C=O	-9058	24.21	-6582	13.14
AAD-1 C=O	-12862	33.80	-1581	-2.27
AAM-1 C=O	-10813	29.51	-5429	9.87
ABD-1 C=O	-6782	18.07	-6511	13.25
ALF C=O	-5394	13.49	-6341	12.50
ARC1 C=O	-4868	11.90	-8496	18.95
ARC2 C=O	-10475	27.53	-7924	14.58
AZ1-1 C=O	-5977	14.95	-4313	5.99
MCR C=O	-5177	12.96	-7534	15.84
MCU C=O	-6663	16.88	-9647	21.52
MN1-4 C=O	-7764	20.38	-4734	7.25

This observation, generally considered state of the art at the time these tests were completed, can result either by a source dependent mechanism or because carbonyl alone does not reflect the rate limiting step of a more universal mechanism. If such a universal mechanism exists, then the Arrhenius (temperature dependency) parameters could be, in theory, determined once and for all, and a method for characterization of asphalt binder oxidation rates could be devised that does not require testing over a range of temperatures. The thrust of this work is to find a universal mechanism by identifying the rate limiting step, and using that information to find the best way to track the progress of the reaction.

Once the rate of oxidation is reasonably understood to at least provide prediction capabilities, then the question remains of how these chemical changes affect the mechanical properties of the binder, particularly the rheological properties. As a first step in understanding how the oxidation products cause changes in rheological properties, correlations between these two measurements were sought. These are currently empirical in nature, but should provide clues to a better conceptual idea of how this process works at the molecular level.

The dual oxidation mechanism proposed by Petersen (1998) was the starting point for deriving a mathematical form of the dual oxidation pathways. The dual mechanism proposes two primary

paths to form oxidation products, a fast and a slow reaction that occur in parallel. When an asphalt binder is oxidized, the form of the isothermal integrated rate equation appears to be first order changing to zero order (figure 35).

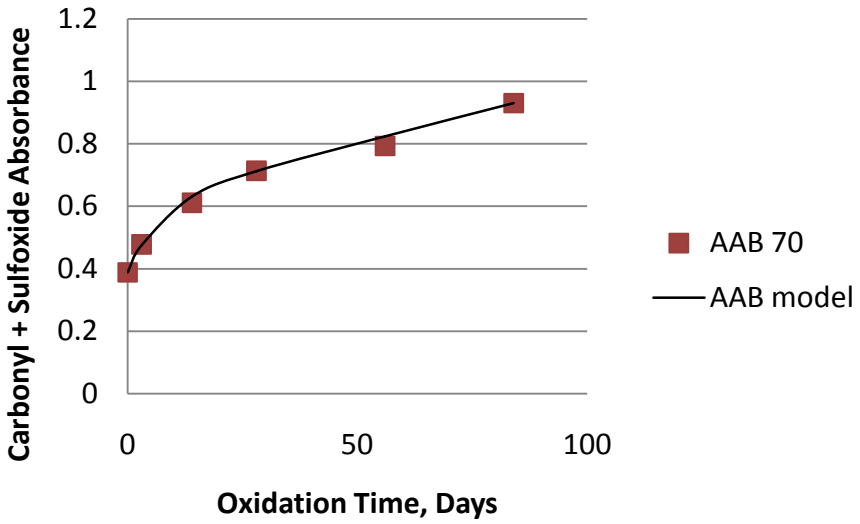

Figure 35. Graph. Oxidation product generation (Sulfoxide +Carbonyl) over time for binder AAB-1 at 70°C.

Fundamentally, first order and parallel zero order reactions are not likely, and the rate limiting steps are most likely bi-molecular (second order). The fast reaction according to the proposed dual reaction scheme produces sulfoxide, alcohol, and possibly carbonyl functional groups, particularly in binders with low sulfide content. In addition, the fast reaction is believed to produce free radicals that can, possibly, participate in the ongoing slow reaction. The slow reaction is proposed to be classic free radical chain. The reactive material in this slow reaction path, as suggested by Petersen, is predominantly benzyl carbons. We modeled this mechanism by assuming the rate limiting step for both paths is at or very near the molecular oxygen collision with reactive materials particular to each pathway. We assume that the slow reaction requires free radical initiation via hydrogen abstraction from a benzyl carbon, which in turn reacts with molecular oxygen in the rate limiting step. Faster reaction steps go on to produce oxide and alcohol products, along with a new free radical to replace the one consumed during hydrogen abstraction. Our mathematical formulation essentially assumes that the oxygen and reactive material react directly in the same step, which would produce a pressure dependency that is directly proportional to the oxygen partial pressure. We and others have found that the pressure correction exponent is fractional (Domke et al. 2000). Our experimental findings and others indicate that a somewhat more complex mechanism involving singlet oxygen or oxygen containing radicals, and accounting for termination steps, will be required to explain pressure dependency.

The important point is that the proposed fast reaction is assumed to produce a free radical in addition to the final reaction products, and this radical, or some descendant of it in a more

complex chain, is responsible for the hydrogen abstraction in the slow pathway. Furthermore, the slow pathway regenerates a new radical for the one used in abstraction. The net result is the fast reaction continues to produce free radicals until its reactive material is consumed. If the hydrogen abstraction step is quite fast relative to the benzyl carbon radical and oxygen step, then the rate of the slow reaction is controlled by the extent of completion of the fast reaction. Once the fast reaction is finished, the slow reaction continues at a constant rate for a very long time since both oxygen and benzylic carbons are available in great abundance. Mathematically, this interaction is actually quite simple. The two reaction pathways can be simplified to

Reaction 1: $C_{fast} + O_2 \xrightarrow{\text{rate limiting}} several\ rapid\ steps \longrightarrow P_{fast} + F^*$

Reaction 2a: $C_{slow} + F^* \xrightarrow[rapid]{} C^*_{slow}$

Reaction 2b: $C^*_{slow} + O_2 \xrightarrow{\text{rate limiting}} several\ rapid\ steps \longrightarrow P_{slow} + F^*$

C_{fast} represents the reactive material for the fast reaction

C_{slow} represents the reactive material for the slow reaction, generally assumed to be benzyl carbons, F^* is a generic symbol for any species of radicals produced. P_{fast} and P_{slow} represent the products produced, which we assume to be proportional to the sum of the carbonyl and sulfoxide concentration as determined from infrared analysis. To do the mathematics properly, the distinction between the product origins must be kept in mind, but once the isothermal integration is completed, these terms can be combined to obtain the values we can measure.

The basic rate equations can be written as:

$$\frac{dP(x)_1}{dt} = A_1 e^{\frac{-E_{a,1}}{RT(x,t)}} \left[C_{fast,0} - P(x,t)_1\right]\left[O(x,t)_2\right]^n \tag{15}$$

$$\frac{dP_2}{dt} = A_2 e^{\frac{-E_{a,2}}{RT(x,t)}} \left[C^*_{slow}(x,t)\right]\left[O(x,t)_2\right]^m \tag{16}$$

Here $C_{fast,0}$ represents the fast reaction reactive material at the beginning of the aging experiment. The slow reaction reactive material is assumed to be a benzyl radical produced in proportion to the products of the fast reaction. During the course of the slow reaction, additional radicals are produced to replace the radical consumed in the hydrogen abstraction of benzyl carbons. Integration of the rate equations above produces the isothermal and isobaric equation used to fit the data:

$$P = C_{fast,0}\left(1 - \frac{k_2}{k_1}\right)\left(1 - e^{-k_1 t}\right) + k_2 C_{fast,0} t + P_o \tag{17}$$

Equation 17 is used to fit the isothermal data to determine the rate constants and amount of reactive material for each binder studied. Note that this isobaric form has the oxygen concentration term combined into the apparent rate constant.

A typical fit of the model to the production of aging products appears in figure 36. For all twelve binders studied, the correlation coeffcients were 0.95 or better.

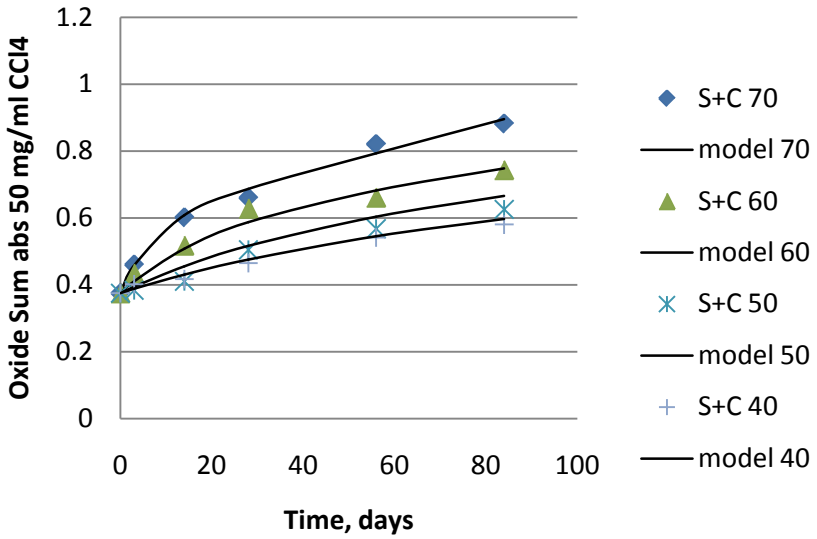

Figure 36. Graph. Oxidation product generation model fits over time for binder MN1-3 at 70°C, 60°C, 50°C and 40°C.

The collection of twelve asphalts results in 48 isothermal oxidized production plots (similar to figure 35) to fit. These were fit simultaneously using nonlinear regression methods (Microsoft Excel Solver utility) to obtain values for the universal rate constants k_1 and k_2 at each of the four temperatures studied and the amount of reactive material in each binder (table 12). The units on the rate constants are reciprocal days. All of the binders produced good fits with the same rate constants (figures 37-48). Individual fits will produce some variance in the rate constants, because of oxygen solubility difference and experimental variance.

Table 12. Isothermal fit rate constants.

Rate Constant	Aging Temperature			
	40°C	50°C	60°C	70°C
k_1	0.0181	0.0274	0.0522	0.1362
k_2	0.0034	0.0060	0.0086	0.0152

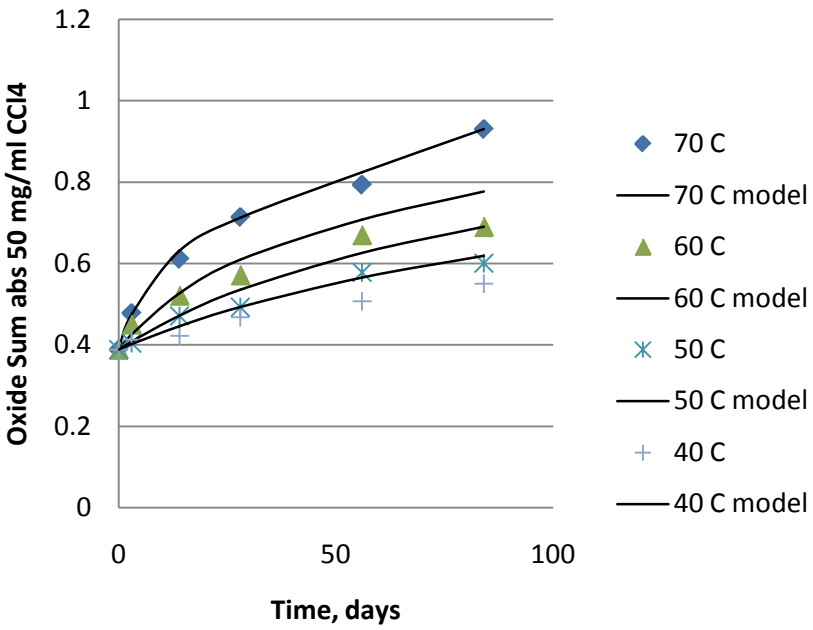

Figure 37. Graph. AAB-1 oxidation at .74 atmospheres compared to model fits at 4 temperatures.

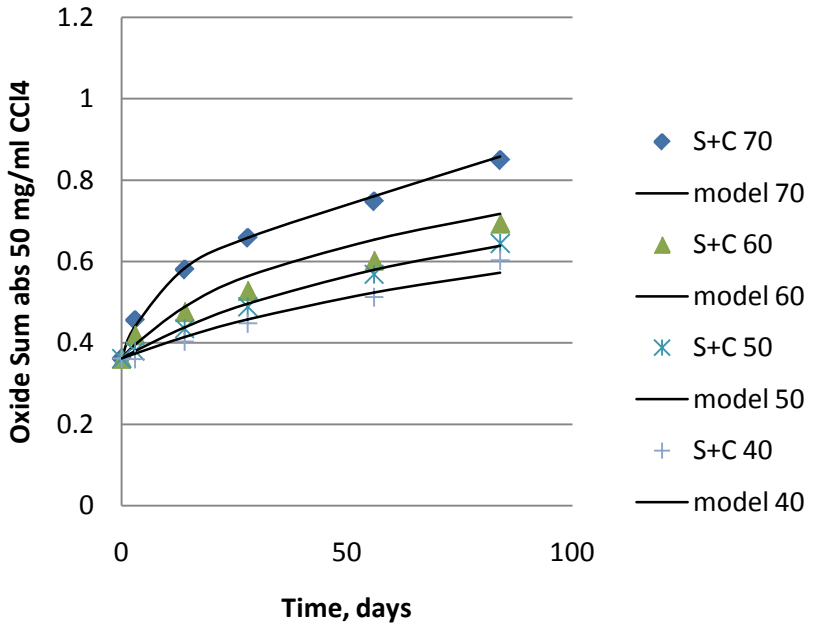

Figure 38. Graph. AAC-1 oxidation at .74 atmospheres compared to model fits at 4 temperatures.

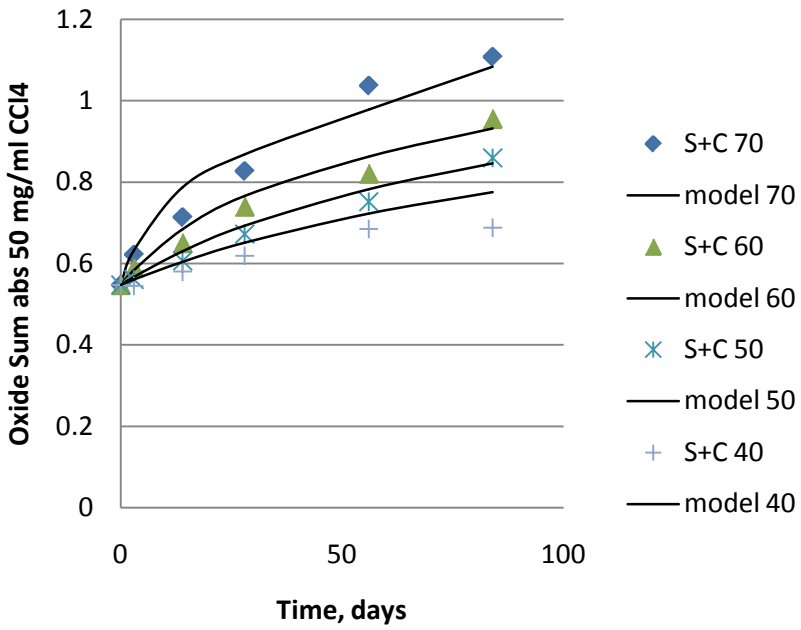

Figure 39. Graph. AAD-1 oxidation at .74 atmospheres compared to model fits at 4 temperatures.

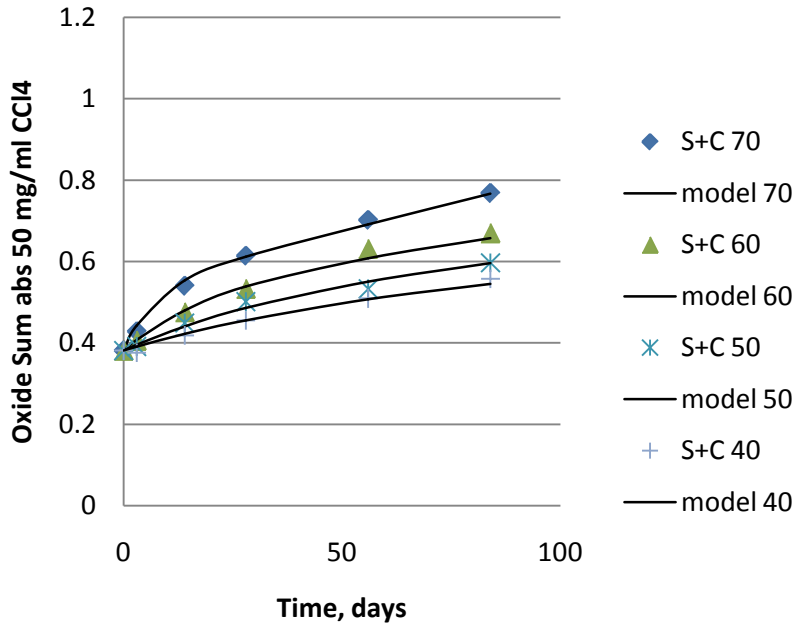

Figure 40. Graph. AAD-1 oxidation at .74 atmospheres compared to model fits at 4 temperatures.

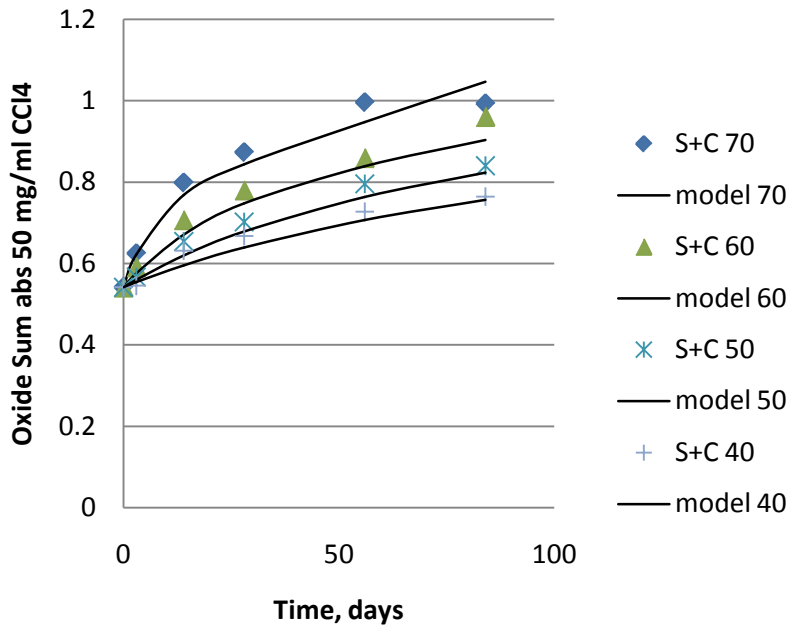

Figure 41. Graph. ABD-1 oxidation at .74 atmospheres compared to model fits at 4 temperatures.

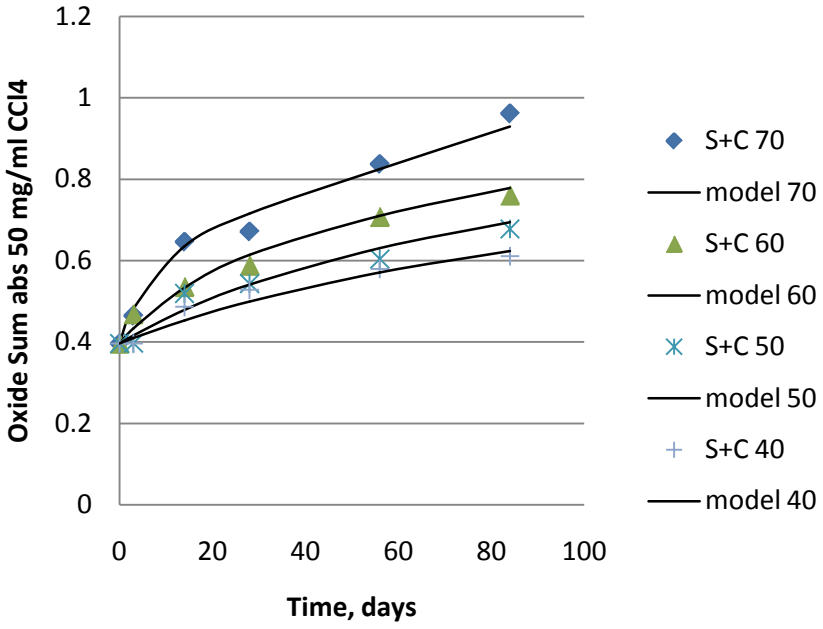

Figure 42. Graph. ALF oxidation at .74 atmospheres compared to model fits at 4 temperatures.

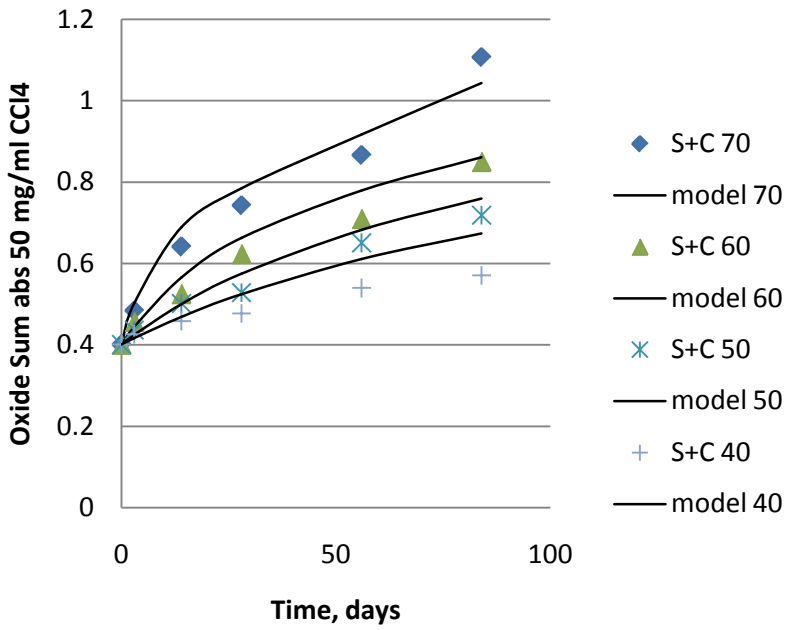

Figure 43. Graph. ARC-1 oxidation at .74 atmospheres compared to model fits at 4 temperatures.

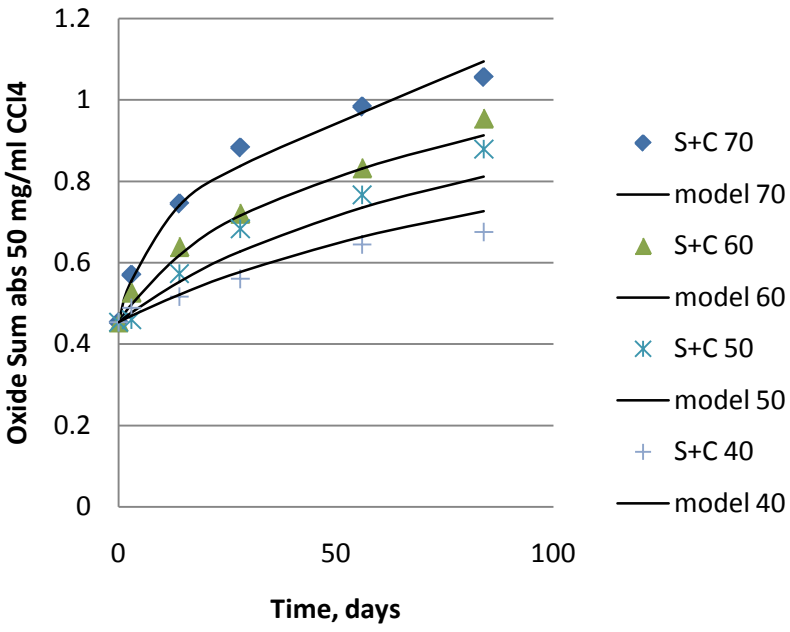

Figure 44. Graph. ARC-2 oxidation at .74 atmospheres compared to model fits at 4 temperatures.

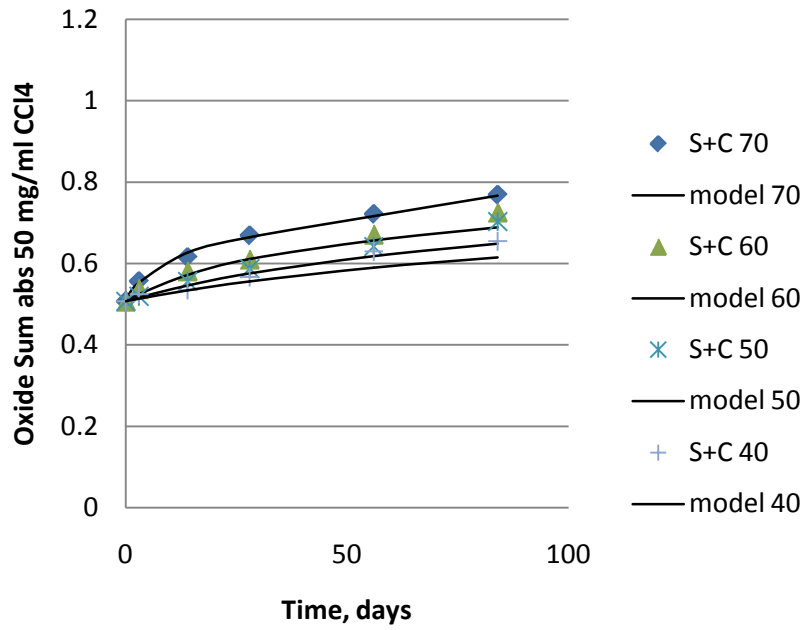

Figure 45. Graph. AZ1-1 oxidation at .74 atmospheres compared to model \fits at 4 temperatures.

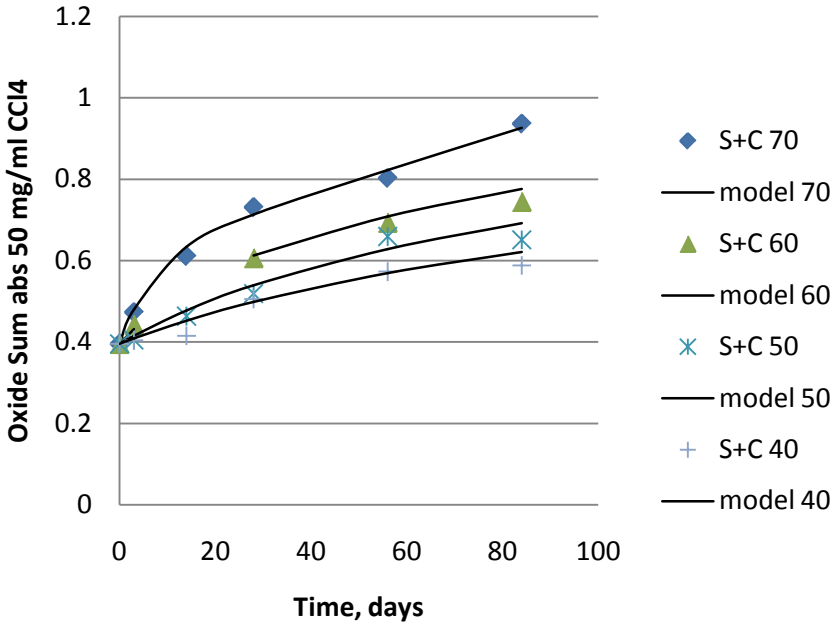

Figure 46. Graph. MCR oxidation at .74 atmospheres compared to model fits at 4 temperatures.

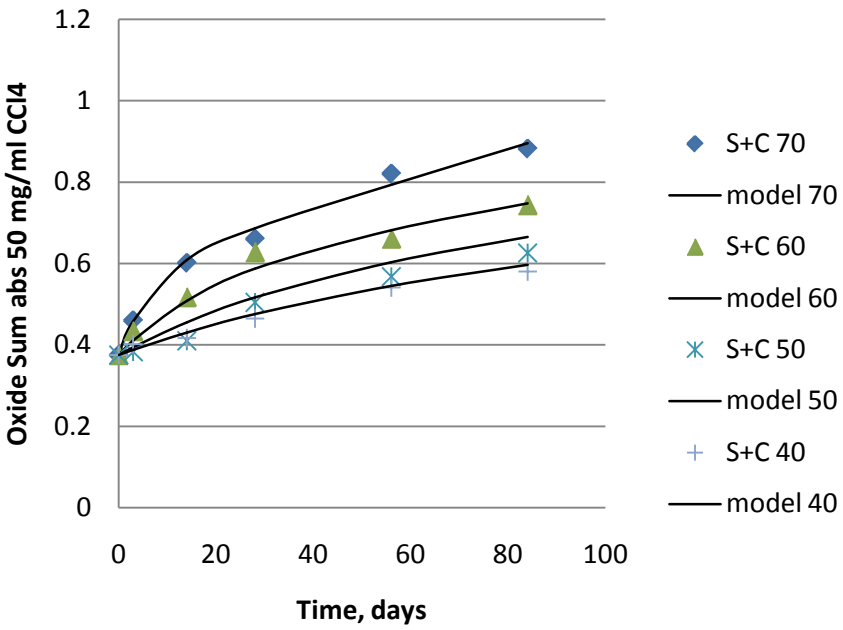

Figure 47. Graph. MN1-3 oxidation at .74 atmospheres compared to model fits at 4 temperatures.

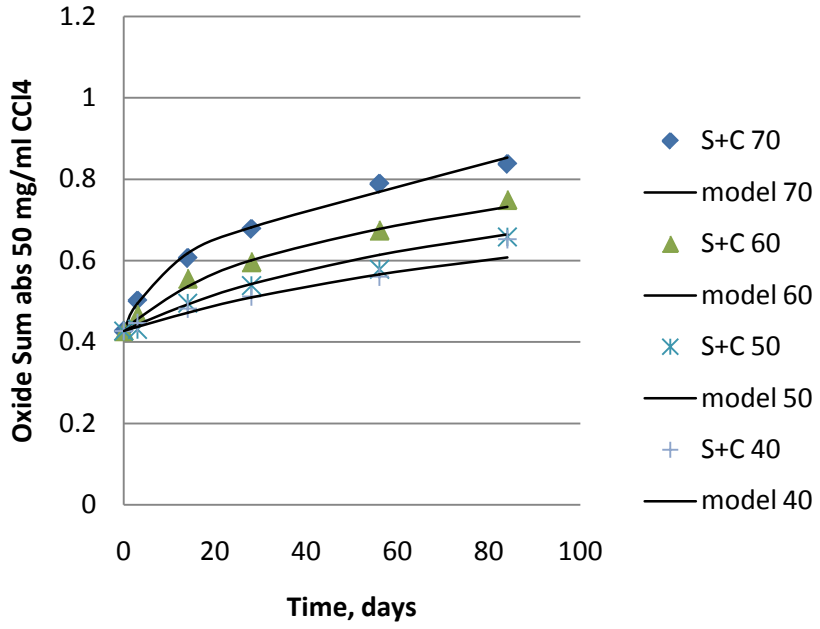

Figure 48. Graph. MN1-4 oxidation at .74 atmospheres compared to model fits at 4 temperatures.

The reactive material for each binder, shown in table 13, is assumed to not change with temperature and is constant through the fitting procedure for each binder. This constant has units of absorbance as determined from a 50 mg/ml solution of asphalt in carbon tetrachloride in a 1 mm path length sodium chloride transmission cell. Other IR measurement methods would require the appropriate corrections.

Table 13. Initial reactive material in the fast reaction.

Binder	$C_{fast,0}$ Absorbance Units
AAB-1	0.250
AAC-1	0.229
AAD-1	0.248
AAM-1	0.178
ABD-1	0.233
ALF	0.246
ARC-1	0.297
ARC-2	0.296
AZ1-1	0.117
MCR	0.245
MN1-3	0.241
MN1-4	0.197

The correlation coefficient (Pearson's R^2) of these fits are summarized in table 14.

Table 14. Isothermal fits correlation coefficients.

Binder	40°C	50°C	60°C	70°C
AAB-1	0.996	0.983	0.982	0.985
AAC-1	0.999	0.981	0.997	0.980
AAD-1	0.963	0.971	0.982	0.968
AAM-1	0.997	0.995	0.983	0.995
ABD-1	0.964	0.994	0.990	0.968
ALF	0.987	0.986	0.960	0.952
ARC-1	0.973	0.978	0.987	0.988
ARC-2	0.988	0.992	0.990	0.987
AZ1-1	0.997	0.985	0.989	0.984
MCR	0.994	0.998	0.960	0.954
MN1-3	0.992	0.980	0.982	0.989
MN1-4	0.994	0.992	0.981	0.967

The rate constants in isothermal aging are temperature dependent and are described by the Arrhenius equation. The slow and fast reaction paths have different temperature dependency parameters (equations 18-19).

$$k_1^{'} = A_1 e^{\frac{-E_{a,1}}{RT}} \tag{18}$$

$$k_2^{'} = A_2 e^{\frac{-E_{a,2}}{RT}} \tag{19}$$

The Arrhenius parameters, pre-exponential constants, $A_{1\&2}$ and activation energies divided by the gas constant, $\frac{E_a}{R}$, were fit using the usual linearization of the natural log of the rate constant plotted against the inverse absolute temperature (equation 15). These relationships used with equations (12) and (13) allow us to calculate the rate of reaction given any temperature history within the range of this mechanism. Equation (14) is the special isothermal solution to equations (12) and (13) and only applies to the isothermal case. More work is required to determine the limits of this temperature range as this information is needed to evaluate acceleration possibilities in the laboratory. Figure 49 shows the Arrhenius plot for the fast reaction and figure 50 shows the Arrhenius plot for the slow reaction. These apply to all the binders studied.

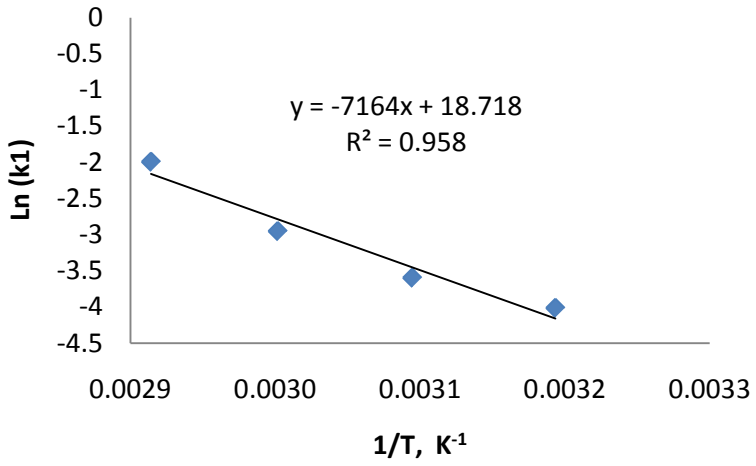

Figure 49. Graph. Arrhenius plot for the fast reaction.

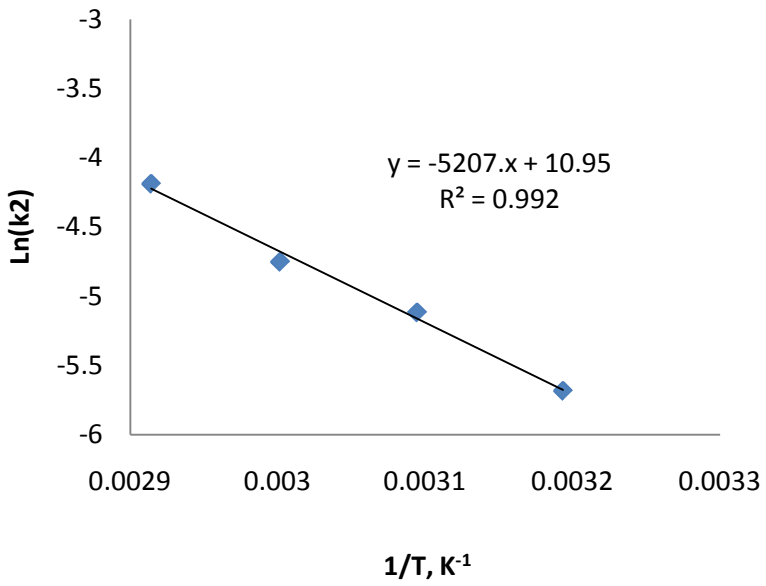

Figure 50. Graph. Arrhenius plot for the slow reaction.

Several more binders were aged and fit using the results from the initial study of twelve binders (table 15). Only the reactive material was adjusted to fit the 70°C data in the table below.

Table 15. Kinetic oxidation model fits of several asphalt binders.

70°C Asphalt Binder Oxidation Summary		k1	k2
		0.136	0.0152
	P0	RM	R^2
SHRP Binders			
AAB-1	0.388	0.250	0.996
AAC-1	0.362	0.229	0.999
AAD-1	0.547	0.248	0.963
AAM-1	0.381	0.178	0.997
ABD-1	0.542	0.233	0.964
AAK-1 (tank)	0.440	0.311	0.983
AAK-1 (RTFO)	0.428	0.292	0.974
AAK-1 (tank)	0.441	0.308	0.991
ALF Binders			
ALF Base	0.397	0.246	0.987
ALF-6281	0.554	0.200	0.985
ALF-6286 TB-CRM	0.695	0.246	0.993
ALF B-6289 (Elvaloy)	0.519	0.246	0.998
ALF B-6295 (SBS-LG)	0.408	0.246	0.994
Arizona Binders			
AZ1-1	0.513	0.117	0.997
AZ1-2	0.451	0.200	0.995
AZ1-3	0.509	0.217	0.987
AZ1-4	0.501	0.248	0.994
Minnesota Binders			
MN1-2	0.407	0.225	0.975
MN1-3	0.375	0.241	0.992
MN1-4	0.427	0.197	0.994
MN1-5	0.475	0.244	0.946
Asphalt Research Consortium			
ARC-1	0.401	0.297	0.973
ARC-2	0.454	0.296	0.987
Other Binders			
Manitoba RTFO	0.396	0.245	0.994
Manitoba Tank	0.343	0.303	0.991
Maya	0.371	0.262	0.971

Table 15. Kinetic oxidation model fits of several asphalt binders (continued).

		k1	k2
RAP Blends	60C	0.0522	0.00863
	P0	RM	R^2
AAC-1	0.436	0.198	0.990
AAC-1/15%MT RAP	0.512	0.169	0.986
AAC-1/50% MT RAP	0.709	0.144	0.989
MT RAP	0.972	0.050	0.911
AAC-1	0.436	0.198	0.990
AAC-1/15% SC RAP	0.499	0.161	0.971
AAC-1/50% SC RAP	0.710	0.143	0.967
SC RAP	0.971	0.050	0.911

SARA SEPARATIONS

The change in the SARA fractions after 12 weeks of aging are shown in figures 51-57:

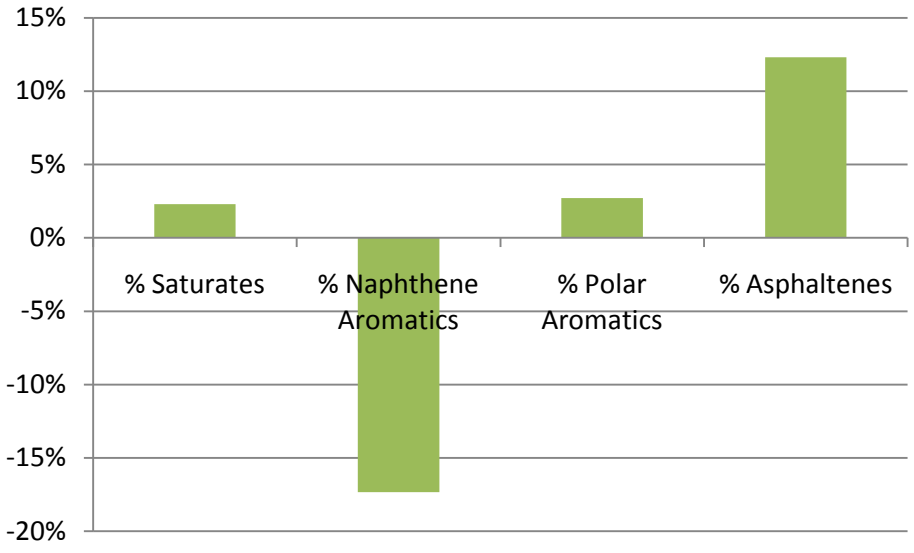

Figure 51. Graph. ALF SARA fraction changes after 12 weeks of oxidation at 70°C.

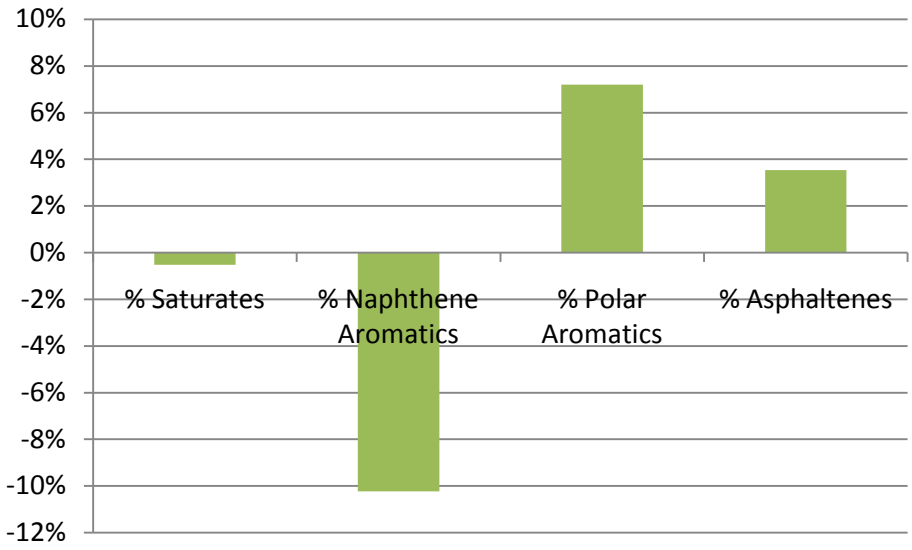

Figure 52. Graph. AZ1-1 SARA fraction changes after 12 weeks of oxidation at 70°C.

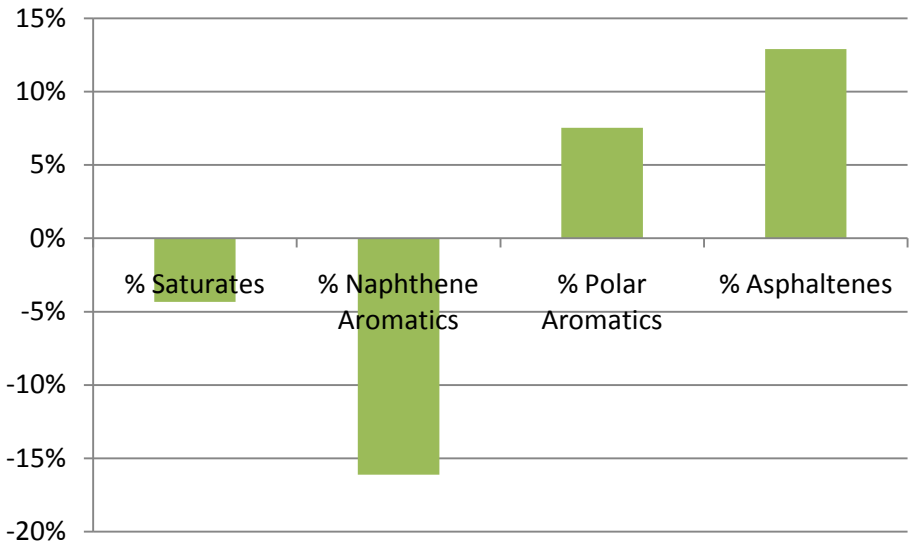

Figure 53. Graph. MCR SARA fraction changes after 12 weeks of oxidation at 70°C.

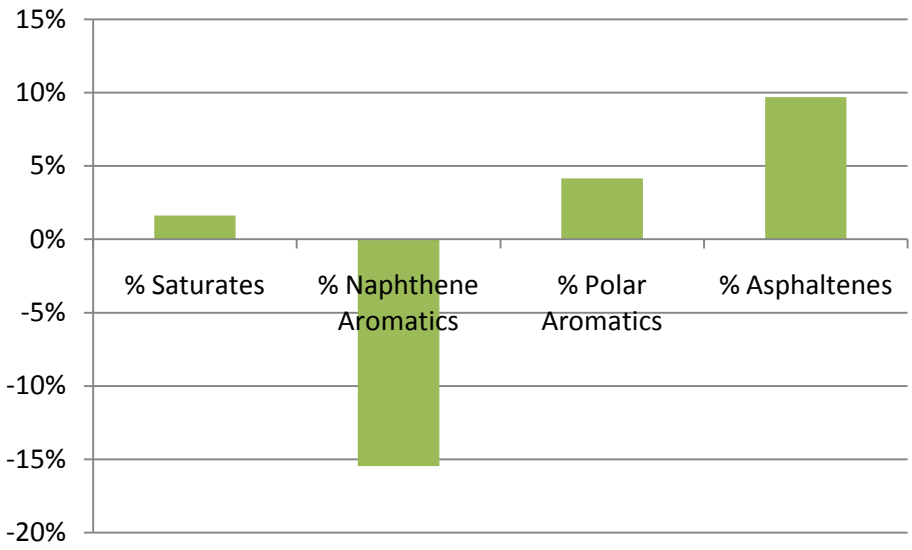

Figure 54. Graph. MN1-3 SARA fraction changes after 12 weeks of oxidation at 70°C.

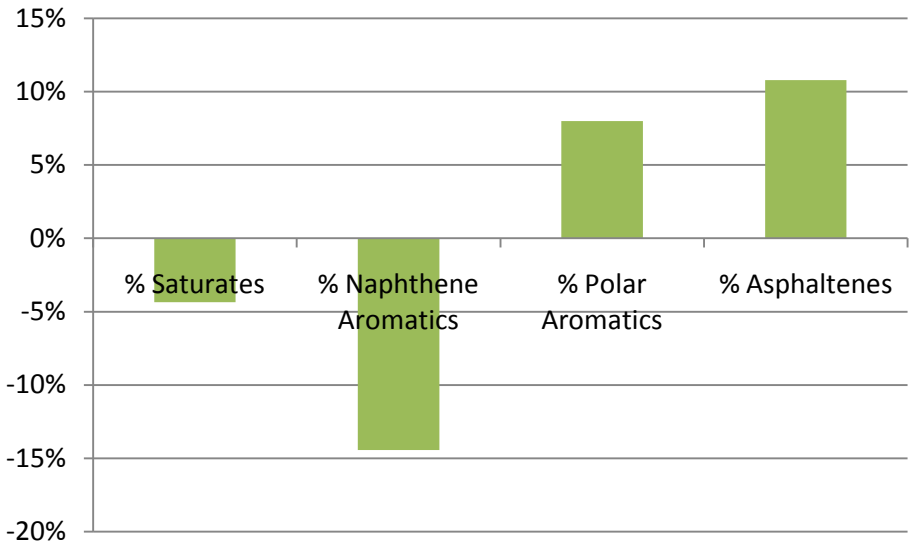

Figure 55. Graph. MN1-4 SARA fraction changes after 12 weeks of oxidation at 70°C.

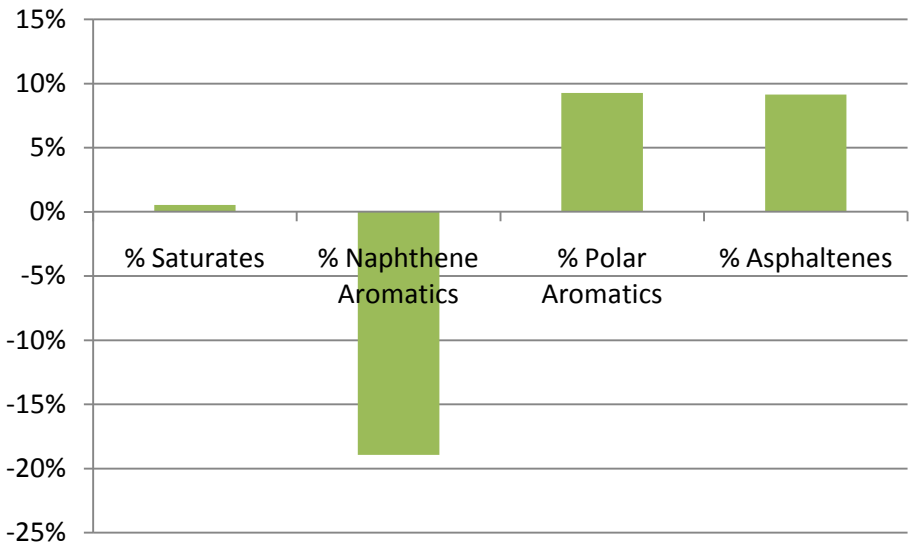

Figure 56. Graph. ARC-1 SARA fraction changes after 12 weeks of oxidation at 70°C.

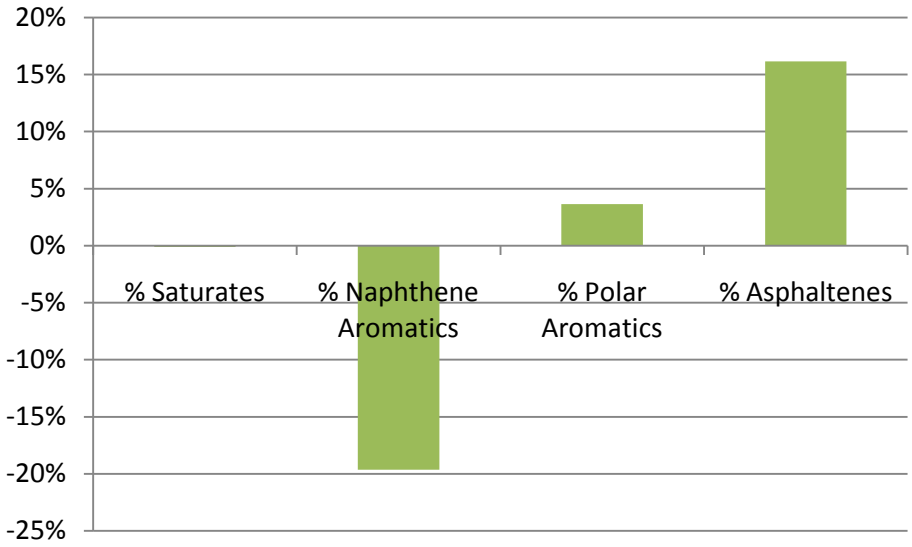

Figure 57. Graph. ARC-2 SARA fraction changes after 12 weeks of oxidation at 70°C.

The data presents a consistent pattern of decreasing naphthene aromatics and increasing polar aromatics and asphaltenes over the course of oxidation. The naphthene aromatics mass fractions in the time zero material correlate well with the reactive material determinations from the kinetic model fits (figure 58).

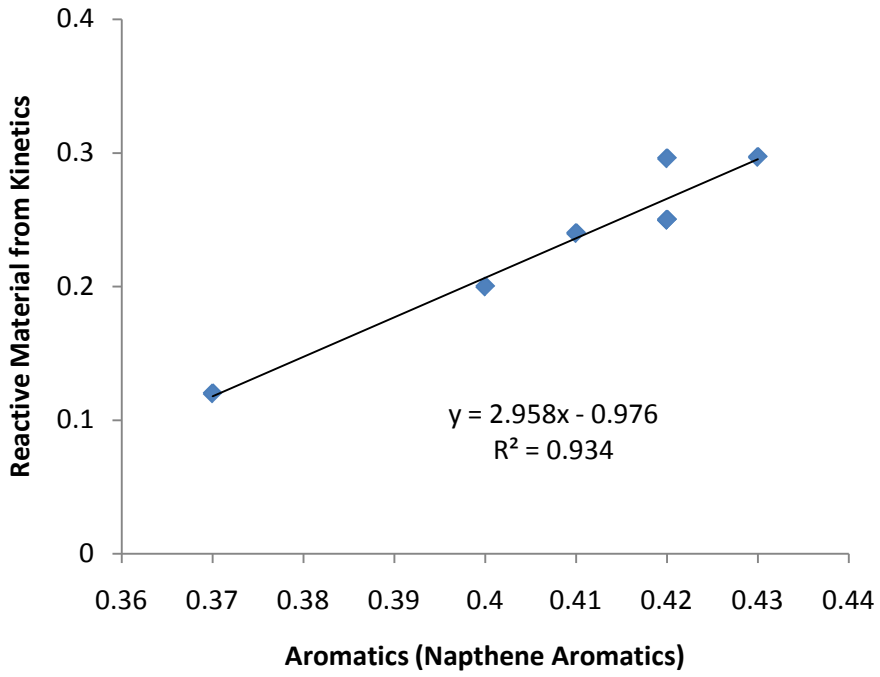

Figure 58. Graph. Naphthene aromatics correlated against reactive material.

The changes in crossover parameters also correlate well with the naphthene aromatic content in the starting material (figures 59, 60).

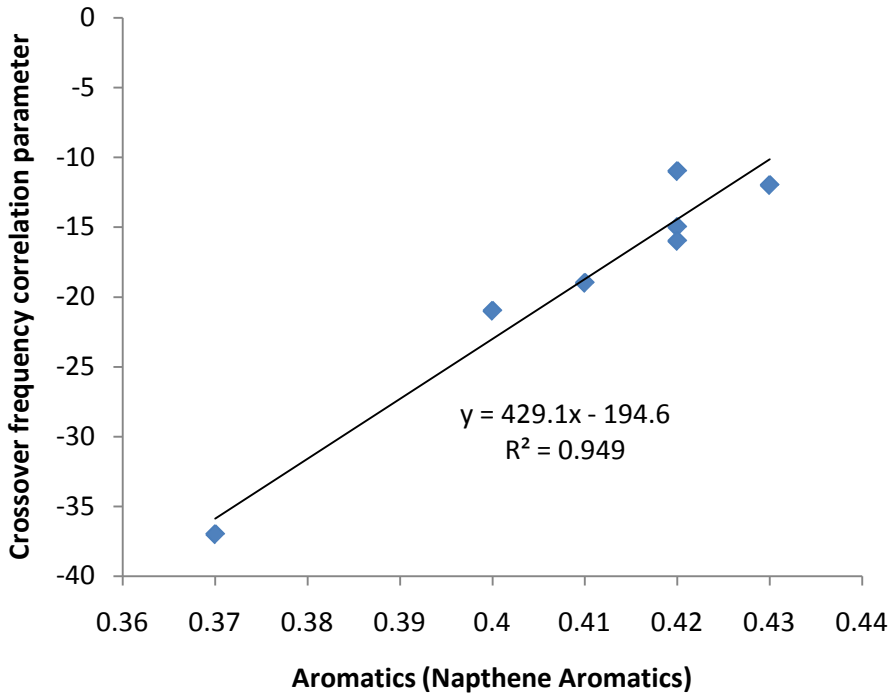

Figure 59. Graph. Naphthene aromatics correlated against reactive crossover frequency correlation parameter.

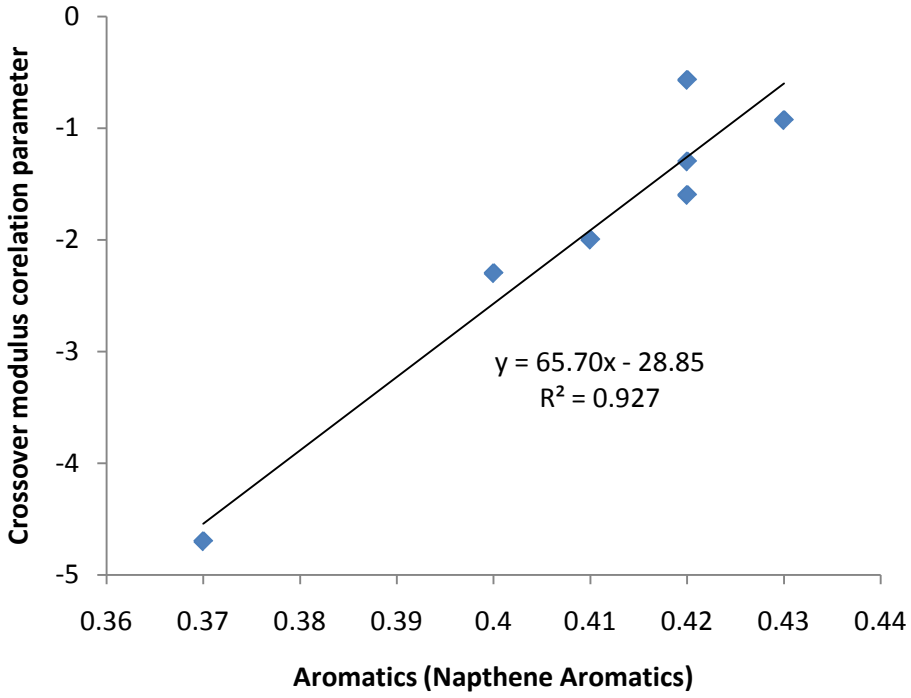

Figure 60. Graph. Naphthene aromatics correlated against reactive crossover modulus correlation parameter.

Several of the binder time series samples were also separated into SARA fractions to investigate the shape of the napthene depletion over time. If both fast and slow reaction materials are contained in the napthene aromatics, then this reactant plot would resemble a horizontal reflection of the products curve obtained from IR oxide sums. (There would be no change after depletion of all the reactive material, usually in a few weeks under these conditions) Alternatively, a decaying exponential would represent reactive material depletion alone, and mirror the fast reaction. These plots are shown in figures 61-65.

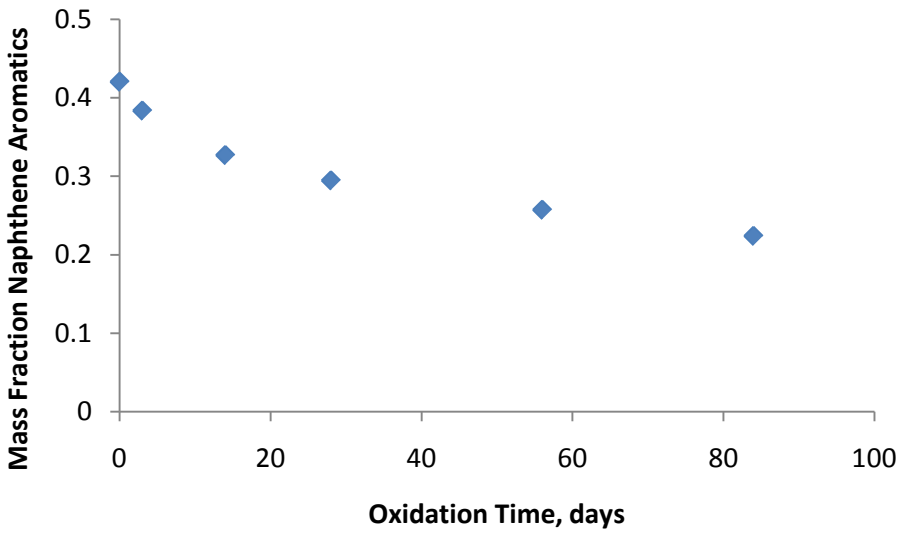

Figure 61. Graph. Naphthene aromatics consumption profile for binder ARC2.

The figure above suggests the naphthene aromatics contribute to both reaction paths.

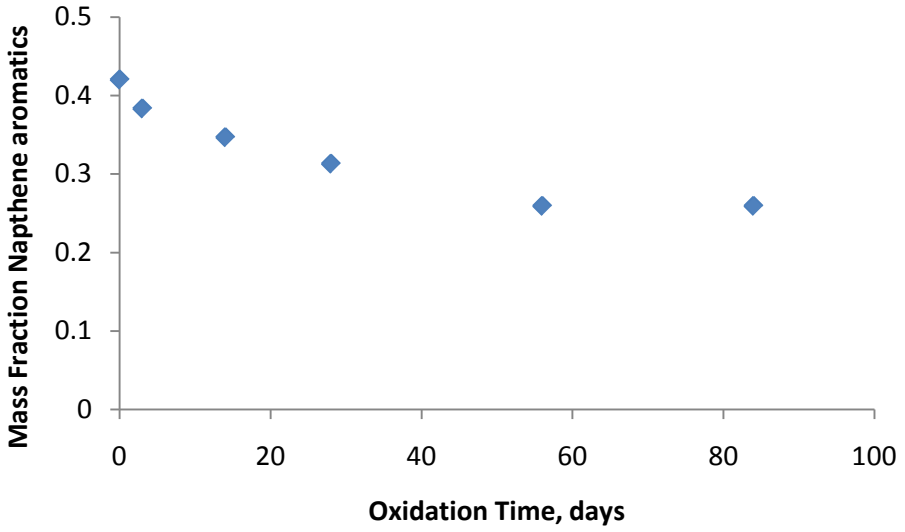

Figure 62. Graph. Naphthene aromatics consumption profile for binder MCR.

The figure above suggests the naphthene aromatics contribute to the fast path.

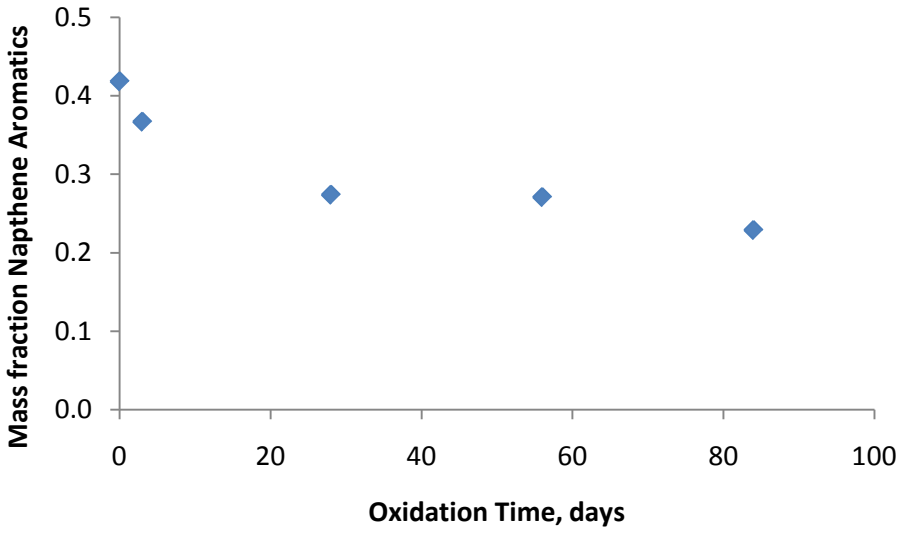

Figure 63. Graph. Naphthene aromatics consumption profile for binder ARC1.

The figure above suggests the naphthene aromatics contribute to both reaction paths.

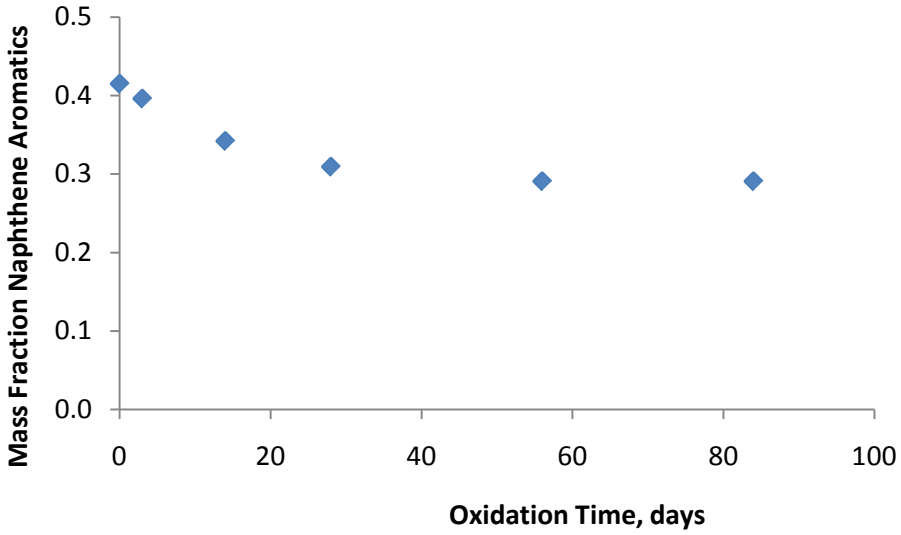

Figure 64. Graph. Naphthene aromatics consumption profile for binder MN1-3.

The figure above suggests the naphthene aromatics contribute to the fast path.

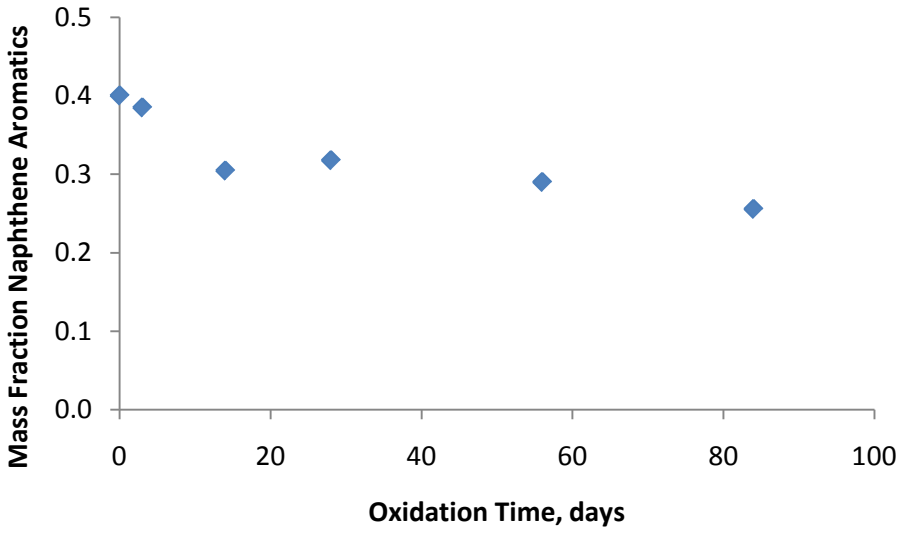

Figure 65. Graph. Naphthene aromatics consumption profile for binder MN1-4.

The figure above suggests the naphthene aromatics contribute to both paths.

This preliminary work suggests that very approximate kinetic expressions and resulting master-curve changes can be obtained from a simple SARA separation of the RTFO material. A chemical test that better targets the responsible chemical species types would produce more precise determinations but will require further study to validate this chemometric method and assess the suitability of the obtainable precision and accuracy for specification and rational design pavement performance modeling.

PRESSURE DEPENDENCY

The isothermal integrated rate equation derived for the low pressure aging analysis can be adapted by inserting a partial pressure oxygen term with and exponent for the oxygen concentration, yielding the following equation:

$$P = C_{fast,0}\left(1-\frac{k_2 P_{O_2}^n}{k_1 P_{O_2}^m}\right)\left(1-e^{-k_1 P_{O_2}^m t}\right)+k_2 P_{O_2}^n C_{fast,0} t + P_o \qquad (20)$$

The RITA (2010) data, described previously, was fit with the equation above, using the results from the ambient pressure study, by only changing the oxygen partial pressure exponents. These 4 SHRP binders were aged at 60 and 80°C at 20 atm air pressure in a PAV vessel. The best fit, using the .74 atmosphere fit constants for all other parameters, was an exponent of 1/3. A pressure exponent of ½ is almost as good. The RITA (2010) samples were aged at 2 temperatures, so we can test the consistency of the Arrhenius values at elevated pressure. The 0.74 atmosphere values appear to work well with a uniform pressure exponent for all 4 binders. Will the same exponent work with many binder sources when carbonyl and sulfoxide are used in the measurement of extent of reaction? The answer to that question remains to be seen until

additional work is done. However, determining a consistent pressure correction, contrary to the findings of previous investigators that monitored only carbonyl, would lead to a simple accelerated test whose results can be mapped to pavement conditions reliably. The fits of the 20 atmosphere air pressure oxidation aging with a 1/3 pressure exponent are shown in figures 66-73.

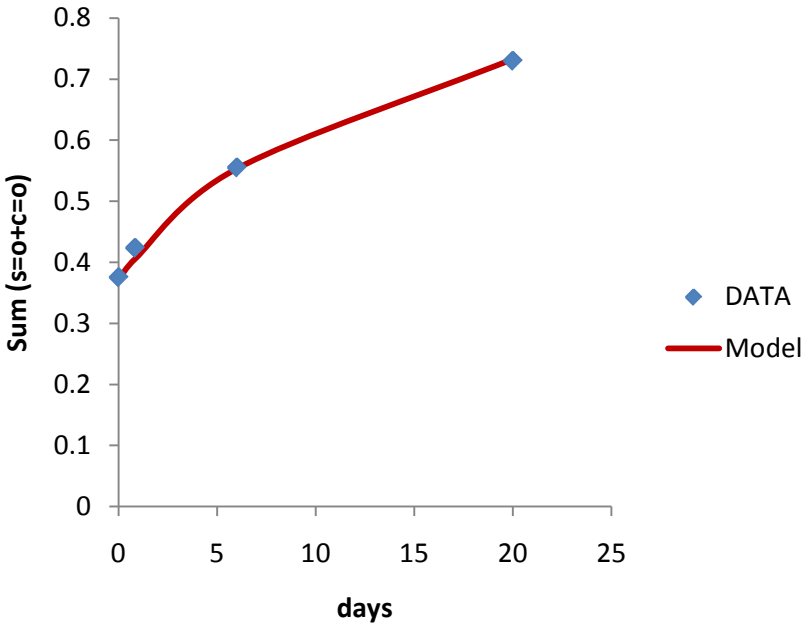

Figure 66. Graph. AAB-1 PAV prediction at 60°C.

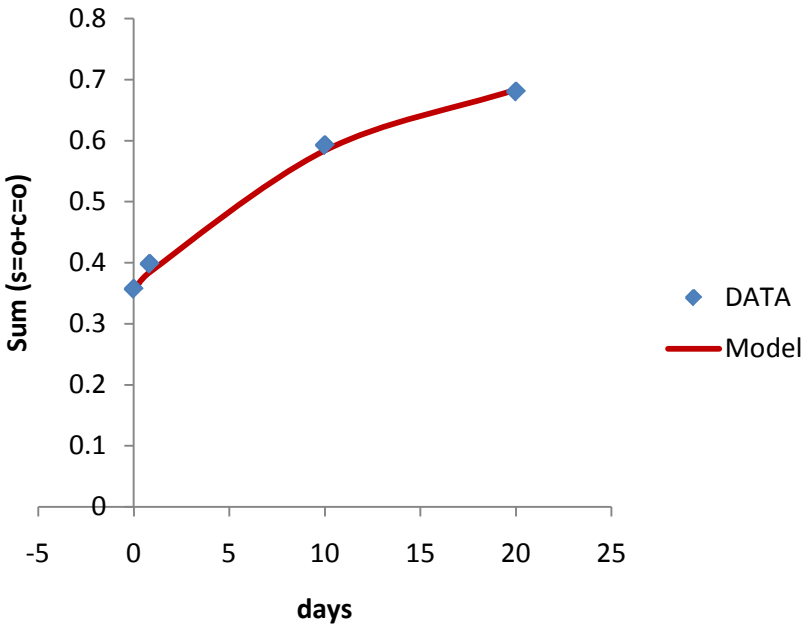

Figure 67. Graph. AAC-1 PAV prediction at 60°C.

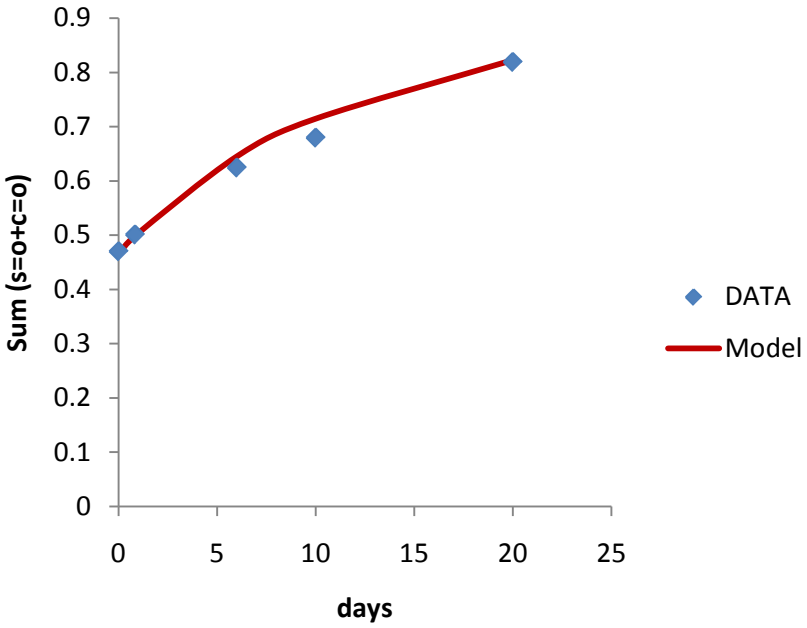

Figure 68. Graph. AAC-1 PAV prediction at 60°C.

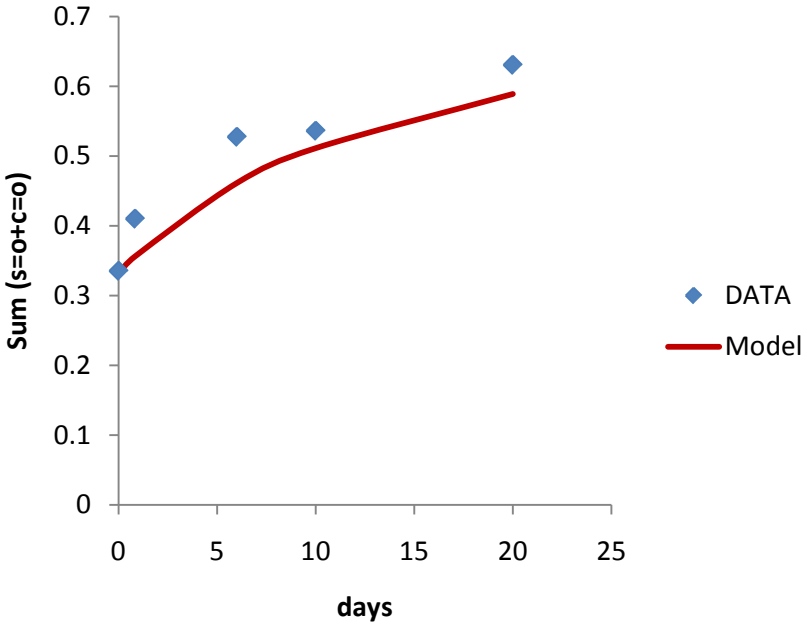

Figure 69. Graph. AAM-1 PAV prediction at 60°C.

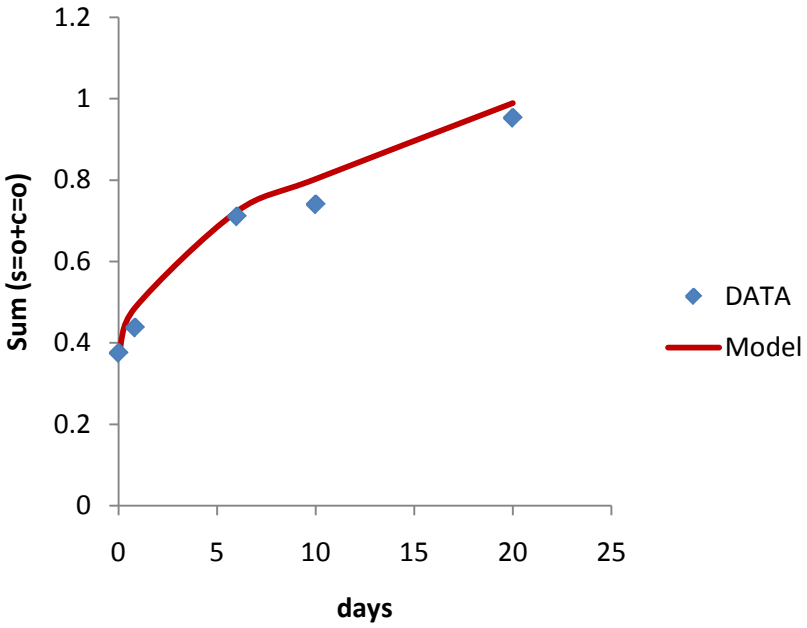

Figure 70. Graph. AAB-1 PAV prediction at 80°C.

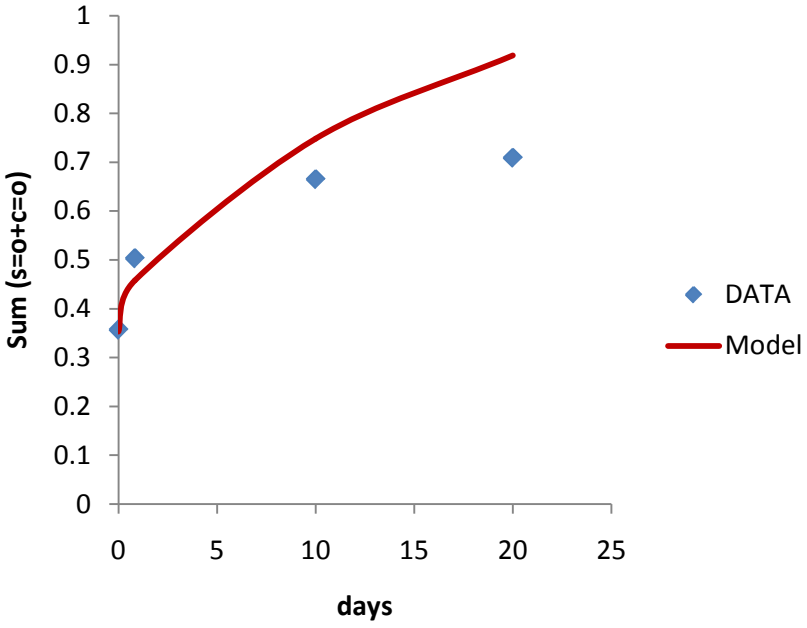

Figure 71. Graph. AAC-1 PAV prediction at 80°C.

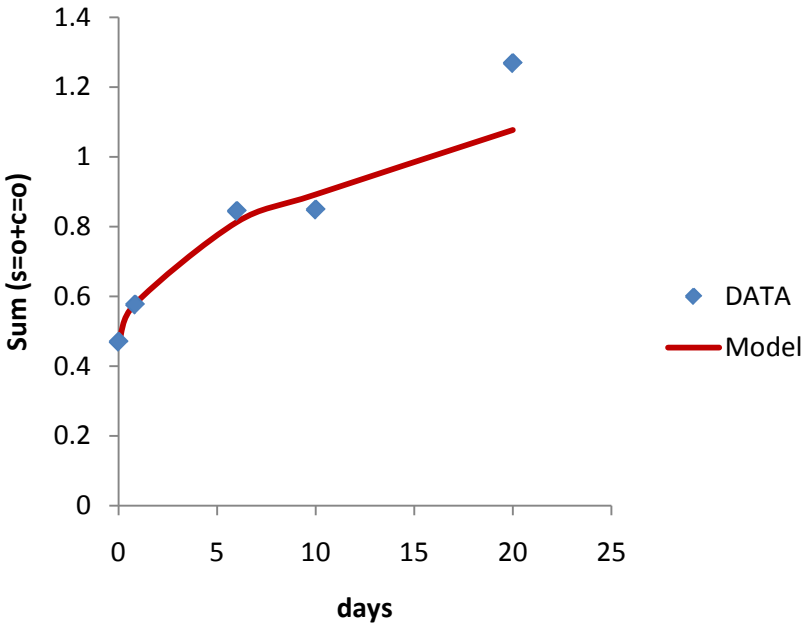

Figure 72. Graph. AAD-1 PAV prediction at 80°C.

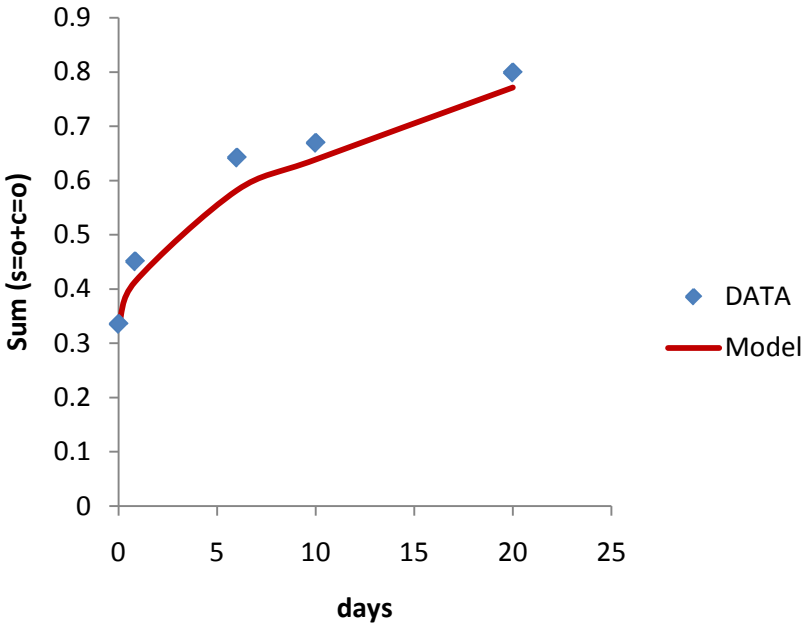

Figure 73. Graph. AAM-1 PAV prediction at 80°C.

RAP BLEND OXIDATION

The IR data from the RAP extract blend aging was fit to the oxidation model by only adjusting the reactive material and initial time zero IR responses. Pure SHRP binders AAC-1 and AAA-1 were used in the study, and two rap extracts, one from Manitoba and a second from South Carolina. Two blends were made and aged as well at 15% rap and 50% RAP from each virgin binder and RAP material. The reactive materials for the pure binder and pure RAP extract samples were obtained by fitting the model. The reactive materials for the blends were also obtained by fitting the model to the aging data, and compared to using a mass fraction weighted average of reactive material in the model to make a prediction.

$$RM_{Blend} = (1 - X_{Rap})RM_{Binder} + X_{Rap}RM_{Rap} \quad (21)$$

where:
RM_{Blend} = reactive material in the blend
RM_{Binder} = reactive material in the binder
RM_{Rap} = reactive material in the rap
X_{Rap} = mass fraction rap
$(1\text{-}X_{Rap})$ = mass fraction binder

The mass fraction weighted average kinetic behavior prediction compared well with the measured behavior. A summary of the IR responses is shown in tables 16-27. A summary of the fits are also shown in tables 16-27. The kinetic parameters used in the fits are summarized in tables 28-30.

Table 16. AAA-1 oxidation kinetics results compared to mixing model.

Aging Days	wn 1693	wn 1034	sum	model
0	0.144	0.303	0.447	0.447
2	0.152	0.339	0.491	0.463
14	0.165	0.376	0.541	0.535
28	0.177	0.406	0.582	0.587
56	0.198	0.452	0.651	0.649
84	0.214	0.478	0.692	0.692

Table 17. AAC-1 oxidation kinetics results compared to mixing model.

Aging Days	wn 1693	wn 1034	sum	model
0	0.155	0.281	0.436	0.436
2	0.159	0.312	0.471	0.455
14	0.191	0.346	0.537	0.546
28	0.228	0.374	0.602	0.611
56	0.287	0.401	0.688	0.688
84	0.360	0.406	0.766	0.743

Table 18. MT-RAP oxidation kinetics results compared to mixing model.

Aging Days	wn 1693	wn 1034	sum	model
0	0.360	0.586	0.945	0.945
4	0.379	0.598	0.977	0.961
14	0.390	0.616	1.007	0.991
28	0.392	0.619	1.011	1.018
56	0.422	0.642	1.064	1.051
84	0.418	0.655	1.074	1.074

Table 19. SC-RAP oxidation kinetics results compared to mixing model.

Aging Days	wn 1693	wn 1034	sum	model
0	0.382	0.590	0.972	0.972
4	0.382	0.610	0.992	0.981
14	0.391	0.601	0.991	0.999
28	0.387	0.611	0.997	1.016
56	0.409	0.626	1.035	1.035
84	0.414	0.652	1.067	1.049

Table 20. AAC-1-15% MT oxidation kinetics results compared to mixing model.

Aging Days	wn 1693	wn 1034	sum	blend prediction	model
0	0.196	0.316	0.512	0.512	0.512
2	0.202	0.324	0.526	0.530	0.529
14	0.235	0.377	0.612	0.613	0.606
28	0.259	0.399	0.658	0.672	0.661
56	0.297	0.423	0.720	0.743	0.727
84	0.323	0.438	0.761	0.793	0.774

Table 21. AAC-1-50% MT oxidation kinetics results compared to mixing model.

Aging Days	wn 1693	wn 1034	sum	blend prediction	model
0	0.293	0.416	0.709	0.709	0.709
2	0.300	0.422	0.723	0.723	0.723
14	0.327	0.474	0.801	0.787	0.789
28	0.347	0.489	0.836	0.833	0.836
56	0.377	0.515	0.892	0.888	0.893
84	0.400	0.540	0.939	0.927	0.933

Table 22. AAA-1-15% MT oxidation kinetics results compared to mixing model.

Aging Days	wn 1693	wn 1034	sum	blend prediction	model
0	0.189	0.363	0.552	0.552	0.552
2	0.193	0.378	0.570	0.567	0.565
14	0.209	0.415	0.625	0.633	0.624
28	0.217	0.436	0.654	0.681	0.667
56	0.243	0.475	0.718	0.739	0.718
84	0.257	0.504	0.760	0.779	0.754

Table 23. AAA-1-50% MT oxidation kinetics results compared to mixing model.

Aging Days	wn 1693	wn 1034	sum	blend prediction	model
0	0.266	0.454	0.719	0.719	0.719
2	0.264	0.456	0.720	0.732	0.728
14	0.278	0.471	0.749	0.786	0.767
28	0.292	0.498	0.789	0.826	0.796
56	0.315	0.514	0.829	0.873	0.829
84	0.334	0.548	0.882	0.906	0.853

Table 24. AAC-1-15% SC oxidation kinetics results compared to mixing model.

Aging Days	wn 1693	wn 1034	sum	blend pred	model
0	0.177	0.322	0.499	0.499	0.499
2	0.205	0.346	0.551	0.516	0.515
14	0.227	0.377	0.604	0.596	0.588
28	0.246	0.396	0.641	0.654	0.641
56	0.286	0.427	0.713	0.723	0.704
84	0.308	0.435	0.743	0.772	0.749

Table 25. AAC-1-50% SC oxidation kinetics results compared to mixing model.

Aging Days	wn 1693	wn 1034	sum	blend pred	model
0	0.276	0.433	0.710	0.710	0.710
2	0.302	0.458	0.760	0.722	0.724
14	0.316	0.485	0.801	0.778	0.789
28	0.329	0.504	0.833	0.819	0.836
56	0.355	0.519	0.874	0.868	0.892
84	0.382	0.549	0.931	0.902	0.931

Table 26. AAA-1-15% SC oxidation kinetics results compared to mixing model.

Aging Days	wn 1693	wn 1034	sum	blend pred	model
0	0.194	0.378	0.572	0.572	0.572
14	0.205	0.410	0.615	0.651	0.632
28	0.214	0.438	0.653	0.698	0.667
56	0.239	0.483	0.722	0.753	0.709
84	0.244	0.495	0.739	0.792	0.739

Table 27. AAA-1-50% SC oxidation kinetics results compared to mixing model.

Aging Days	wn 1693	wn 1034	sum	blend pred	model
0	0.272	0.487	0.759	0.759	0.759
2	0.278	0.488	0.766	0.769	0.767
14	0.270	0.492	0.762	0.816	0.802
28	0.291	0.524	0.815	0.850	0.828
56	0.311	0.552	0.863	0.891	0.859
84	0.321	0.560	0.881	0.920	0.881

Table 28. Oxidation kinetics parameters for pure materials.

	AAC-1	AAA-1	MT RAP	SC-RAP
k1	0.0522	0.0522	0.0522	0.0522
RM	0.199	0.158	0.083	0.050
P0	0.436	0.447	0.945	0.972
k2	0.00863	0.00863	0.00863	0.00863
r squared	0.990	0.951	0.951	0.911

Table 29. Oxidation kinetics parameters for AAC-1 RAP blends.

	AAC-1-15% MT RAP	AAC-1-50% MT-RAP	AAC-1-15% SC RAP	AAC-1-50% SC-RAP
k1	0.0522	0.0522	0.0522	0.0522
RM	0.169	0.144	0.161	0.143
P0	0.512	0.709	0.499	0.710
k2	0.00863	0.00863	0.00863	0.00863
r squared	0.986	0.989	0.971	0.968

Table 30. Oxidation kinetics parameters for AAA-1 RAP blends.

	AAA-1-15% MT RAP	AAA-1 -50% MT-RAP	AAA-1-15% SC RAP	AAA-1 -50% SC-RAP
k1	0.0522	0.0522	0.0522	0.0522
RM	0.130	0.086	0.108	0.079
P0	0.552	0.719	0.572	0.759
k2	0.00863	0.00863	0.00863	0.00863
r squared	0.951	0.951	0.951	0.951

The oxidation behavior of the pure materials and various blends are shown in figures 74-77, along with predicted behavior based upon a mass averaged amount of reactive material in the blends.

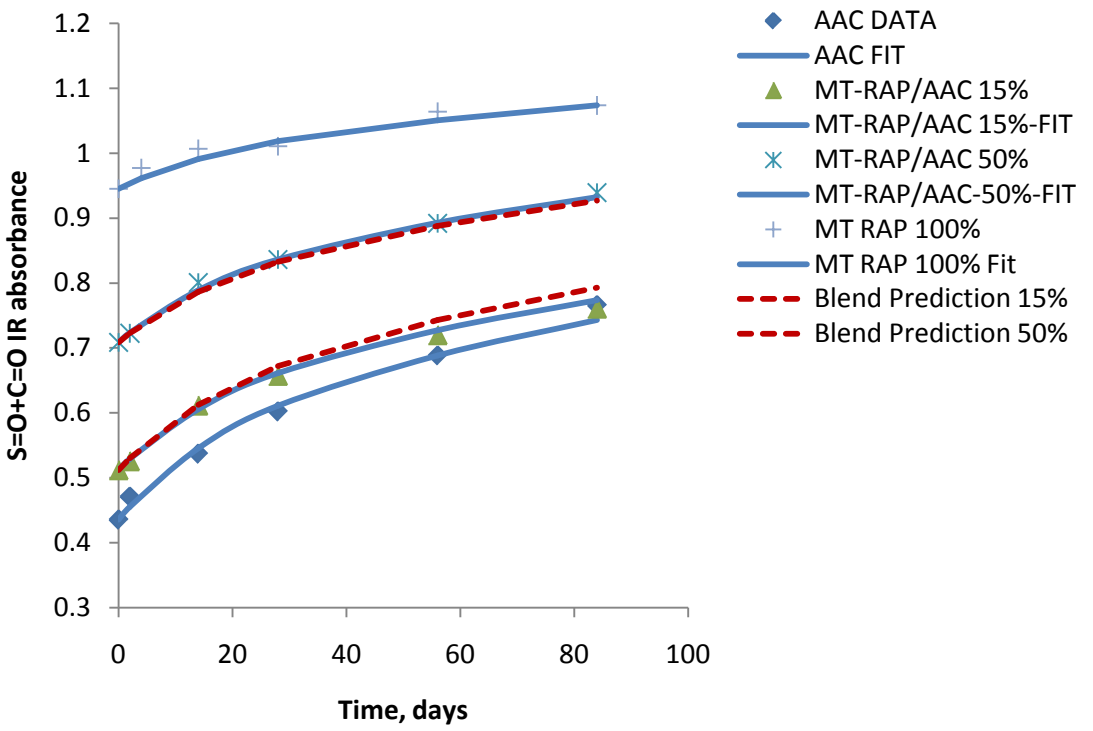

Figure 74. Graph. AAC-1 and Manitoba RAP blend oxidation.

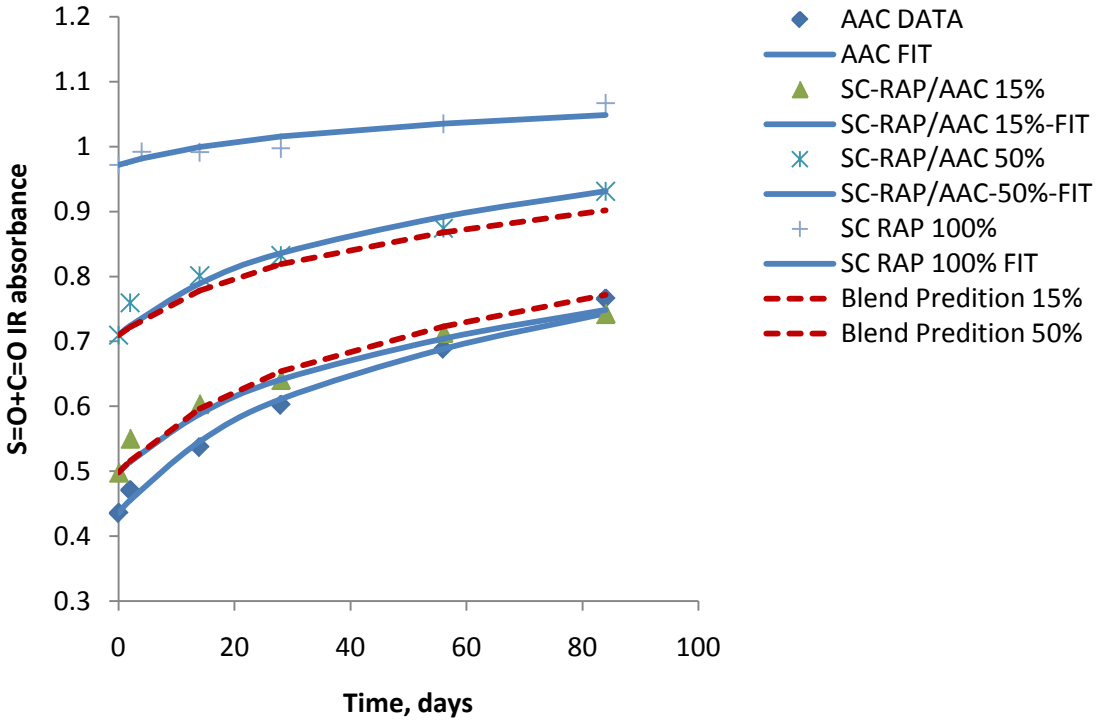

Figure 75. Graph. AAC-1 and South Carolina RAP blend oxidation.

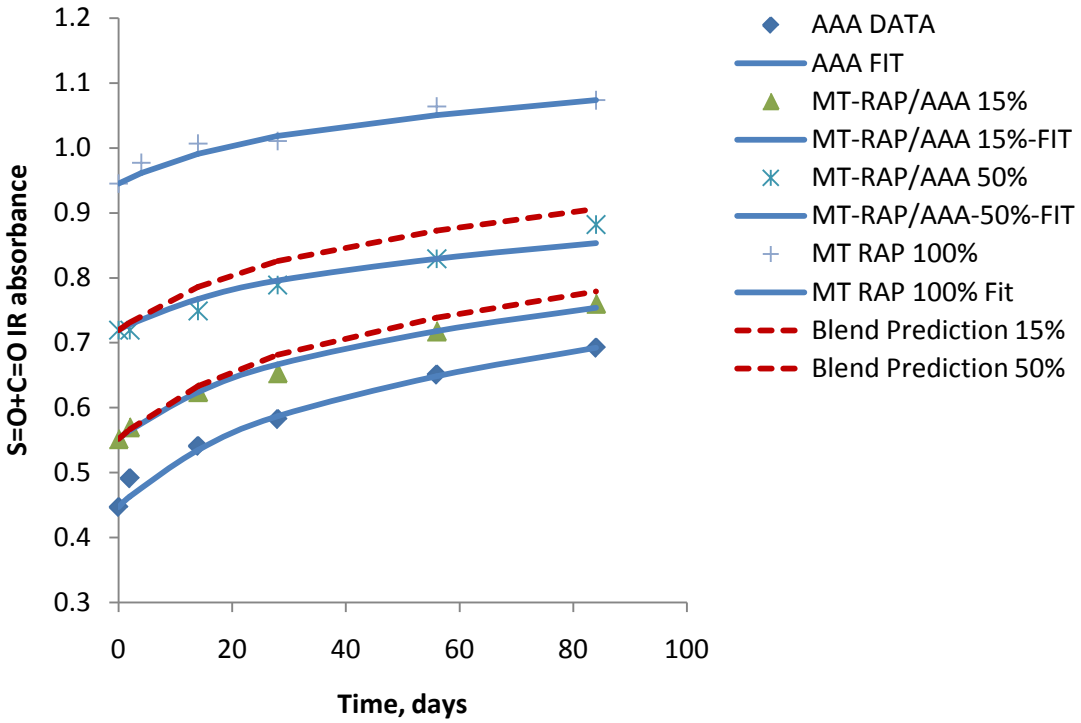

Figure 76. Graph. AAA-1 and Manitoba RAP blend oxidation.

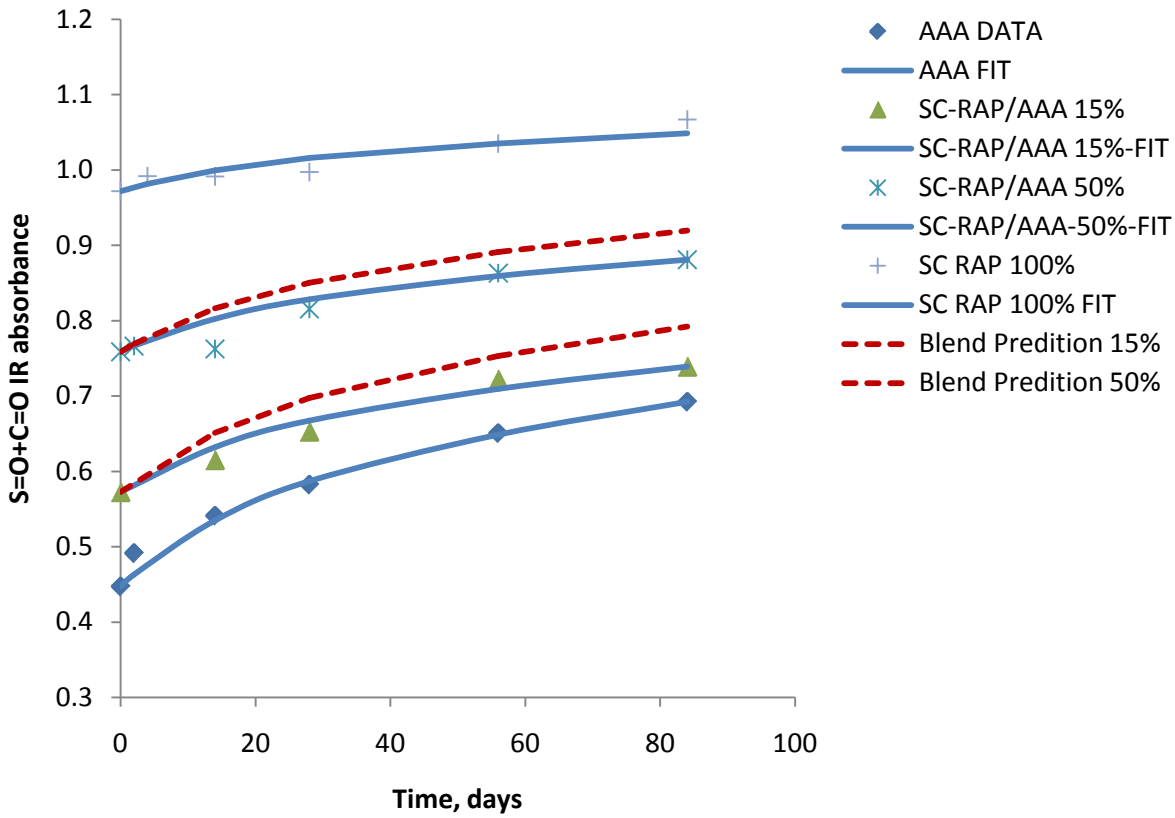

Figure 77. Graph. AAA-1 and South Carolina RAP blend oxidation.

ALF BINDER OXIDATION ANALYSIS

Several of the ALF binder materials are unique relative to the other binders investigated in that they are modified materials. Since these are our only examples of modified materials, it is instructive to examine their kinetic behaviors in a bit more detail. The kinetic model fits for these materials are presented again in table 31.

Table 31. Kinetic model fit parameters for ALF base binder and modified binders.

	P_0	RM	R^2
ALF Base	0.397	0.246	0.987
ALF-6281	0.554	0.200	0.985
ALF-6286 TB-CRM	0.695	0.246	0.993
ALF B-6289 (Elvaloy)	0.519	0.246	0.998
ALF B-6295 (SBS-LG)	0.408	0.246	0.994

The P_0 term represent the infrared response at time zero, and is higher for the modified materials because modifiers (SBS, Elvaloy, Rubber) contain these functional groups (carbonyl and sulfoxide) . The ALF-6281 is pre-oxidized and it contains a large amount of carbonyl plus sulfoxide and less reactive material (RM) because some was consumed during pre-treatment. All of the binders provide good fits with the same activation energies (rate constants are the same) and all have the same amount of reactive material as the unmodified binder within experimental precision with the exception of the pre-oxidized material.

ALF CORE OXIDATION ANALYSIS

The details of sampling and analysis of the sliced cores from the Turner Fairbank Aging Facility are presented in a separate technical white paper FP 19 Chemical Changes with Oxidative Aging. These materials present us with an opportunity to compare oxidation model predictions based upon laboratory measurements, and compare those to measurements obtained in the field. The oxidation model, in differential form (equations 22, 23) is

$$\frac{dP_1}{dt} = k_1^{'}\left[O_2\right]^n\left[C_{fast,0} - P_1\right] \tag{22}$$

and

$$\frac{dP_2}{dt} = k_2^{'}\left[P_1\right]\left[O_2\right]^m \tag{23}$$

The rate constants, $k_2^{'}$, $k_1^{'}$ are only constant at constant temperature, and field aging temperatures vary considerably over the seasons, and with pavement depth as well. Consequently, the rate constants in the model need to be replaced with the temperature dependence of the rate constant, the Arrhenius expression for each rate constant:

$$\frac{dP_1}{dt} = A_1 e^{\frac{-E_{a,1}}{RT}}\left[O_2\right]^n\left[C_{fast,0} - P_1\right] \tag{24}$$

$$\frac{dP_2}{dt} = A_2 e^{\frac{-E_{a,2}}{RT}}\left[P_1\right]\left[O_2\right]^m \tag{25}$$

$$P_T = [S=O] + [C=O] = P_1 + P_2 \tag{26}$$

In addition, the dissolved oxygen concentration term is also time variant, and would have to be known or accurately modeled for an accurate estimate of the severity of oxidation with depth over the life of the pavement. A temperature history (a function of time and depth) of the naturally aged lane was provided from Nelson Gibson at Turner-Fairbank over the eight year life of the cores. This history was obtained from model calculations based upon the MEPDG-EICM model (figure 78).

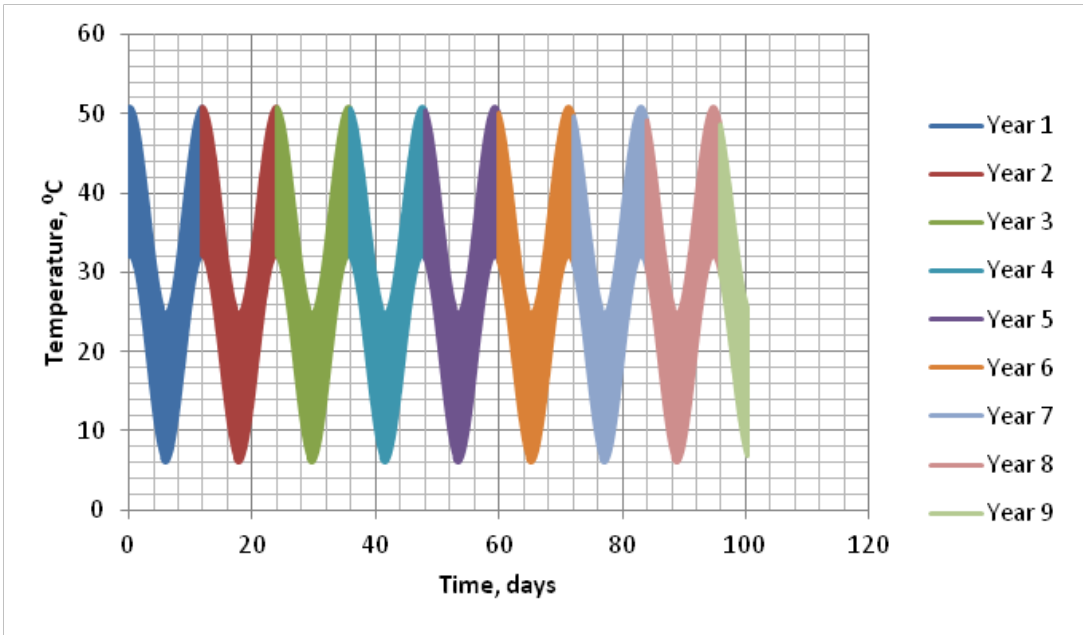

Figure 78. Graph. ALF thermal history model temperatures at ½ inch depth.

The differential form of the oxidation model was then numerically integrated to provide an estimate of aging if no significant depletion of atmospheric oxygen occurred. Also, this estimate does not account for a rate reduction due to mass transfer rates (permeation and diffusion) being lower than reaction rates. Computations made by simply integrating the rate model over time produce the maximum possible level of oxidation, and would require no oxygen reduction in the air voids with depth, and no significant restriction due to diffusion path lengths. This maximum case is obviously not likely, but in the absence of detailed oxygen partial pressure measurements, or a very good mathematical model, the computation is limited to this case. However, these results can be compared to the measured cored values, and an "average apparent partial pressure of oxygen" profile with depth can be computed. A fairly flat profile would suggest that mass transfer limitations are not significant vertically, but significant horizontally. This behavior could be the result of a very permeable air void network, and rather large (>100 micron) distances between fresh air supply conduits. The opposite behavior, a sharply decreasing partial pressure oxygen correction, could imply depletion of oxygen in the pores, and/or mass transfer limitations at both the permeation and molecular diffusion scales. As one might expect, the non-isothermal extent of oxidation as a function of time plots are similar to the isothermal laboratory plots. The major difference is that the non isothermal plots are modulated by seasonal and daily oscillations. These oscillations cannot be approximated by simple averages as the rate constant dependence is exponential. Numerical integration is simple and routine with modern computers, but a hand calculator estimate could be computed using an Arrhenius exponentially weighted average temperature. The authors do not see much advantage to this degradation in rigor. The results of this comparison, and a mass transfer correction factor, are presented in table 32. The mass transfer corrections are also plotted in figure 79 against depth from the pavement surface.

Table 32. Mass transfer free oxidation prediction compared to measured core values.

Sample	Description	CS_2 Solution FTIR Absorbance			Model Prediction		
		~1700 cm^{-1} C=O	~1032 cm^{-1} S=O	Net C=O plus S=O	Net C=O plus S=O	P_{o2} correction	Oxygen reduction % based on ½ pressure exponent
1	ALF L2S3 0/8"(1/2 midpoint)	0.4595	0.5859	0.6114	1.83	.334	88
2	ALF L2S3 5/8"(1" midpoint)	0.3742	0.5389	0.4821	1.71	.282	92
3	ALF L2S3 20/8"(3" midpoint)	0.2269	0.3650	0.1609	1.37	.117	98

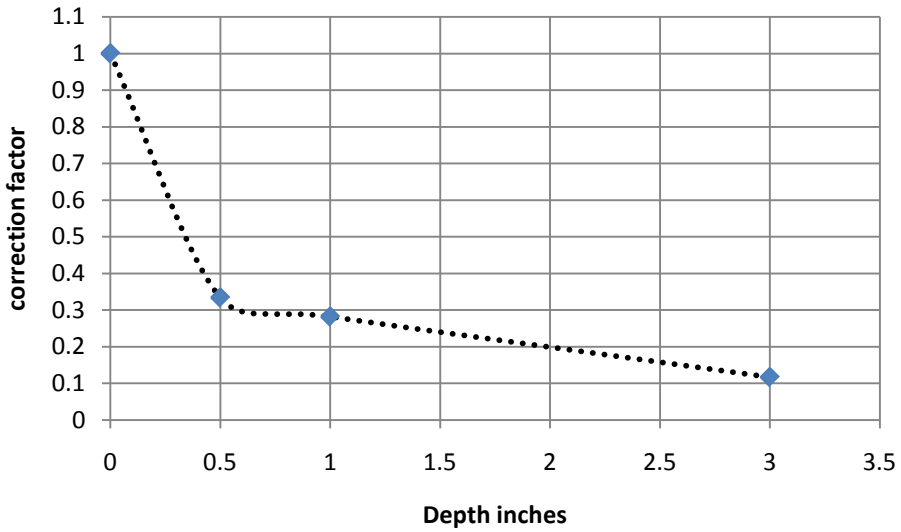

Figure 79. Graph. Mass transfer corrections with depth into core.

Are these results reasonable? If we consider a limiting case, a pavement with no connected pores, then we have oxygen movement into the core by molecular diffusion only. Under these conditions, information from our film thickness investigation can provide some idea of how fast the oxidation penetrates into the core, that is, at what point is all the oxygen consumed. This is, of course, a time dependant phenonmena. Let's revisit the film thickness aging data again in figure 80:

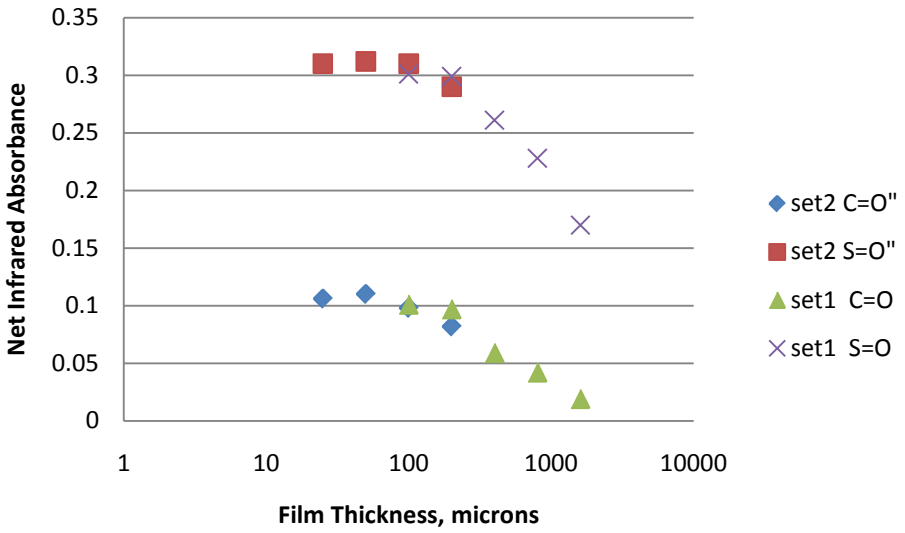

Figure 80. Graph. Oxidation extent compared at various film thicknesses.

These materials (SHRP binder AAK-1) were aged for 2 weeks at 70°C. Our measurements of the top core slice after 8 years in the field shows about the same amount of oxidation as our thin films for 84 days at 70°C. So, roughly, this is 1.3 years of aging. The figure above displays net absorbance, so no oxidation has occurred at depths greater than the zero value. This depth appears to be about 10000 microns, or only 0.4 inches. So, perhaps it is not unreasonable to see 88% reduction in dissolved oxygen below saturation at only ½ inch below the surface. Alternatively, a small error in the thermal model results can have huge effect on the resulting oxidation rate when integrated over very long periods of time. Precision thermal instrumentation would be preferred for this type of analysis. A small error of a few degrees in the thermal calculation could drastically change the prediction as well. Han et al. (2011) suggests that MEPDG model errors can exceed 20°C:

> "Although temperatures predicted with the EICM model satisfy pavement design needs in general, there have been some large errors when compared to measured pavement temperature. In one study of Ohio pavements, differences as high as 20°C were observed in the top 10 in. of pavement and there was an average difference of 10°C at the 30 in. depth (Liang et al. 2006). Similar results are seen in the studies on New Jersey pavements (Ahmed et al. 2005), for which an average difference of 15°C over the top 20 in. was calculated from their reported data."

A simple re-calculation for the ½ inch deep slice was performed by subtracting 5°C from the modeled temperatures provided by Gibson. This results in a 22% reduction in oxidation of over the 8 year life of the test, or, an increase of 22% in the correction factor. Because the partial pressure of oxygen effect roughly follows the square root power, the reduction in dissolved oxygen is only 83 %, compare to the alternative warmer estimate of 88%. So, it seems obvious, that in spite of possible errors in the temperature estimates, the data indicates that for this mix

design and this climate, a good deal of the oxygen in the pavement is consumed by oxidation as the air penetrates the pavement.

If the temperatures used in this prediction are sufficiently precise, then the rapid depletion of oxygen with depth suggests that mix design, particularly with regard to permeability and distance between connected oxygen arterials, has a huge effect of the aging of the material and is probably of greater concern than the reactivity of the binder.

OXIDATION AND RHEOLOGICAL CHANGES

The aged materials from the thin film 0.74 atmosphere oven tests DSR frequency sweep data were shifted to 0°C and fit with the Christensen Andersen (CA) model. These are shown for each binder as they age in figures 81-99.

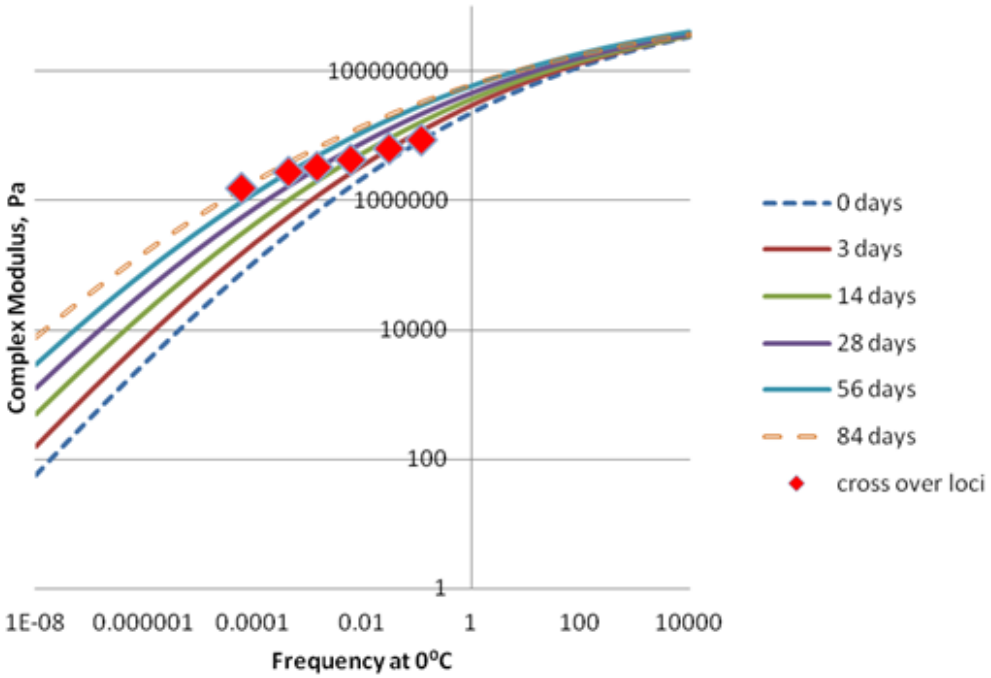

Figure 81. Graph. AAB-1 aging master curves 0°C reference, oxidized at 70°C.

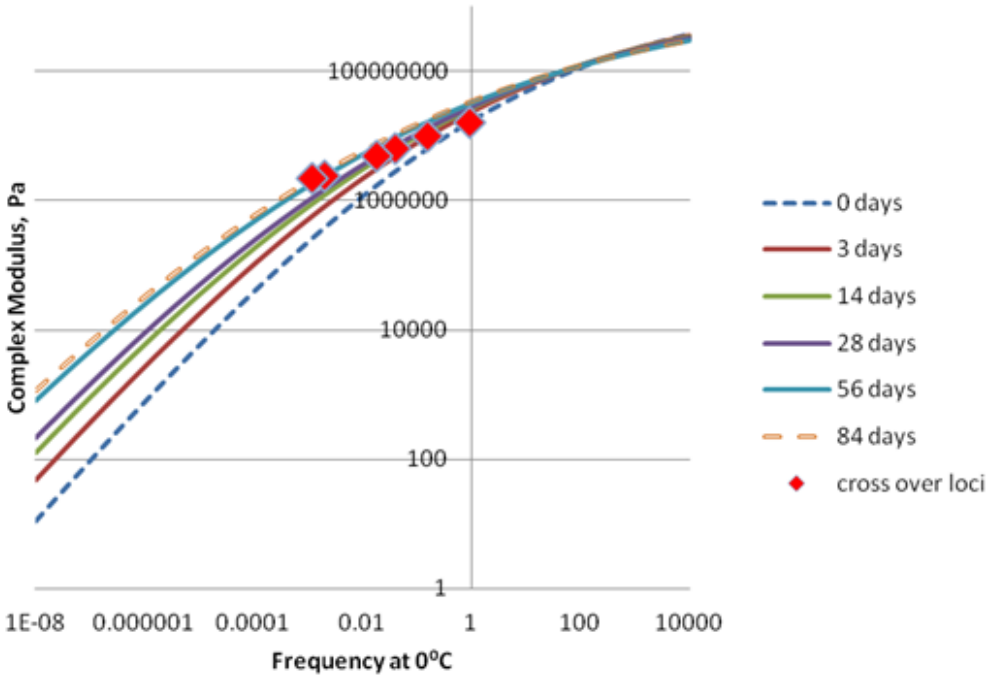

Figure 82. Graph. AAC-1 aging master curves 0°C reference, oxidized at 70°C.

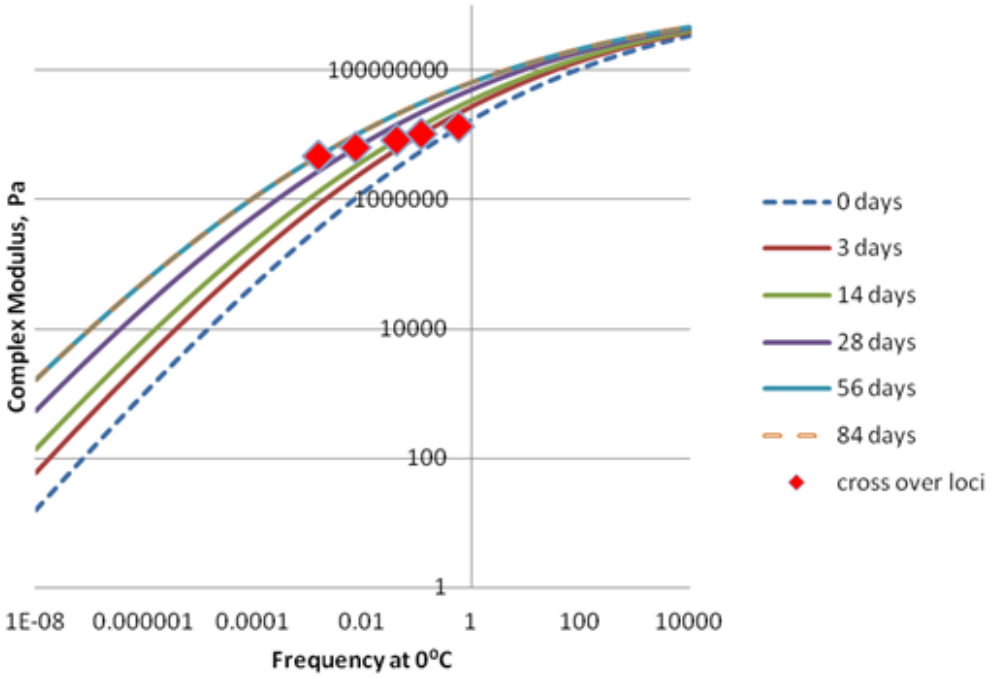

Figure 83. Graph. AAD-1 aging master curves 0°C reference, oxidized at 70°C.

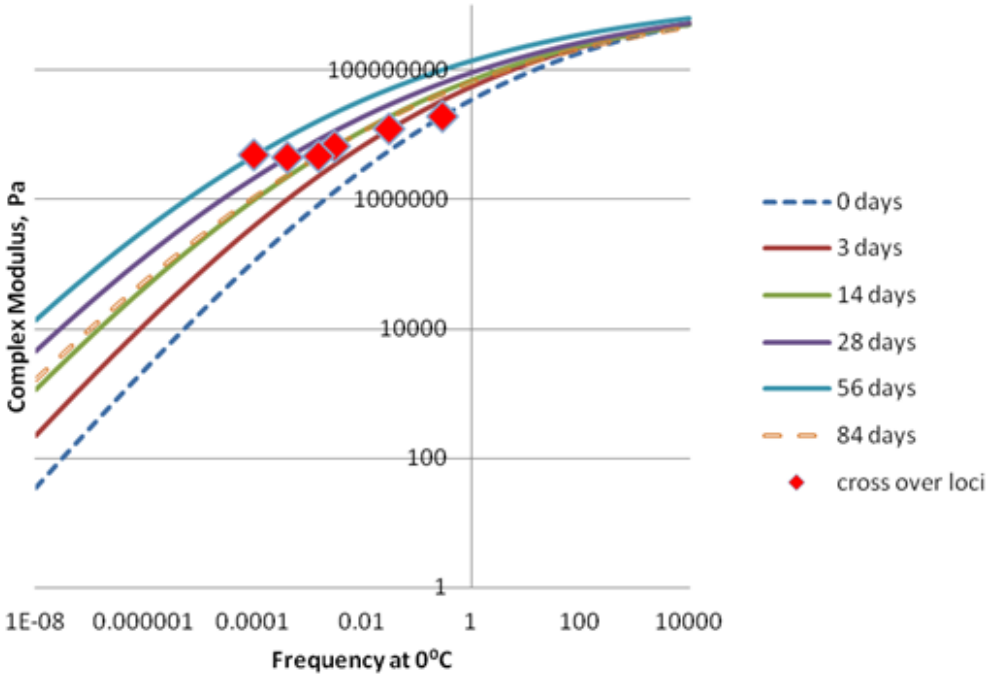

Figure 84. Graph. AAK-1 aging master curves 0°C reference, oxidized at 70°C.

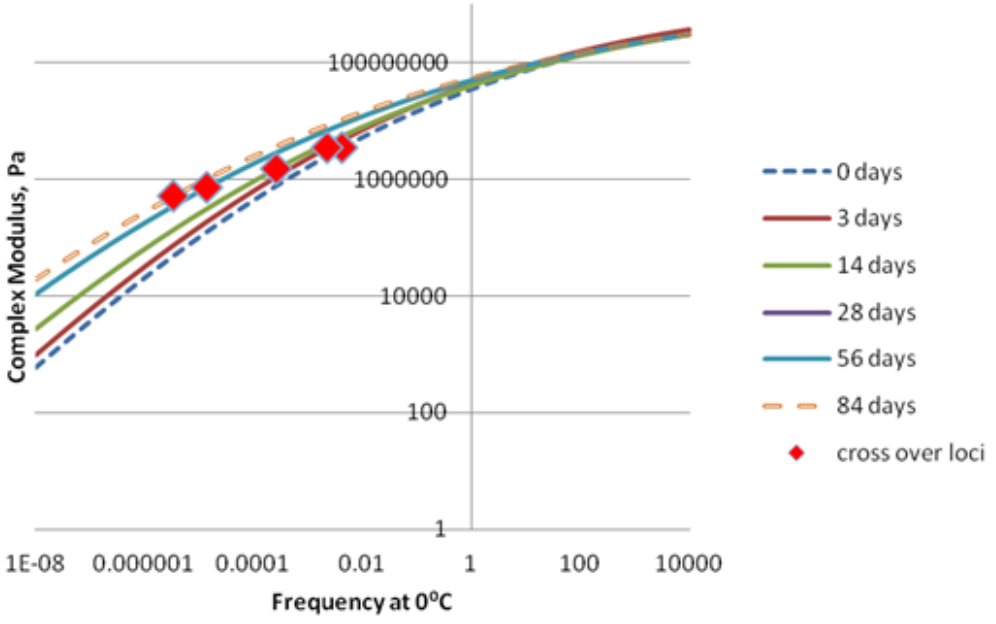

Figure 85. Graph. AAM-1 aging master curves 0°C reference, oxidized at 70°C.

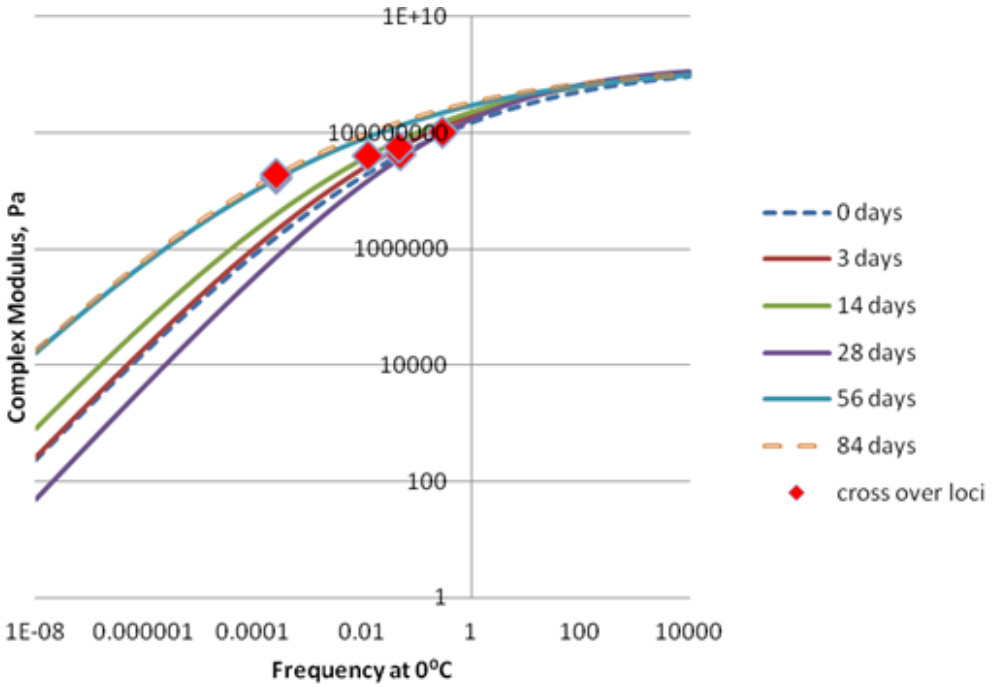

Figure 86. Graph. ABD-1 aging master curves 0°C reference, oxidized at 70°C.

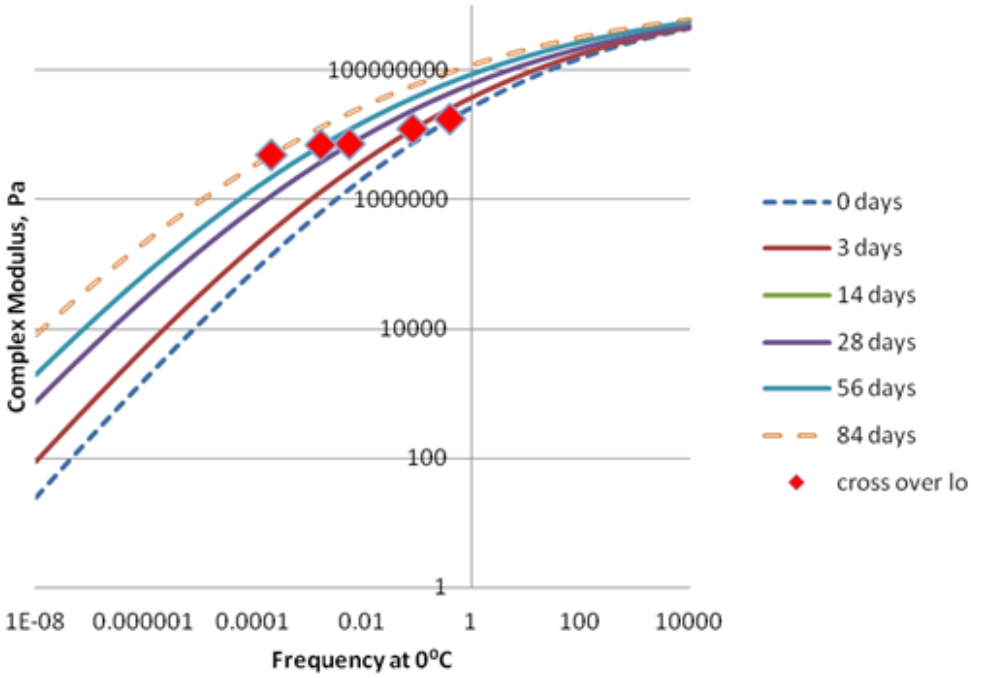

Figure 87. Graph. ARC-1 aging master curves 0°C reference, oxidized at 70°C.

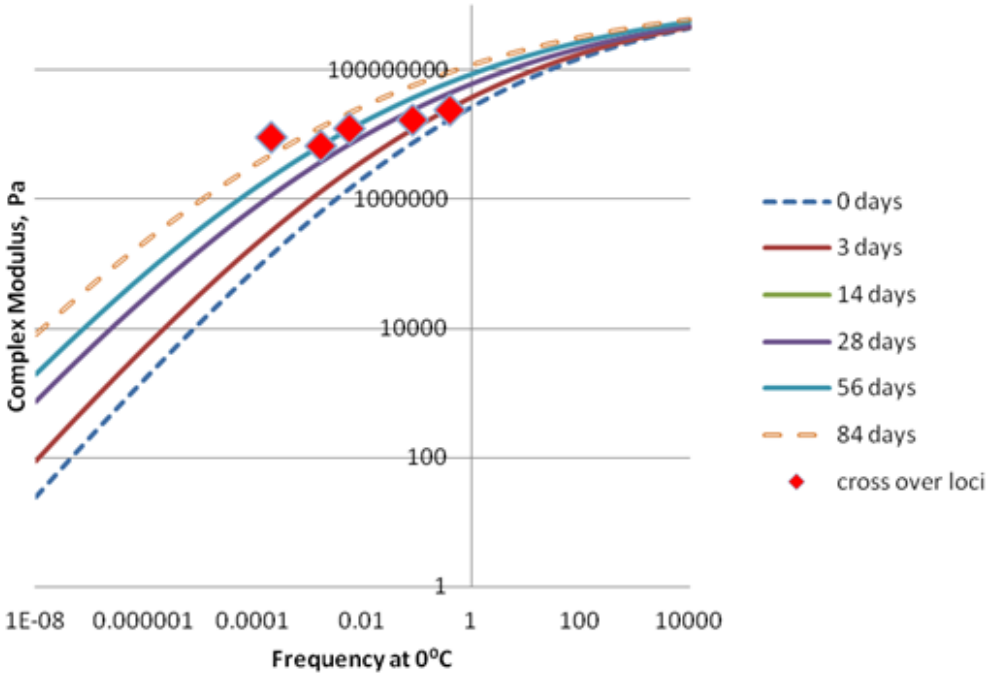

Figure 88. Graph. ARC-2 aging master curves 0°C reference, oxidized at 70°C.

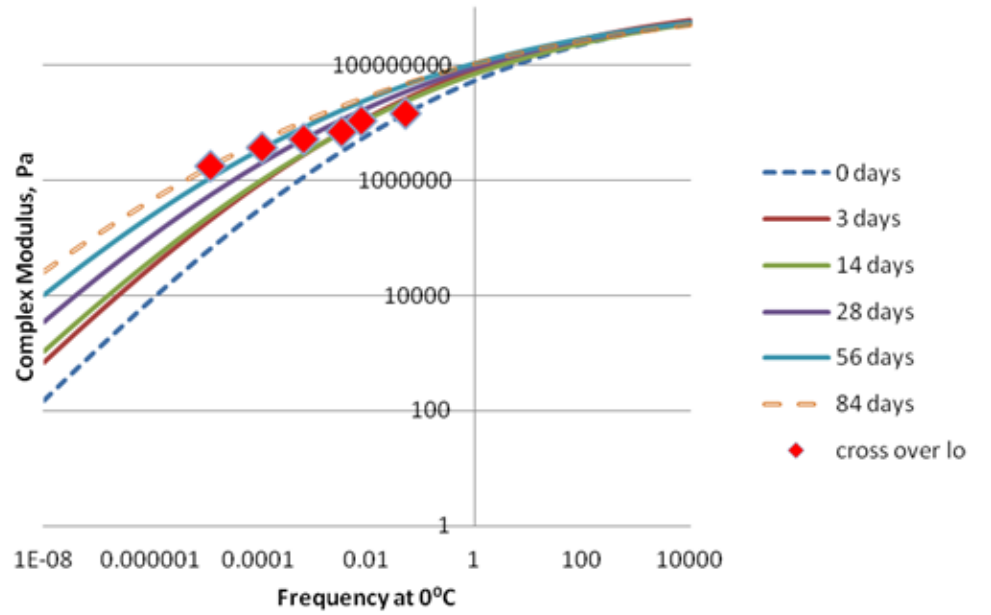

Figure 89. Graph. ALF-Base aging master curves 0°C reference, oxidized at 70°C.

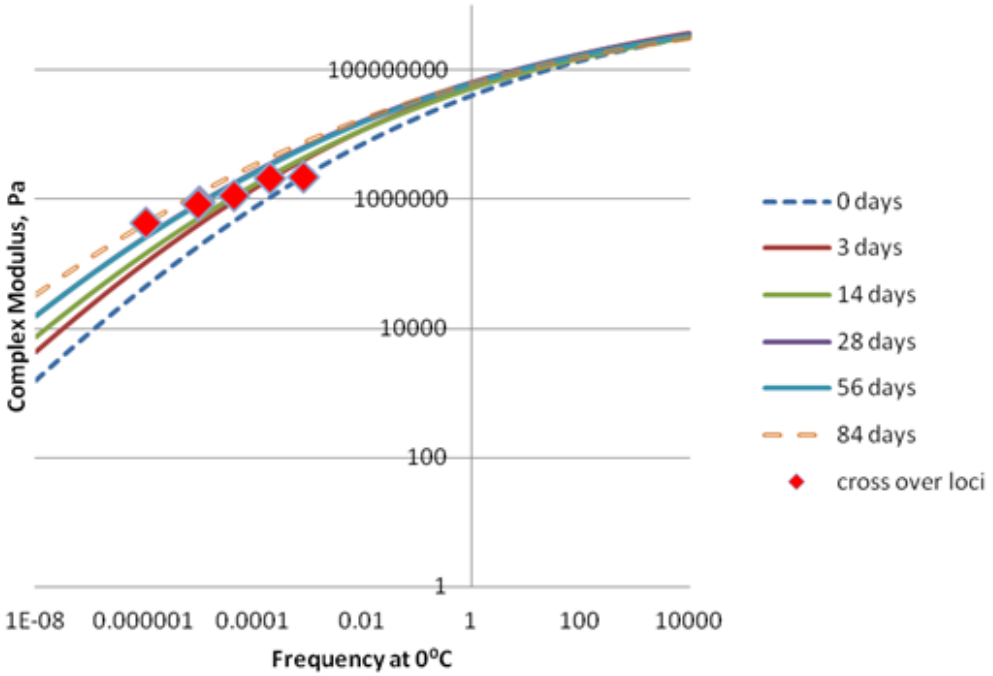

Figure 90. Graph. AZ1-1 aging master curves 0°C reference, oxidized at 70°C.

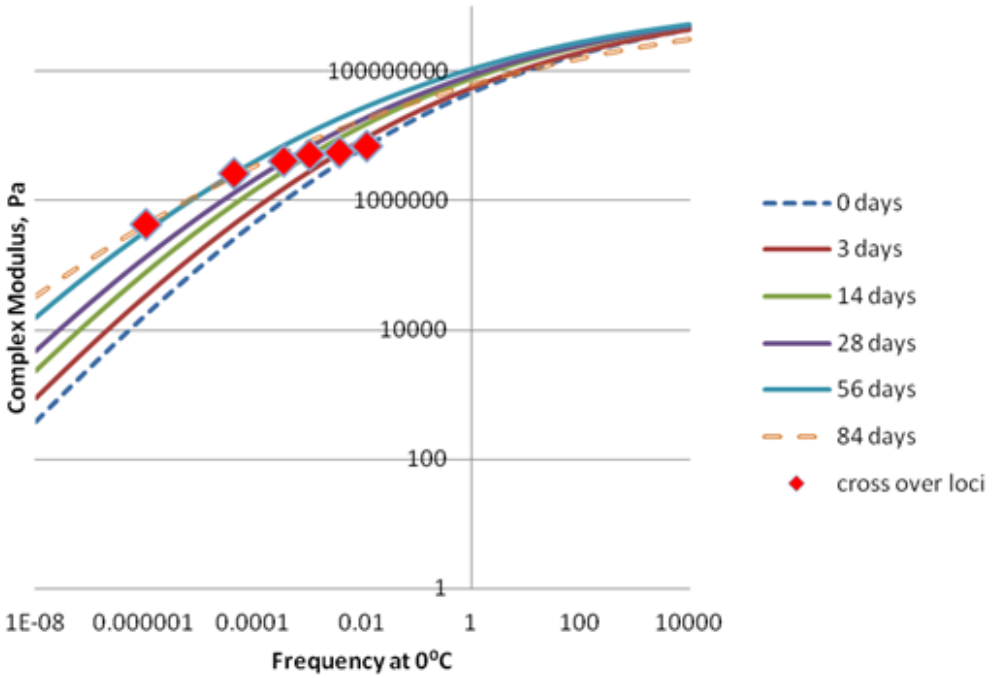

Figure 91. Graph. AZ1-2 aging master curves 0°C reference, oxidized at 70°C.

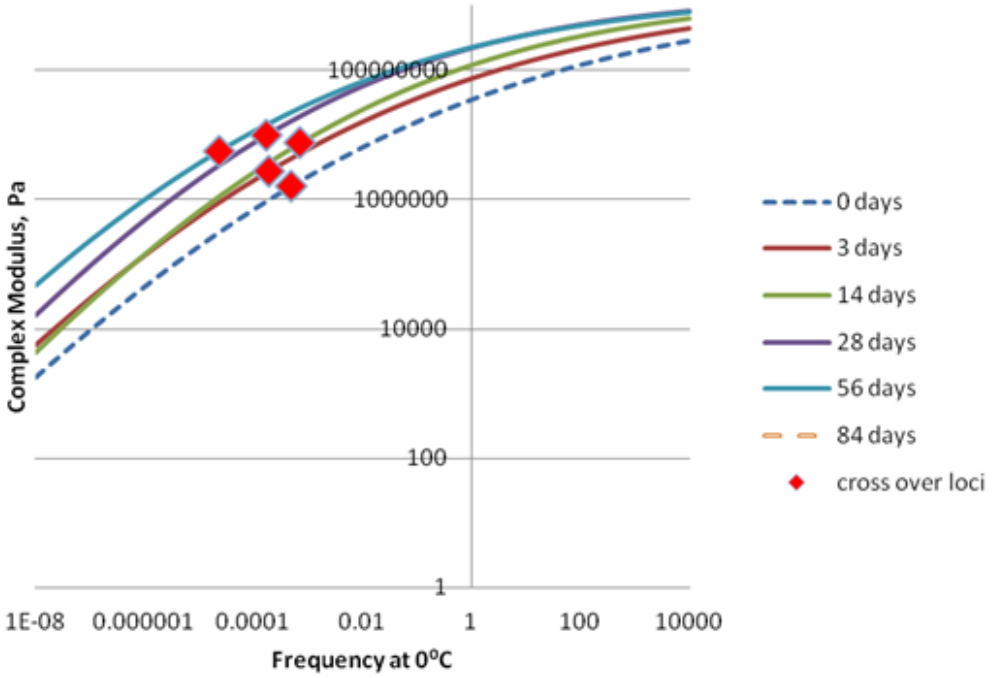

Figure 92. Graph. AZ1-3 aging master curves 0°C reference, oxidized at 70°C.

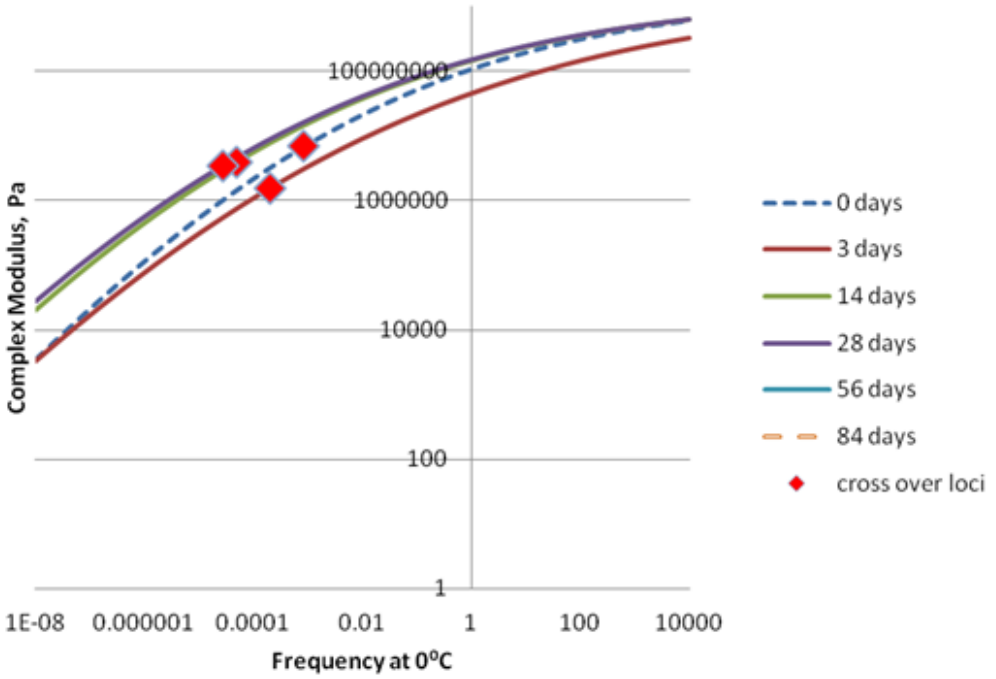

Figure 93. Graph. AZ1-4 aging master curves 0°C reference, oxidized at 70°C.

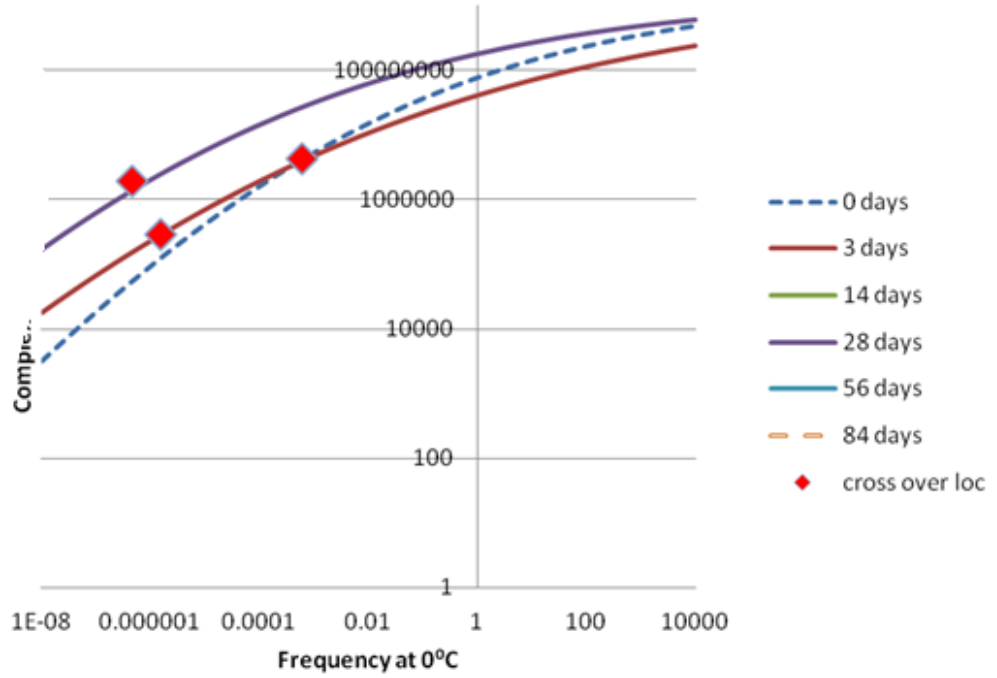

Figure 94. Graph. MAYA aging master curves 0°C reference, oxidized at 70°C.

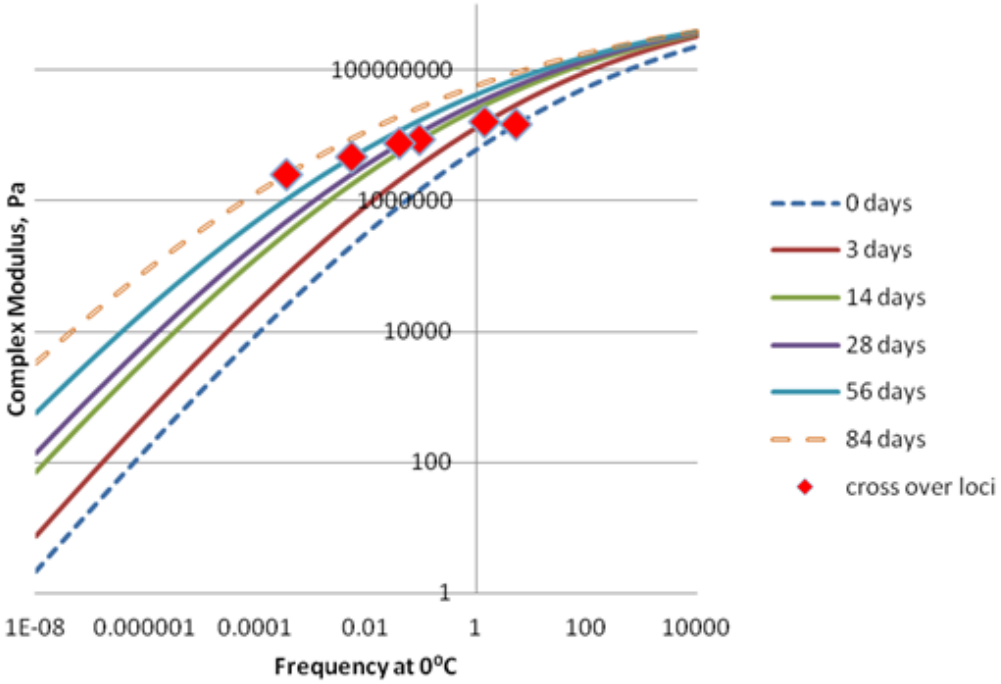

Figure 95. Graph. MCR aging master curves 0°C reference, oxidized at 70°C.

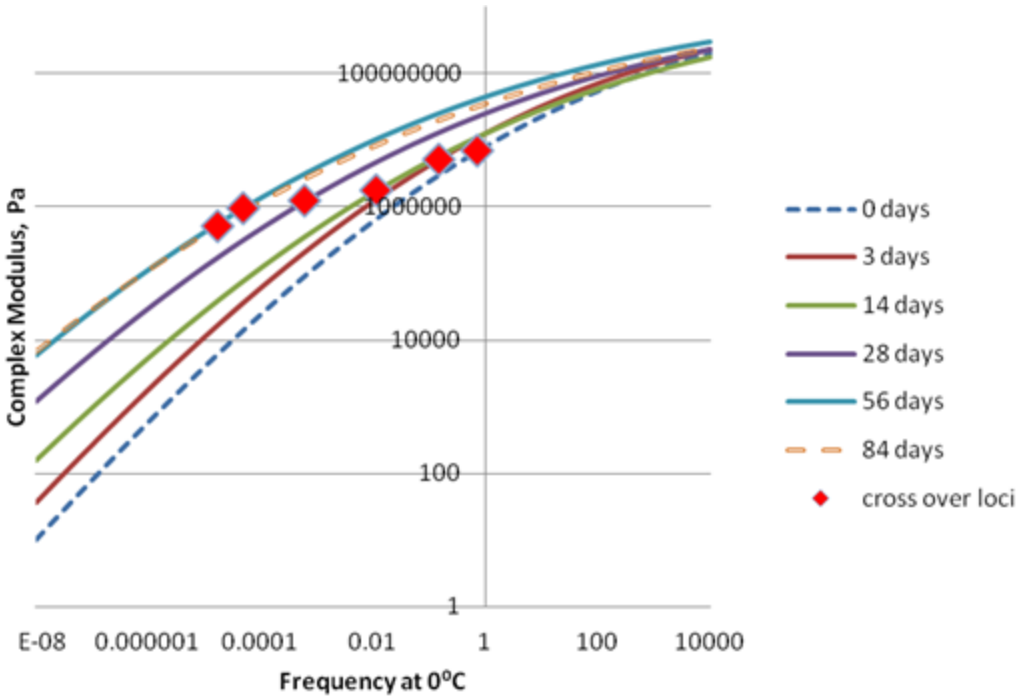

Figure 96. Graph. MN1-2 aging master curves 0°C reference, oxidized at 70°C.

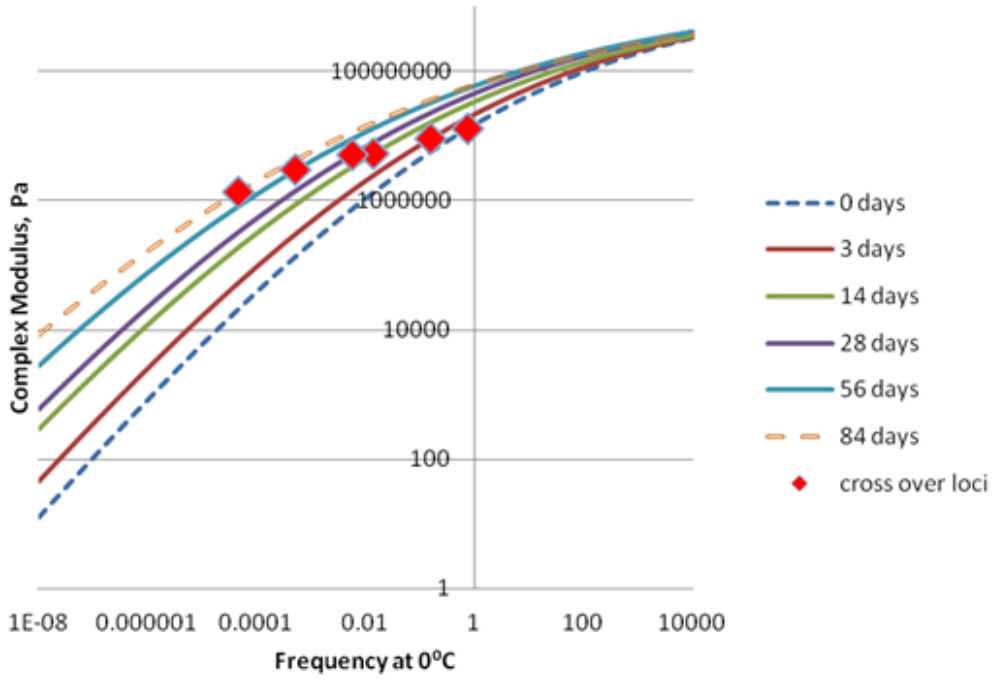

Figure 97. Graph. MN1-3 aging master curves 0°C reference, oxidized at 70°C.

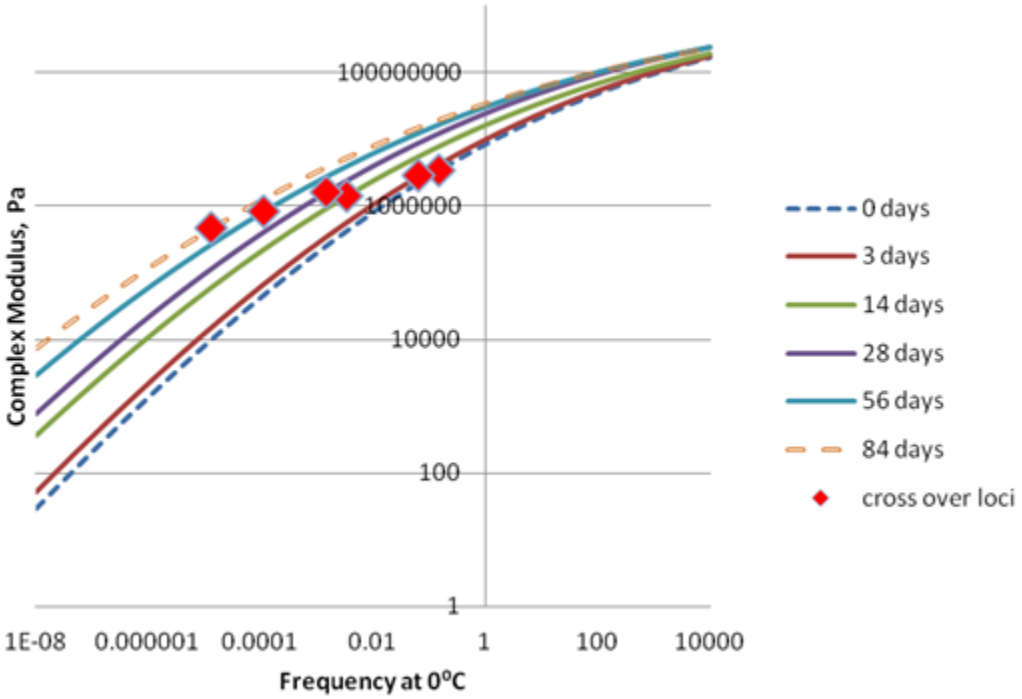

Figure 98. Graph. MN1-4 aging master curves 0°C reference, oxidized at 70°C.

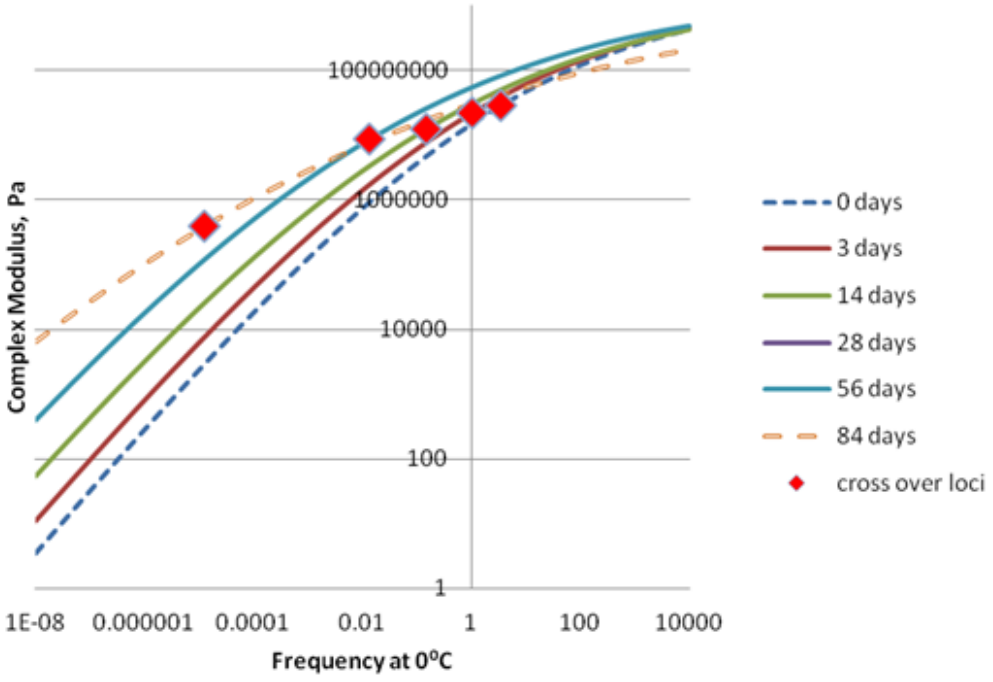

Figure 99. Graph. MN1-5 aging master curves 0°C reference, oxidized at 70°C.

There is currently no detailed mathematical model derived from fundamentals of how chemical changes in an oxidized asphalt binder affect changes in rheological parameters. It is generally accepted that increased polarity from oxygen containing heteroatom functional groups can create hydrogen bonding, or polar-polar interactions that in turn can lead to changes in binder microstructure continuous and suspended phases, even sol-gel transitions, causing the observed changes in rheological behavior (Petersen 2009). These changes are related to increases in asphaltene precipitation amounts observed as oxidation proceeds. However, the Joback equation for viscosity (Joback and Reid 1987), which relates functional group contributions to viscosities of pure Newtonian hydrocarbons, suggests a log-linear form may provide reasonable fits. This approach appears to work well and provides a convenient method for relating oxidation chemistry changes to changes in the CA model parameters, allowing chemistry changes to be mapped to rheological change, albeit empirically at the current time. Table 33 summarizes the changes in rheological behavior of several oxidized binders over time in CA model terms. Also included in table 33 are the changes in the sum of sulfoxide and carbonyl absorbencies used to gauge the extent of aging. The fitsum term is the minimized value for the sum of relative residuals and, much like the regression coefficient, is measure of data scatter for each curve.

Table 33. Christensen-Anderson master curve parameters for oxidized asphalt binders.

AAB-1						
days	0	3	14	28	56	84
fitsum	264	268	271	251	181	149
G_g	1.50E+09	1.50E+09	1.50E+09	1.50E+09	1.50E+09	1.50E+09
log2/R	0.134	0.126	0.118	0.113	0.110	0.100
ω_c	1.23E-01	3.07E-02	6.28E-03	1.53E-03	4.50E-04	6.00E-05
r^2	1.000	0.999	1.000	1.000	0.999	1.000
slope	0.979	0.985	0.996	1.000	1.030	1.010
R	2.24	2.38	2.54	2.67	2.74	3.00
G_c	8.59E+06	6.24E+06	4.29E+06	3.22E+06	2.73E+06	1.51E+06
$\log(\omega_c/\omega_{c0})$	0.000	-0.602	-1.290	-1.910	-2.440	-3.310
oxides	0.260	0.320	0.397	0.457	0.483	0.525
Δ(oxides)	0.000	0.060	0.137	0.197	0.223	0.265
$\log(G_c/G_{c0})$	0.000	-0.139	-0.302	-0.427	-0.498	-0.755

Table 33. Christensen-Anderson master curve parameters for oxidized asphalt binders (continued).

AAC-1						
days	0	3	14	28	56	84
fitsum	335	311	394	377	271	242
G_g	1.50E+09	1.50E+09	1.50E+09	1.50E+09	1.50E+09	1.50E+09
log2/R	0.153	0.138	0.126	0.121	0.108	0.106
ω_c	9.36E-01	1.55E-01	3.96E-02	1.85E-02	2.03E-03	1.20E-03
r^2	1.000	1.000	1.000	1.000	1.000	0.999
slope	0.954	0.980	0.958	0.963	1.010	0.999
R	1.97	2.18	2.38	2.49	2.80	2.84
G_c	1.63E+07	1.00E+07	6.24E+06	4.86E+06	2.40E+06	2.19E+06
$\log(\omega_c/\omega_{c0})$	0.000	-0.780	-1.370	-1.700	-2.660	-2.890
oxides	0.362	0.456	0.580	0.658	0.748	0.849
Δ(oxides)	0.000	0.095	0.218	0.297	0.386	0.487
$\log(G_c/G_{c0})$	0.000	-0.211	-0.416	-0.524	-0.831	-0.871
AAD-1						
days	0	3	14	28	56	84
fitsum	420	222	151	291	170	285
G_g	1.50E+09	1.50E+09	1.50E+09	1.50E+09	1.50E+09	1.50E+09
log2/R	0.147	0.140	0.134	0.126	0.120	0.118
ω_c	5.99E-01	1.24E-01	4.35E-02	7.55E-03	1.56E-03	1.48E-04
r^2	0.999	0.999	0.999	0.999	0.999	0.999
slope	1.060	1.040	1.030	1.070	1.060	1.100
R	2.05	2.16	2.25	2.38	2.50	2.55
G_c	1.33E+07	1.05E+07	8.40E+06	6.24E+06	4.69E+06	4.18E+06
$\log(\omega_c/\omega_{c0})$	0.000	-0.684	-1.140	-1.900	-2.580	-3.610
oxides	0.547	0.622	0.714	0.827	1.040	1.110
Δ(oxides)	0.000	0.075	0.167	0.280	0.490	0.560
$\log(G_c/G_{c0})$	0.000	-0.102	-0.198	-0.327	-0.451	-0.501
AAK-1						
days	0	3	14	28	56	84
fitsum	137	130	418	199	164	
G_g	1.50E+09	1.50E+09	1.50E+09	1.50E+09	1.50E+09	
log2/R	0.159	0.144	0.128	0.119	0.120	
ω_c	2.89E-01	3.16E-02	3.16E-03	4.17E-04	1.01E-04	
r^2	1.000	1.000	0.997	0.999	0.998	
slope	1.020	1.020	0.890	0.962	1.080	
R	1.90	2.09	2.35	2.53	2.50	
G_c	1.90E+07	1.22E+07	6.68E+06	4.43E+06	4.75E+06	
$\log(\omega_c/\omega_{c0})$	0.000	-0.961	-1.960	-2.840	-3.460	
oxides	0.440	0.590	0.706	0.852	0.997	
Δ(oxides)	0.000	0.150	0.266	0.412	0.556	
$\log(G_c/G_{c0})$	0.000	-0.192	-0.454	-0.632	-0.602	

Table 33. Christensen-Anderson master curve parameters for oxidized asphalt binders (continued).

AAM-1						
days	0	3	14	28	56	84
fitsum	414	289	161		256	206
G_g	1.50E+09	1.50E+09	1.50E+09		1.50E+09	1.50E+09
log2/R	0.114	0.114	0.100		0.091	0.087
ω_c	4.24E-03	2.30E-03	2.65E-04		1.38E-05	3.46E-06
r^2	0.999	0.999	1.000		0.998	0.999
slope	0.967	1.020	1.010		1.100	1.080
R	2.64	2.64	3.00		3.32	3.47
G_c	3.42E+06	3.45E+06	1.51E+06		7.23E+05	5.06E+05
$\log(\omega_c/\omega_{c0})$	0.000	-0.265	-1.200		-2.490	-3.090
oxides	0.381	0.429	0.540		0.702	0.768
Δ(oxides)	0.000	0.048	0.159		0.321	0.387
$\log(G_c/G_{c0})$	0.000	0.004	-0.355		-0.675	-0.830
ABD-1						
days	0	3	14	28	56	84
fitsum	812	429	1000	413	427	254
G_g	1.50E+09	1.50E+09	1.50E+09	1.50E+09	1.50E+09	1.50E+09
log2/R	0.194	0.209	0.192	0.255	0.153	0.158
ω_c	5.01E-02	4.69E-02	1.30E-02	2.95E-01	2.70E-04	2.58E-04
r^2	0.993	0.996	0.991	0.976	0.996	1.000
slope	0.886	0.838	0.745	0.716	0.877	0.957
R	1.55	1.44	1.57	1.18	1.97	1.91
G_c	4.22E+07	5.48E+07	4.03E+07	9.93E+07	1.61E+07	1.86E+07
$\log(\omega_c/\omega_{c0})$	0.000	-0.029	-0.587		-2.270	-2.290
oxides	0.542	0.625	0.799	0.874	0.996	0.993
Δ(oxides)	0.000	0.084	0.257	0.332	0.455	0.451
$\log(G_c/G_{c0})$	0.000	0.113	-0.021	0.371	-0.418	-0.355
ALF-Base						
days	0	3	14	28	56	84
fitsum	380	210	235	180	156	191
G_g	1.50E+09	1.50E+09	1.50E+09	1.50E+09	1.50E+09	1.50E+09
log2/R	0.149	0.140	0.128	0.122	0.115	0.102
ω_c	5.22E-02	8.13E-03	3.48E-03	6.65E-04	1.12E-04	1.24E-05
r^2	0.997	1.000	0.999	0.997	0.999	0.998
slope	0.885	0.992	0.963	0.951	0.981	0.939
R	2.02	2.15	2.34	2.47	2.63	2.95
G_c	1.44E+07	1.07E+07	6.79E+06	5.10E+06	3.53E+06	1.69E+06
$\log(\omega_c/\omega_{c0})$	0.000	-0.808	-1.180	-1.900	-2.670	-3.620
oxides	0.397	0.465	0.646	0.672	0.838	0.961
Δ(oxides)	0.000	0.068	0.249	0.275	0.441	0.564
$\log(G_c/G_{c0})$	0.000	-0.128	-0.327	-0.451	-0.610	-0.930

Table 33. Christensen-Anderson master curve parameters for oxidized asphalt binders (continued).

ARC-1						
days	0	3	14	28	56	84
fitsum	375	194		254	311	293
G_g	1.50E+09	1.50E+09		1.50E+09	1.50E+09	1.50E+09
log2/R	0.155	0.144		0.129	0.128	0.121
ω_c	4.00E-01	8.62E-02		5.72E-03	1.73E-03	2.11E-04
r^2	1.000	0.999		0.999	0.998	0.980
slope	0.996	1.040		0.966	0.963	0.992
R	1.94	2.09		2.32	2.34	2.49
G_c	1.72E+07	1.22E+07		7.10E+06	6.79E+06	4.84E+06
$\log(\omega_c/\omega_{c0})$	0.000	-0.667		-1.840	-2.360	-3.280
oxides	0.401	0.485		0.743	0.866	1.110
Δ(oxides)	0.000	0.084		0.342	0.465	0.706
$\log(G_c/G_{c0})$	0.000	-0.147		-0.383	-0.402	-0.549
ARC-2						
days	0	3	14	28	56	84
fitsum	333	276	408	412	231	119
G_g	1.50E+09	1.50E+09	1.50E+09	1.50E+09	1.50E+09	1.50E+09
log2/R	0.167	0.154	0.142	0.144	0.127	0.135
ω_c	1.07E-01	2.14E-02	1.89E-03	9.98E-04	6.81E-05	2.96E-05
r^2	0.999	0.999	0.999	0.996	0.999	0.999
slope	0.936	0.969	0.978	1.020	0.924	0.898
R	1.81	1.95	2.12	2.09	2.36	2.23
G_c	2.34E+07	1.68E+07	1.14E+07	1.23E+07	6.48E+06	8.86E+06
$\log(\omega_c/\omega_{c0})$	0.000	-0.700	-1.750	-2.030	-3.200	-3.560
oxides	0.454	0.570	0.745	0.883	0.983	1.060
Δ(oxides)	0.000	0.116	0.291	0.429	0.530	0.602
$\log(G_c/G_{c0})$	0.000	-0.143	-0.313	-0.280	-0.557	-0.422
AZ1-1						
days	0	3	14	28	56	84
fitsum	284	732	459	909	624	407
G_g	1.50E+09	1.50E+09	1.50E+09	1.50E+09	1.50E+09	1.50E+09
log2/R	0.106	0.105	0.096	0.093	0.093	0.085
ω_c	8.19E-04	1.99E-04	4.35E-05	1.04E-05	9.85E-06	1.07E-06
r^2	0.999	0.995	0.999	0.994	0.993	0.985
slope	1.010	1.270	1.090	1.390	1.190	1.080
R	2.83	2.86	3.13	3.23	3.26	3.54
G_c	2.22E+06	2.05E+06	1.12E+06	8.85E+05	8.32E+05	4.32E+05
$\log(\omega_c/\omega_{c0})$	0.000	-0.616	-1.270	-1.900	-1.920	-2.890
oxides	0.507	0.557	0.616	0.669	0.722	0.769
Δ(oxides)	0.000	0.050	0.109	0.162	0.215	0.262
$\log(G_c/G_{c0})$	0.000	-0.035	-0.297	-0.400	-0.426	-0.711

Table 33. Christensen-Anderson master curve parameters for oxidized asphalt binders (continued).

AZ1-2						
days	0	3	14	28	56	84
fitsum	225	159	170	176	134	
G_g	1.50E+09	1.50E+09	1.50E+09	1.50E+09	1.50E+09	
log2/R	0.129	0.124	0.122	0.117	0.109	
ω_c	1.20E-02	3.82E-03	1.07E-03	3.58E-04	4.47E-05	
r^2	0.999	1.000	0.999	0.999	0.999	
slope	0.928	1.010	1.050	1.070	1.050	
R	2.34	2.44	2.48	2.58	2.76	
G_c	6.92E+06	5.50E+06	5.01E+06	3.98E+06	2.62E+06	
$\log(\omega_c/\omega_{c0})$	0.000	-0.496	-1.050	-1.520	-2.430	
oxides	0.451	0.507	0.605	0.677	0.839	
Δ(oxides)	0.000	0.056	0.154	0.226	0.388	
$\log(G_c/G_{c0})$	0.000	-0.100	-0.140	-0.240	-0.421	
AZ1-3						
days	0	3	14	28	56	84
fitsum	808	571	261	670	273	
G_g	1.50E+09	1.50E+09	1.50E+09	1.50E+09	1.50E+09	
log2/R	0.101	0.110	0.130	0.138	0.124	
ω_c	5.00E-04	1.92E-04	6.99E-04	1.71E-04	2.40E-05	
r^2	0.991	0.995	1.000	0.999	0.999	
slope	0.817	0.854	0.972	0.906	0.963	
R	2.97	2.74	2.31	2.18	2.43	
G_c	1.61E+06	2.74E+06	7.38E+06	1.00E+07	5.63E+06	
$\log(\omega_c/\omega_{c0})$	0.000		0.146	-0.465	-1.320	
oxides	0.509		0.690	0.797	0.907	
Δ(oxides)	0.000		0.181	0.288	0.398	
$\log(G_c/G_{c0})$	0.000		0.661	0.793	0.543	
AZ1-4						
days	0	3	14	28	56	84
fitsum	355	573	274	102		
G_g	1.50E+09	1.50E+09	1.50E+09	1.50E+09		
log2/R	0.128	0.101	0.117	0.114		
ω_c	8.34E-04	1.99E-04	4.99E-05	2.75E-05		
r^2	0.998	0.992	0.999	0.999		
slope	0.914	0.887	0.984	1.000		
R	2.35	2.99	2.58	2.64		
G_c	6.78E+06	1.54E+06	3.96E+06	3.44E+06		
$\log(\omega_c/\omega_{c0})$	0.000		-1.220	-1.480		
oxides	0.501		0.720	0.817		
Δ(oxides)	0.000	-0.501	0.219	0.316		
$\log(G_c/G_{c0})$	0.000		-0.234	-0.295		

Table 33. Christensen-Anderson master curve parameters for oxidized asphalt binders (continued).

MAYA						
days	0	3	14	28	56	84
fitsum	412	729		88		
G_g	1.50E+09	1.50E+09		2.00E+09		
log2/R	0.118	0.081		0.100		
ω_c	6.15E-04	1.55E-06		4.76E-07		
r^2	0.994	0.985		1.000		
slope	0.874	0.885		0.964		
R	2.55	3.72		3.03		
G_c	4.18E+06	2.83E+05		1.89E+06		
$\log(\omega_c/\omega_{c0})$	0.000	-2.600		-3.110		
oxides	0.371	0.525	0.622	0.792	0.797	
Δ(oxides)	0.000	0.154	0.251	0.421	0.426	
$\log(G_c/G_{c0})$	0.000	-1.170		-0.346		
MCR						
days	0	3	14	28	56	84
fitsum	293	121	296	374	454	479
G_g	1.50E+09	1.50E+09	1.50E+09	1.50E+09	1.50E+09	1.50E+09
log2/R	0.150	0.152	0.134	0.131	0.120	0.109
ω_c	5.15E+00	1.41E+00	9.57E-02	4.07E-02	5.63E-03	3.56E-04
r^2	0.996	1.000	0.999	0.998	0.998	0.999
slope	0.895	1.000	1.090	1.120	1.140	1.040
R	2.01	1.98	2.24	2.30	2.51	2.77
G_c	1.47E+07	1.58E+07	8.56E+06	7.52E+06	4.62E+06	2.53E+06
$\log(\omega_c/\omega_{c0})$	0.000	-0.562	-1.730	-2.100	-2.960	-4.160
oxides	0.396	0.474	0.611	0.731	0.803	0.936
Δ(oxides)	0.000	0.078	0.215	0.335	0.407	0.541
$\log(G_c/G_{c0})$	0.000	0.033	-0.234	-0.290	-0.501	-0.763
MN1-2						
days	0	3	14	28	56	84
						no 30°C
fitsum	452	748	386	668	759	412
G_g	1.50E+09	1.50E+09	1.50E+09	1.50E+09	1.50E+09	1.50E+09
log2/R	0.129	0.122	0.103	0.097	0.094	0.087
ω_c	7.11E-01	1.51E-01	1.18E-02	6.10E-04	5.02E-05	1.71E-05
r^2	0.999	0.999	0.999	0.998	0.995	0.996
slope	1.030	1.220	1.060	1.210	1.300	1.140
R	2.34	2.46	2.93	3.09	3.19	3.47
G_c	6.87E+06	5.17E+06	1.77E+06	1.21E+06	9.59E+05	5.05E+05
$\log(\omega_c/\omega_{c0})$	0.000	-0.672	-1.780	-3.070	-4.150	-4.620
oxides	0.407	0.500	0.584	0.706	0.828	
Δ(oxides)	0.000	0.093	0.177	0.299	0.421	
$\log(G_c/G_{c0})$	0.000	-0.124	-0.589	-0.754	-0.855	-1.130

Table 33. Christensen-Anderson master curve parameters for oxidized asphalt binders (continued).

MN1-3						
days	0	3	14	28	56	84
fitsum	295	225	230	458	501	403
G_g	1.50E+09	1.50E+09	1.50E+09	1.50E+09	1.50E+09	1.50E+09
log2/R	0.145	0.136	0.123	0.122	0.111	0.099
ω_c	7.50E-01	1.58E-01	1.38E-02	5.71E-03	5.18E-04	4.67E-05
r^2	0.998	1.000	1.000	0.998	0.997	0.999
slope	0.932	1.020	1.030	1.090	1.130	0.995
R	2.07	2.22	2.45	2.46	2.70	3.04
G_c	1.28E+07	9.07E+06	5.32E+06	5.15E+06	2.97E+06	1.36E+06
$\log(\omega_c/\omega_{c0})$	0.000	-0.676	-1.730	-2.120	-3.160	-4.210
oxides	0.375	0.460	0.602	0.660	0.821	0.882
Δ(oxides)	0.000	0.085	0.226	0.285	0.446	0.507
$\log(G_c/G_{c0})$	0.000	-0.149	-0.381	-0.395	-0.635	-0.974
MN1-4						
days	0	3	14	28	56	84
fitsum	294	340	363	458	590	490
G_g	1.50E+09	1.50E+09	1.50E+09	1.50E+09	1.50E+09	1.50E+09
log2/R	0.114	0.110	0.099	0.101	0.092	0.086
ω_c	1.48E-01	6.57E-02	3.37E-03	1.47E-03	1.12E-04	1.35E-05
r^2	0.999	0.998	0.999	0.995	0.994	0.996
slope	1.040	1.080	1.060	1.150	1.260	1.150
R	2.64	2.73	3.03	2.97	3.26	3.51
G_c	3.46E+06	2.79E+06	1.39E+06	1.60E+06	8.19E+05	4.59E+05
$\log(\omega_c/\omega_{c0})$	0.000	-0.352	-1.640	-2.000	-3.120	-4.040
oxides	0.427	0.502	0.606	0.678	0.788	0.838
Δ(oxides)	0.000	0.075	0.179	0.251	0.361	0.411
$\log(G_c/G_{c0})$	0.000	-0.094	-0.395	-0.337	-0.626	-0.878
MN1-5						
days	0	3	14	28	56	84
fitsum	146	152	206	579	160	235
G_g	1.50E+09	1.50E+09	1.50E+09	1.50E+09	1.50E+09	1.50E+09
log2/R	0.174	0.163	0.144	0.107	0.134	0.084
ω_c	3.50E+00	1.03E+00	1.51E-01	1.13E-01	1.34E-02	1.25E-05
r^2	1.000	0.999	0.999	0.997	0.999	0.998
slope	0.976	0.983	0.972	0.874	1.040	1.090
R	1.73	1.84	2.09	2.81	2.24	3.58
G_c	2.82E+07	2.15E+07	1.23E+07	2.33E+06	8.54E+06	3.93E+05
$\log(\omega_c/\omega_{c0})$	0.000	-0.530	-1.370	-1.490	-2.420	-5.450
oxides	0.475	0.538	0.692	0.725	0.958	
Δ(oxides)	0.000	0.063	0.217	0.250	0.483	
$\log(G_c/G_{c0})$	0.000	-0.118	-0.361	-1.080	-0.519	-1.860

The relationship between extent of oxidation and CA model parameter changes is fit to the following empirical log-linear equation (equation 27, 28):

$$Ln(G_c^* / G_{c,0}^*) = A_g \Delta([c=o]+[s=o])$$
$$Ln(\omega_c / \omega_{c,0}) = A_\omega \Delta([c=o]+[s=o]) \quad (27, 28)$$

where:

G_g = glassy modulus = 1.5 *GPa*

G_c^* = complex modulus at phase angle = 45°

$G_{c,0}^*$ = complex modulus at phase angle = 45°; time = 0

ω_c^* = frequency at phase angle = 45°

$\omega_{c,0}^*$ = frequency at phase angle = 45°; time = 0

$[c = o] + [s = o]$ = sum of absorbances of sulfoxide and carbonyl

A_g = crossover modulus fit coefficient

A_ω = crossover frequency fit coefficient

The materials examined, all unmodified or air blown binders, behave in a log-linear fashion. The changes in CA parameters plotted against the changes carbonyl and sulfoxide are shown for several of the binders in figures 100 and 101.

The CA model parameter values fit to extent of aging are listed in table 34.

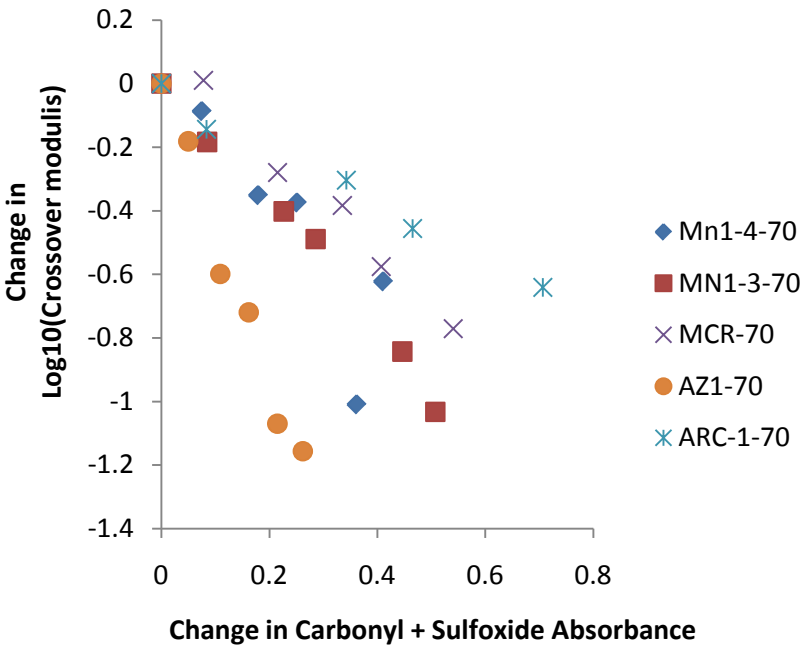

Figure 100. Graph. Crossover modulus change with aging.

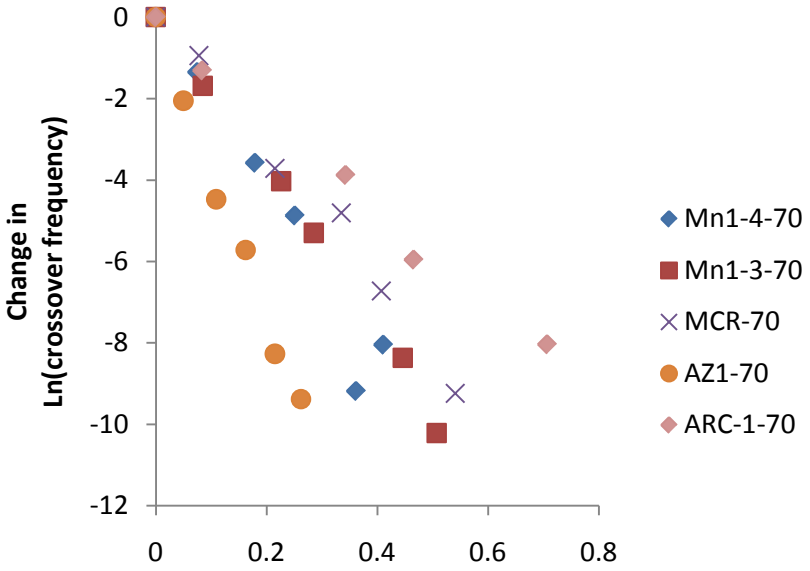

Figure 101. Graph. Crossover frequency change with aging.

Table 34. Rheology and chemical change fit parameters.

Binder	Change in ln (crossover frequency) slope	R^2	Change in $\log_{10}$ (crossover modulus) slope	R^2
AAB-1	-21.	.99	-2.1	.99
AAC-1	-14	.97	-0.95	.77
AAD-1	-14	.97	-0.90	.93
AAM-1	-18	.98	-2.6	.87
ABD-1	-13	.99	-0.94	.97
ALF	-15	.95	-1.6	.96
ARC-1	-12	.99	-0.93	.98
ARC-2	-11	.98	-0.57	.86
AZ1-1	-37	.99	-4.7	.98
MCR	-16	.99	-1.3	.95
MN1-3	-19	.99	-2.0	.99
MN1-4	-21	.95	-2.3	.87

The shift function for the master curves changes very little as the material ages, perhaps less than experiment precision, so no attempt was made at correlating any change. When the Arrhenius shift function is employed, the stability of the visco-elastic analogue to the activation energy of flow can be readily examined and is shown for all 13 binders in table 35, along with the standard deviations of the 6 values obtained at the 6 aging times:

Table 35. Comparison of shift activation energies.

Binder	Shift Activation Energies (K)	
	AVE	STD %
AAB-1	11331	4
AAC-1	11508	1
AAD-1	11113	3
AAK-1	11452	3
AAM-1	12483	2
ABD-1	11859	2
ALF	11434	1
ARC1	11151	1
ARC2	12007	2
AZ1-1	11133	2
MCR	10684	3
MN1-3	10863	2
MN1-4	10805	3

Chemometric Studies of Extent of Oxidation and Rheological Change

Using the software tool developed for correlating spectra to physical properties (FP 06), and analysis of the unmodified binders (including pre-oxidzied AZ1-1) in the original data, a study was conducted to determine the significant wave numbers (and associated functional groups) that play roles in the changes in rheology as asphalt oxidizes. The software requires a cross correlation threshold to be selected for original independent variable reduction, and a typical value of 0.9 was employed, producing 98 groups quantified by selecting the largest indivual response in the group. Carbon tetrachloride solution transmission spectra were obtained over the range of 830-4000 and in some cases 830-2000 to exclude non-linear responses in the 2900 C-H region. The first study attempted to correlated changes in IR (effectively removing non reactive regions) with the natural log of changes in the CA model crossover parameters. The usual procedure in these studies is to perform the correlation repeatedly, removing wave numbers one at a time based upon a significance calculation, usually the F test. The correlation coefficents are then plotted against the number of independent variables, and the number of independent variables is tyically noted at a “break point” in the plot where overfitting has been eliminated. For this attempt, no clear break point was observed (figure 102). It was suspected that inert materials, particular the aliphatic content, which are removed in the spectra subtraction, play an important role in the changes in the master curves with aging.

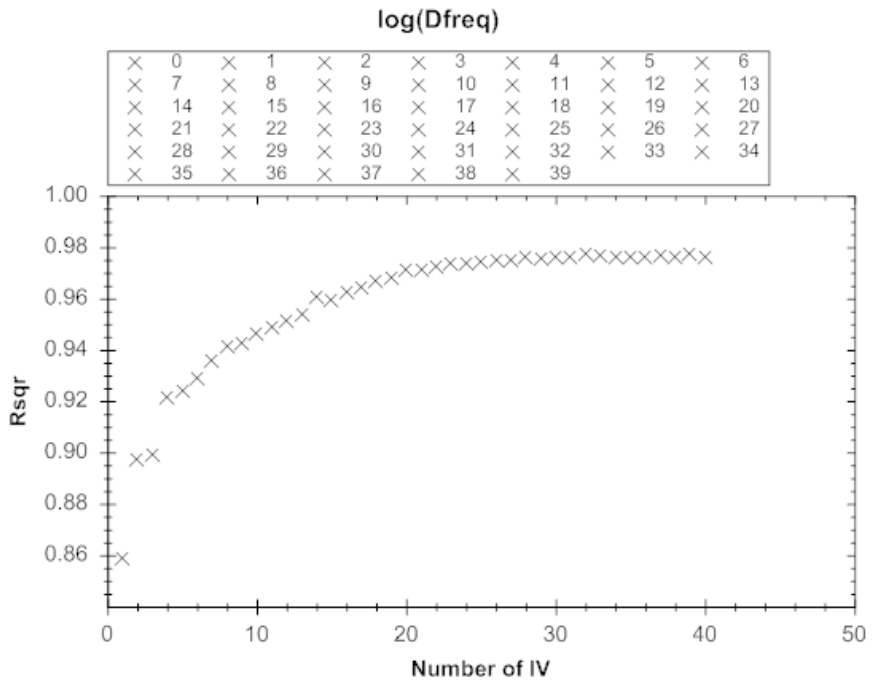

Figure 102. Screenshot. Overfit plot of change spectra against the change in logarithm of crossover frequency.

The correlation was repeated using raw spectra, not net spectra.

It was suspected that inert materials, particular the aliphatic content, which are removed in the spectra subtraction, play an important role in the changes in the master curves with aging. The study was repeated using the raw spectra, not the change spectra. The overfit plot indicated that about 6 wave number can be used to explain most of the change in the master curve parameters (figure 103). Table 36 lists the six significant wave numbers in the correlation and the fit coefficients.

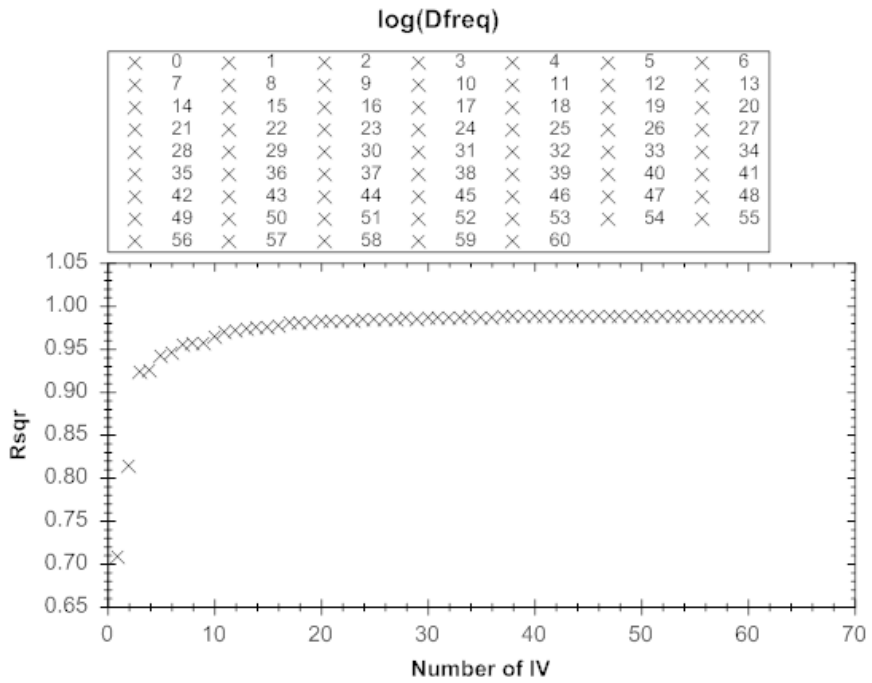

Figure 103. Screenshot. Overfit plot of the raw spectra against the change in logarithm of crossover frequency.

Table 36. Significant wave numbers involved in the crossover frequency change caused by oxidation.

Coefficient of determination (rsqr ACTUAL MATRIX) = 0.9545				
Regression data				
IV x	Coefficient	Group no.	F	Good
x(0)	-2.641E000			
x10	-6.180E000	1699.0000	02001.236	YES
x14	-7.359E000	1034.0000	03368.642	YES
x25	9.948E000	1470.0000	01215.244	YES
x49	-3.190E000	2848.0000	01236.148	YES
x64	2.029E000	2905.0000	00318.679	YES
x65	-1.433E000	2908.0000	00338.973	YES

Figure 104 shows the predicted value compared to the measured value for change in crossover frequency using full spectra. The black dots represent measured data; the red diamonds are a sampling of the synthetic replicates.

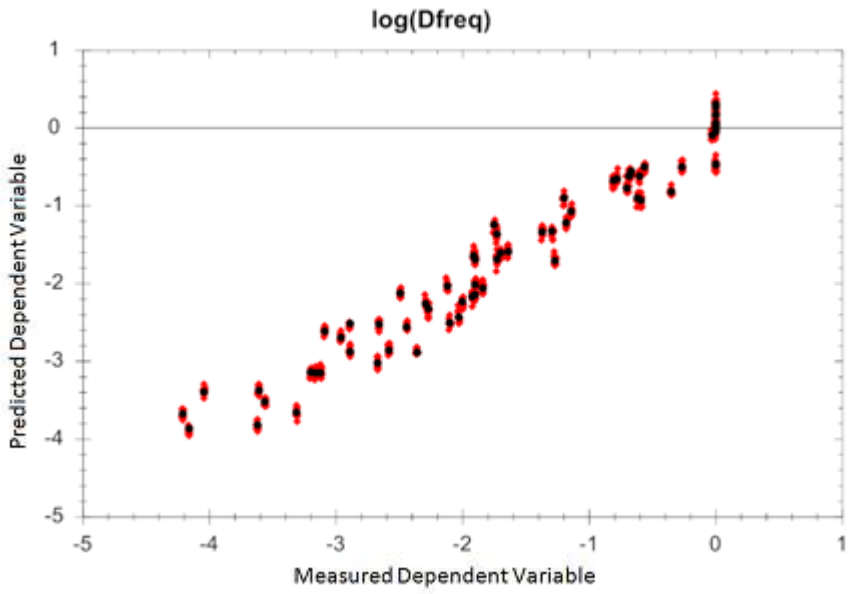

Figure 104. Screenshot. Predicted change in the log of the crossover frequency using 6 parameters.

An examination of figure 104 indicates that the error bound for this master curve parameter is of the order of 1 natural log cycle (roughly 3 fold), meaning that such a correlation used to generate a master curve would be very approximate and probably not suitable for engineering purposes. However, the significant wave numbers in table 36 are a combination of polar functional groups, and aliphatic carbon response, much as one might expect.

It should be noted that high correlation coefficients are often reported for PLS and PCA fits. These should always be checked against parameter to observation ratios, but the projection methods employ all of the wave numbers, making a critical understanding of the significance of the latent variables difficult.

This dataset contains 60 observations. Based upon observation and parameter counts, 20 parameters would provide 3 points in each dimension, and therefore represent a maximum of parameters possible where over fit is not certainly occurring. (Statistical considerations would reduce this number further.) The overall regression coefficient is now improved to 0.98 (figure 105), but the actual error spread is still about half a log cycle (1.5 fold).

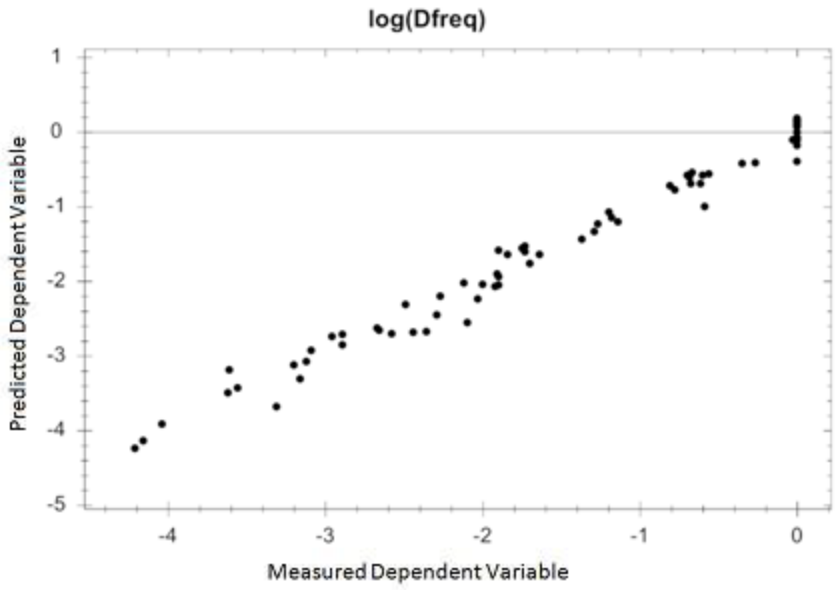

Figure 105. Screenshot. Predicted change in the log of the crossover frequency using 20 parameters.

In figure 106, the aging master curves for AAB-1, is shown again. The abscissa is the frequency, on a logarithmic scale. On this type of plot, ½ natural log cycle (50% error bounds) seems fairly close to the measured value, but in absolute terms, (not logarithm) there is a significant difference. It also should be noted that high frequency, or low temperature values for modulus are less sensitive to crossover parameter estimation errors. Consequently, IR based master curve estimates would be much better at predicting stress accumulation related phenomena (cracking) than permanent deformation phenomena (rutting).

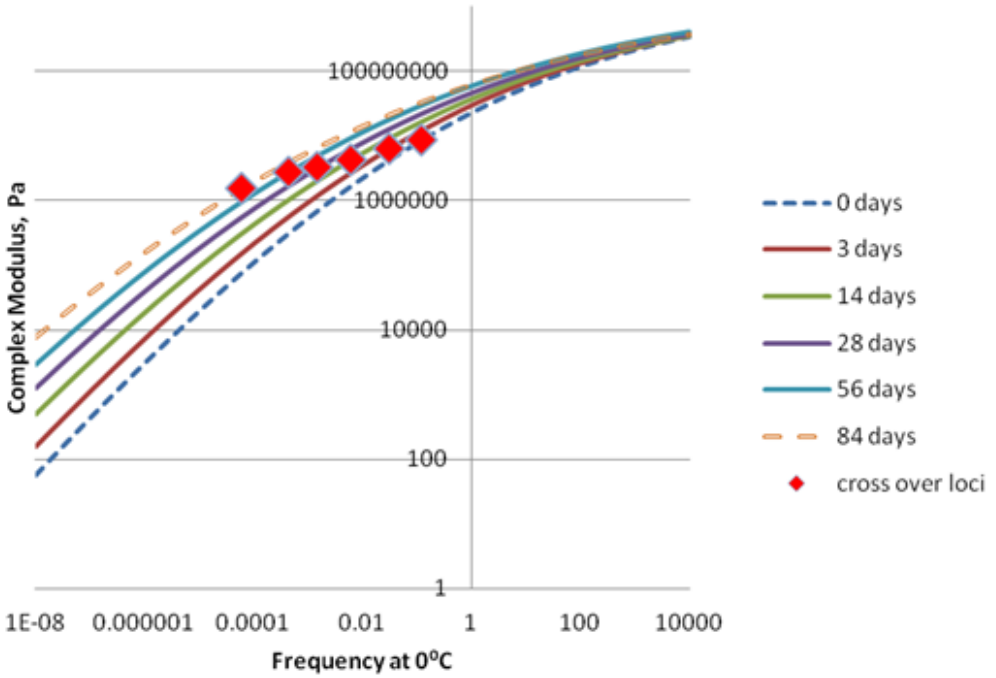

Figure 106. Graph. AAB-1 aging master curves 0°C reference, oxidized at 70°C.

In the preceding study, the correlation was against the change in the log of the crossover frequency. This correlation would require knowledge of the RTFO master curve parameter to add the change to. Similar fits can be obtained for the crossover modulus. The six wave number result using raw spectra against change in crossover modulus is shown in table 37. The predicted values compared to the measured values are shown in figure 107.

Table 37. Significant wave numbers involved in the crossover modulus change caused by oxidation.

Coefficient of determination = 0.8227				
Regression data				
IV x	Coefficient	Group no.	F	Good
x(0)	2.704E000			
x10	-1.332E000	1699.0000	00830.841	YES
x14	-9.059E-001	1034.0000	00401.865	YES
x52	-1.936E000	2852.0000	00358.186	YES
x78	-1.102E000	2946.0000	00173.482	YES
x79	2.188E000	2951.0000	00283.683	YES
x95	2.306E000	3477.0000	00259.663	YES

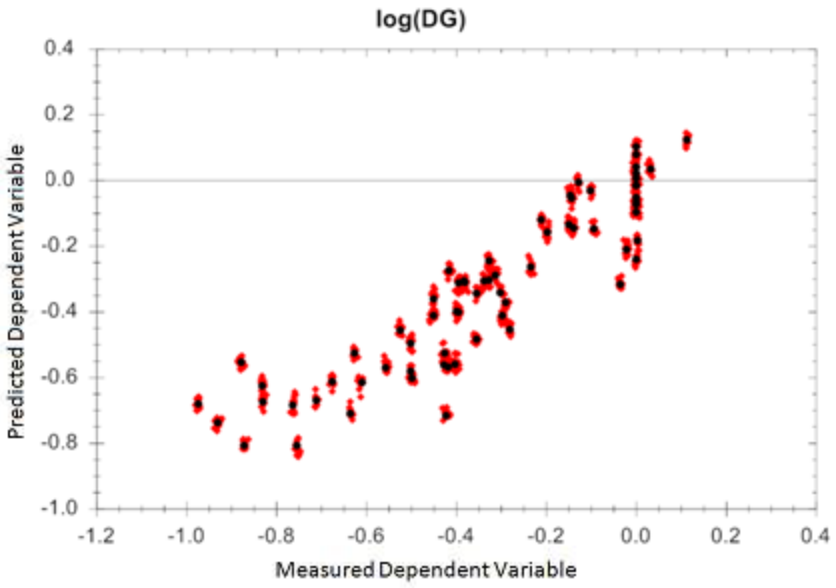

Figure 107. Screenshot. Predicted change in the log of the crossover modulus using 6 parameters.

This initial study indicates that only very approximate estimates of the crossover parameters for binders in general, can be obtained from IR spectra alone. To improve precision, additional or alternative information is likely needed. IR can provide some insight into relative concentrations of aliphatic, aromatic carbons and polar functional groups, but not molecular weight. The addition of molecular weight into these types of correlations will likely improve precision.

The preceding correlations included regions in the spectra around wave number 2900 that are non-linear with regard to Beer's law at the concentrations of asphalt in solvent employed in this study. The correlations were repeated, this time correlating to log crossover frequency, not change in crossover frequency, using the "finger print" region from wave number 830 to 2000 only with similar results to the fits of change in crossover frequency. These results would provide an estimate of master curve parameters directly without having to add the change to a reference master curve. Consequently, estimates could be made without time zero information. This is useful for the characterization of recycled asphalt piles from unknown sources. The results shown here (figure 108 and table 38) are for 10 parameters fits of wave number groups.

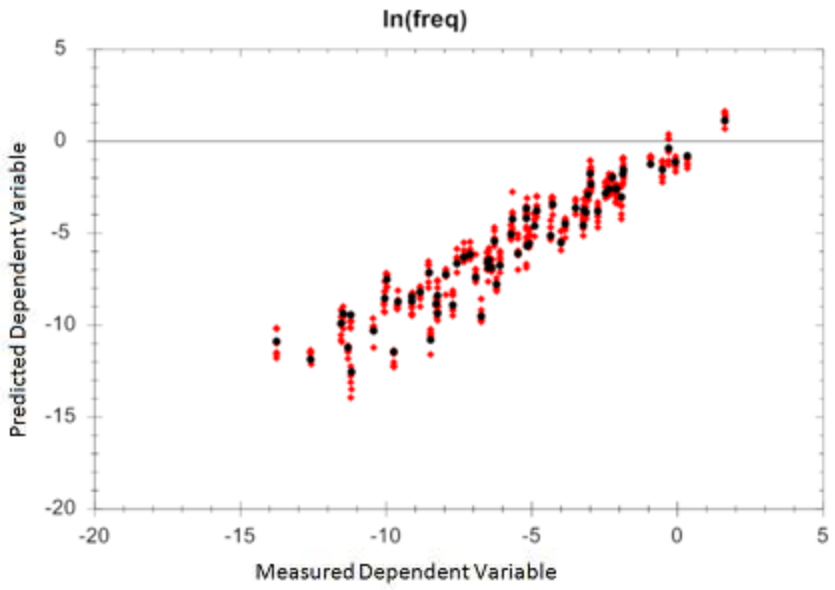

Figure 108. Screenshot. 10 Parameter infrared wave number fit of the Logarithm of crossover frequency.

Table 38. 10 wave number crossover frequency fit results for all binders using finger print region.

Coefficient of determination = 0.8993				
Regression data				
IV x	Coefficient	Group no.	F	Good
x(0)	-1.568E001			
x3	7.663E001	0860.0000	00126.671	YES
x7	-6.485E001	0880.0000	00056.964	YES
x9	-1.794E001	1590.0000	00010.880	YES
x11	-6.856E000	1034.0000	00058.926	YES
x12	-4.723E001	1364.0000	00085.080	YES
x13	4.408E001	1453.0000	00291.373	YES
x16	-3.701E001	1464.0000	00193.516	YES
x18	3.763E001	1470.0000	00065.497	YES
x20	1.228E001	1508.0000	00009.210	YES
x24	-2.467E001	1560.0000	00030.203	YES

An examination of the groups used in the correlation is useful for understanding the significant wave numbers involved. Figures 109-118 are screenshots of the groups involved, with many areas of known functional group assignments, and others not as well known. The selection of some of these wave numbers by the software may mean little more than the best local baseline approximation for overlap correction. These wave numbers have a negative coefficient.

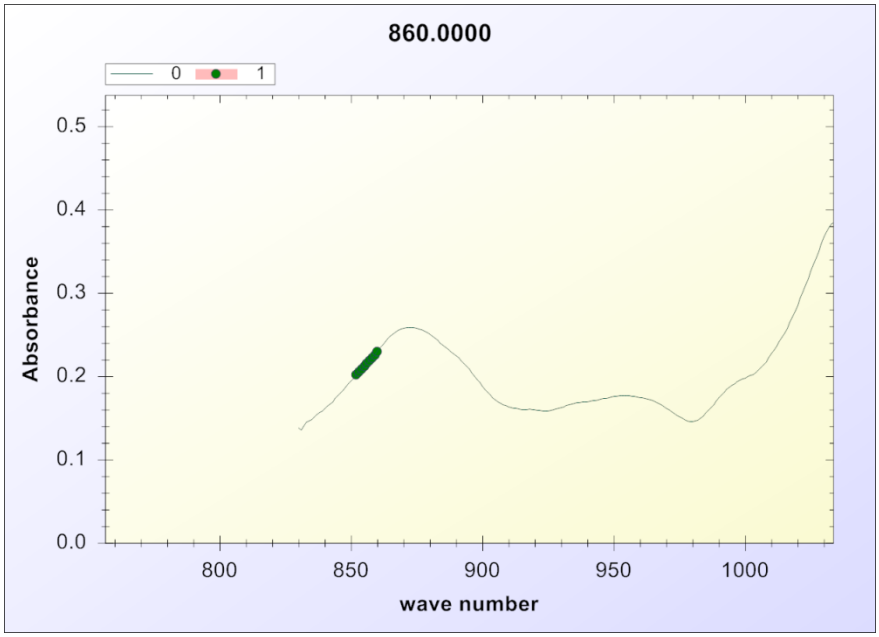

Figure 109. Screenshot. Group 860.

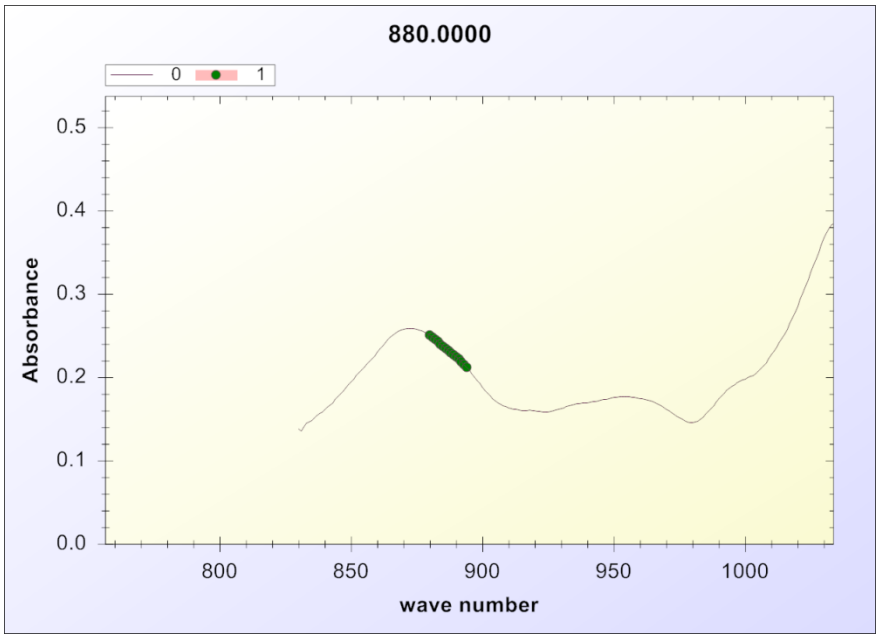

Figure 110. Screenshot. Group 880.

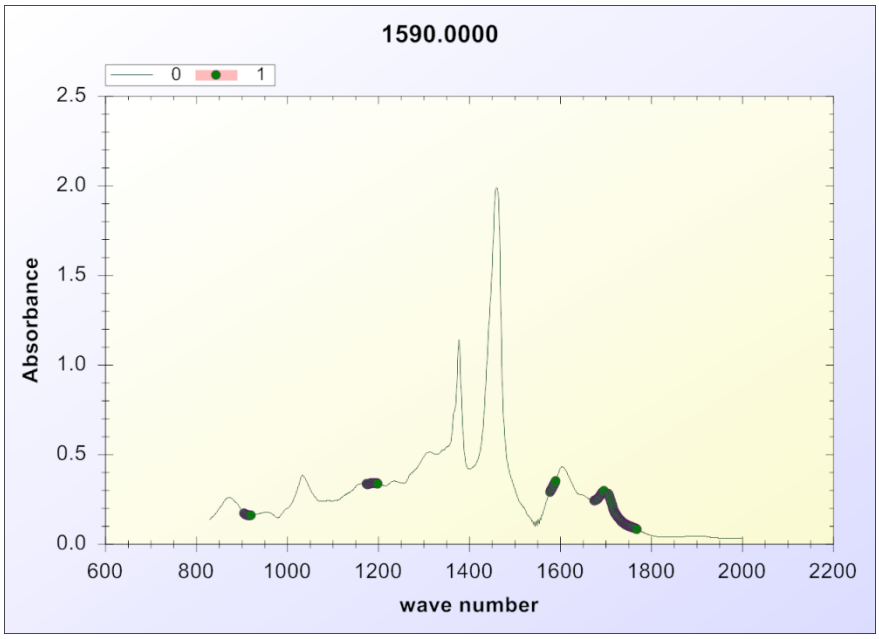

Figure 111. Screenshot. Group 1590.

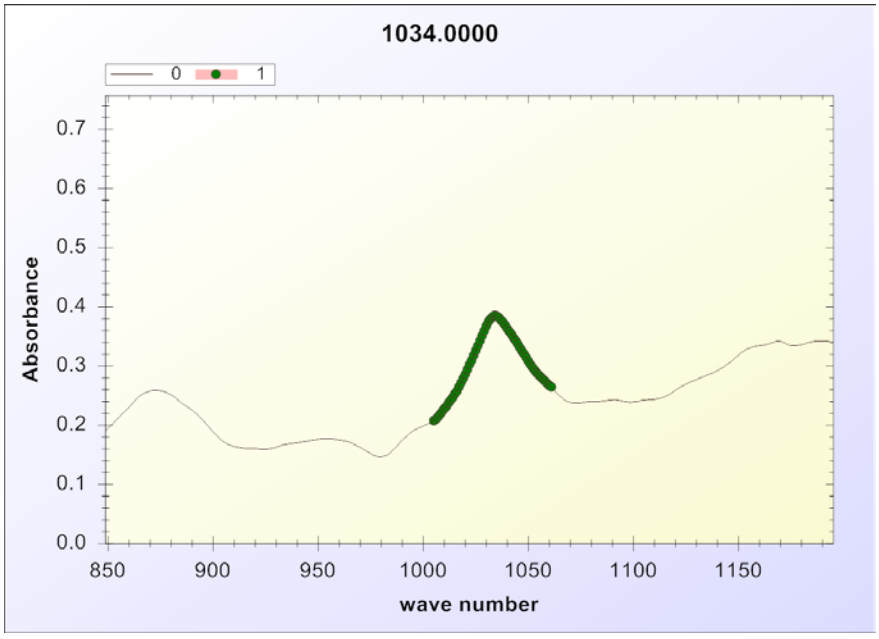

Figure 112. Screenshot. Group 1034.

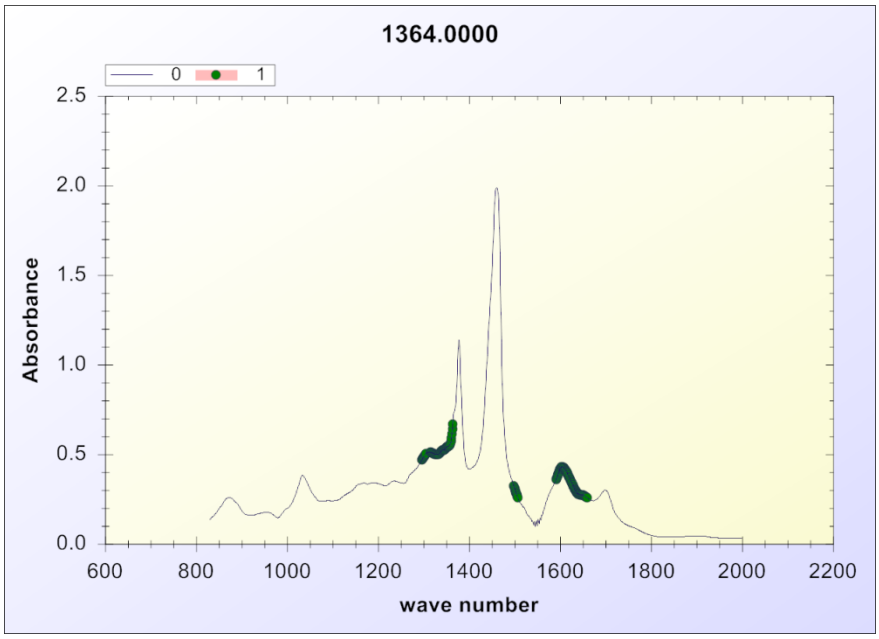

Figure 113. Screenshot. Group 1364.

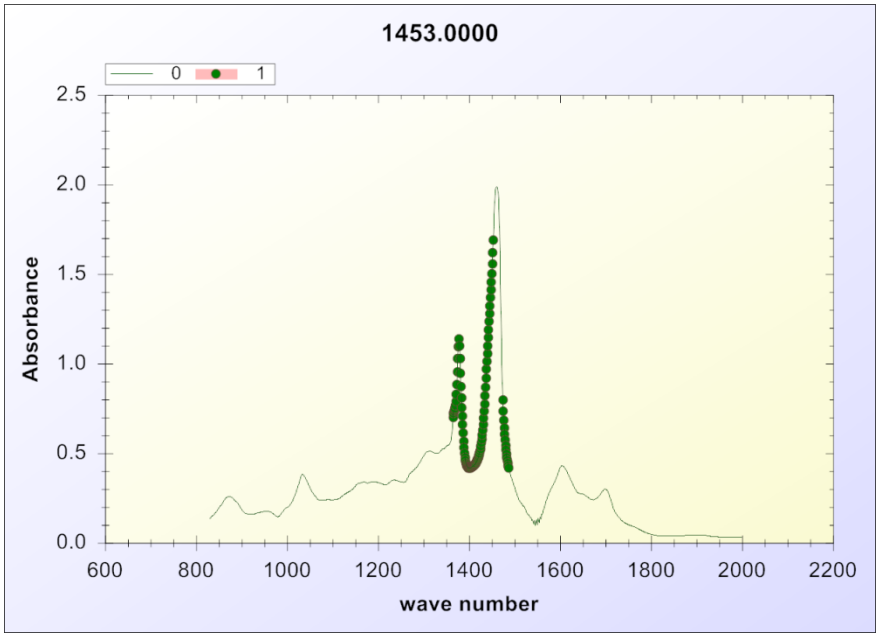

Figure 114. Screenshot. Group 1453.

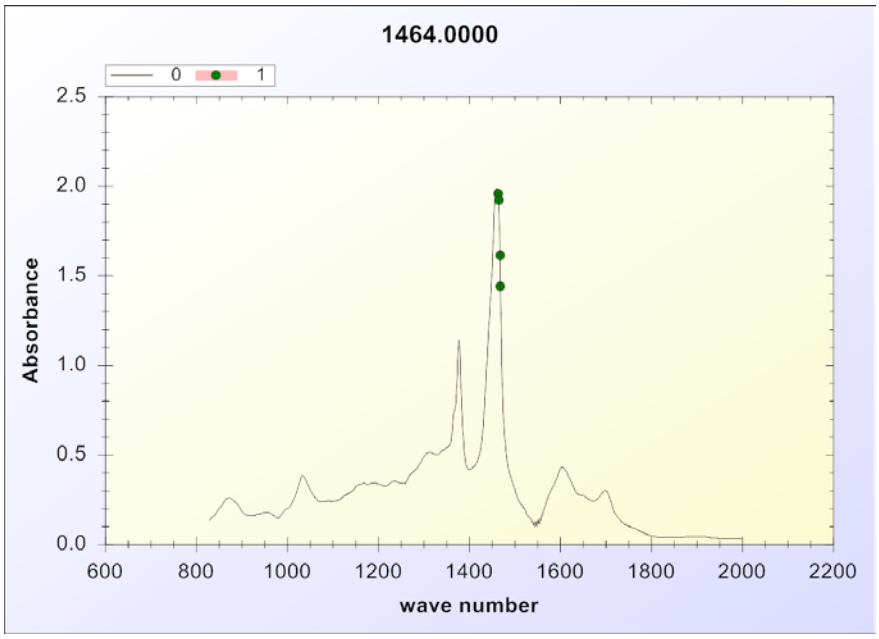

Figure 115. Screenshot. Group 1464.

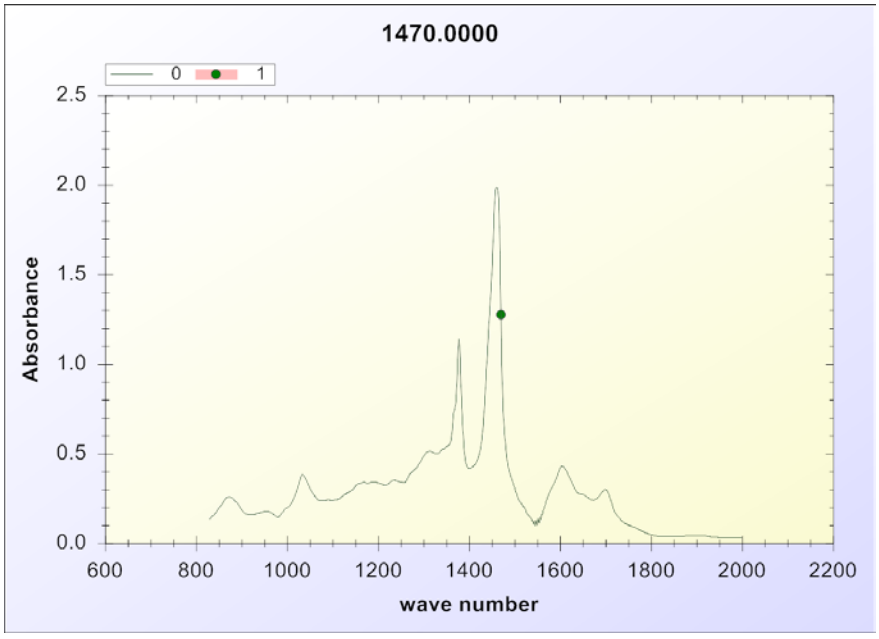

Figure 116. Screenshot. Group 1470.

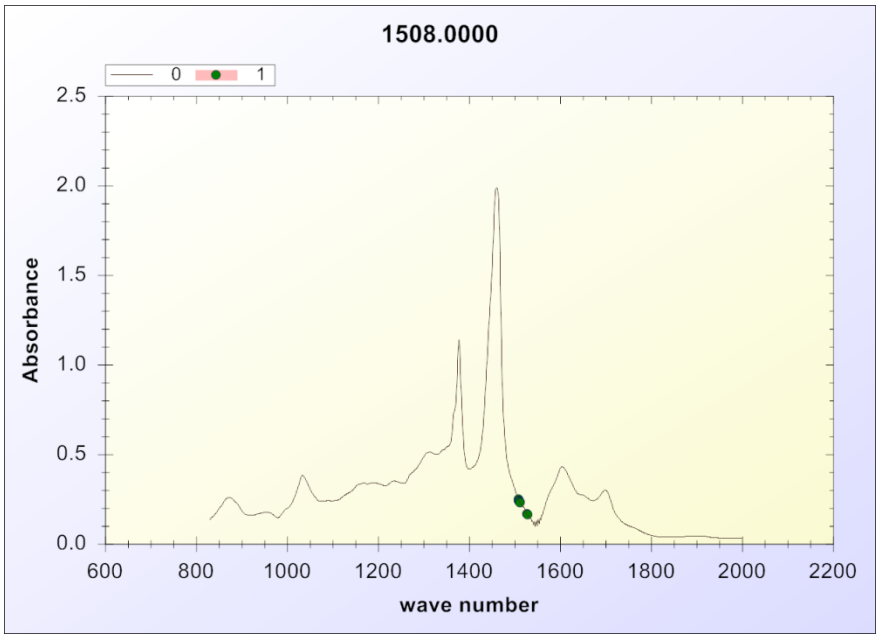

Figure 117. Screenshot. Group 1508.

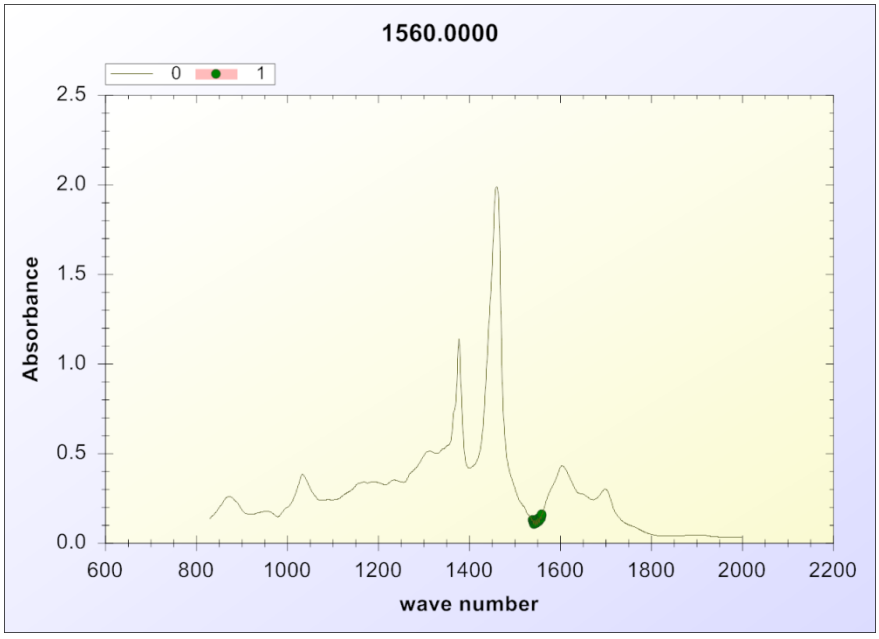

Figure 118. Screenshot. Group 1580.

The correlations were repeated, this time correlating to log crossover modulus, not change in crossover modulus, using the “finger print” region from wave number 830 to 2000 only with similar results to the fits of change in crossover modulus. The results shown here are for 10 parameters fits of wave number groups (figures 119, 120 and table 39).

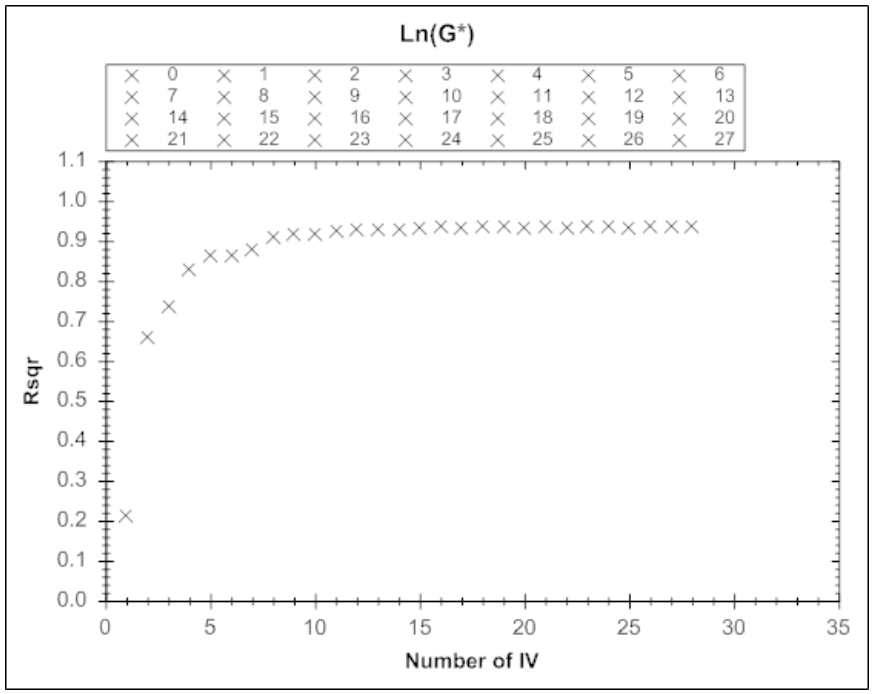

Figure 119. Screenshot. Over fit plot of crossover modulus using finger print region of IR.

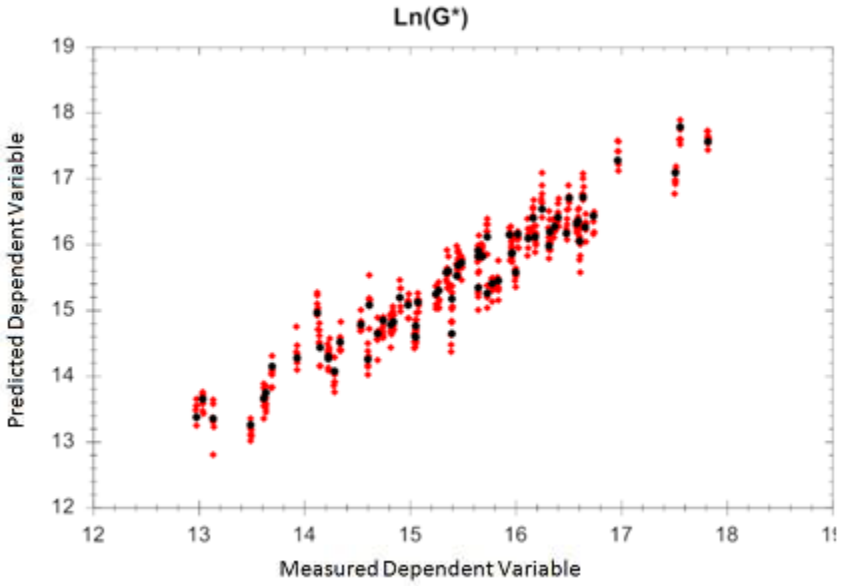

Figure 120. Screenshot. 10 Parameter infrared wavenumber fit of the logarithm of crossover modulus.

Table 39. 10 wave number crossover modulus fit results for all binders using finger print region.

Coefficient of determination = 0.9240				
Regression data				
IV x	Coefficient	Group no.	F	Good
x(0)	1.245E001			
x5	1.579E001	0870.0000	00107.530	YES
x9	-1.127E001	1590.0000	00080.015	YES
x11	-3.188E000	1034.0000	00154.133	YES
x13	9.554E000	1453.0000	00307.145	YES
x16	-1.674E001	1464.0000	00467.136	YES
x18	1.275E001	1470.0000	00077.257	YES
x20	3.093E001	1508.0000	00110.185	YES
x22	-4.629E000	1520.0000	00063.709	YES
x26	-1.863E001	1769.0000	00062.629	YES
x27	-1.529E001	1793.0000	00024.650	YES

The groups involved are similar and are shown in figures 121 through 130.

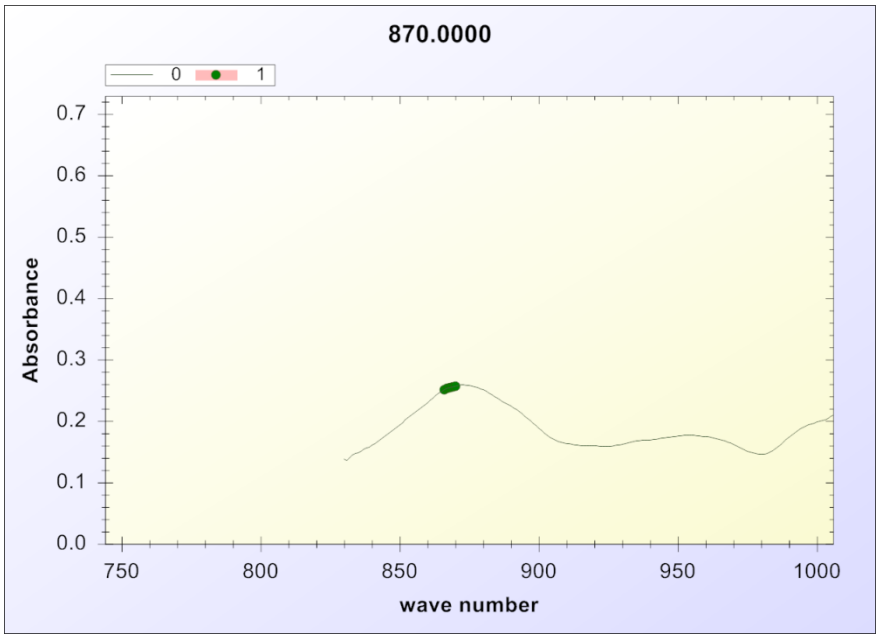

Figure 121. Screenshot. Group 870.

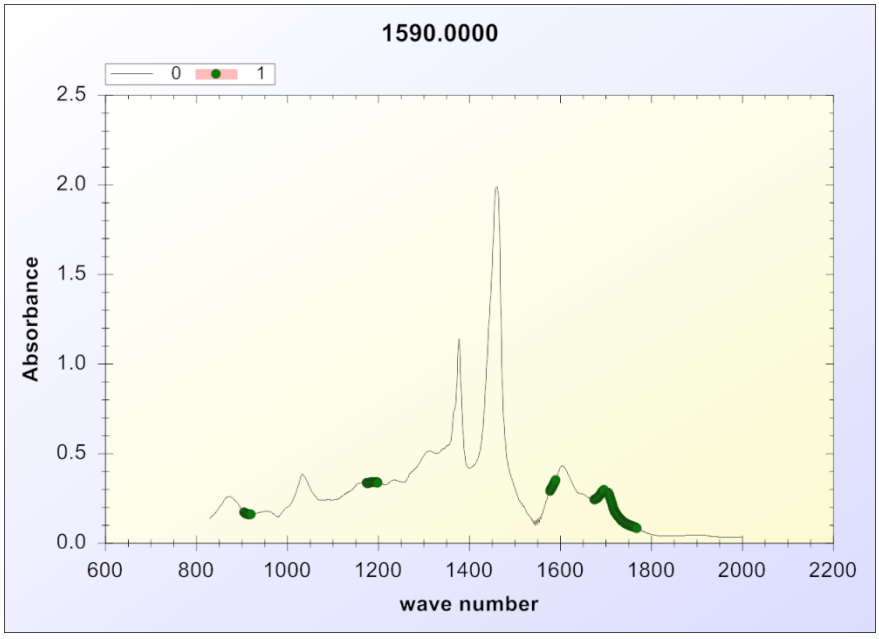

Figure 122. Screenshot. Group 1590.

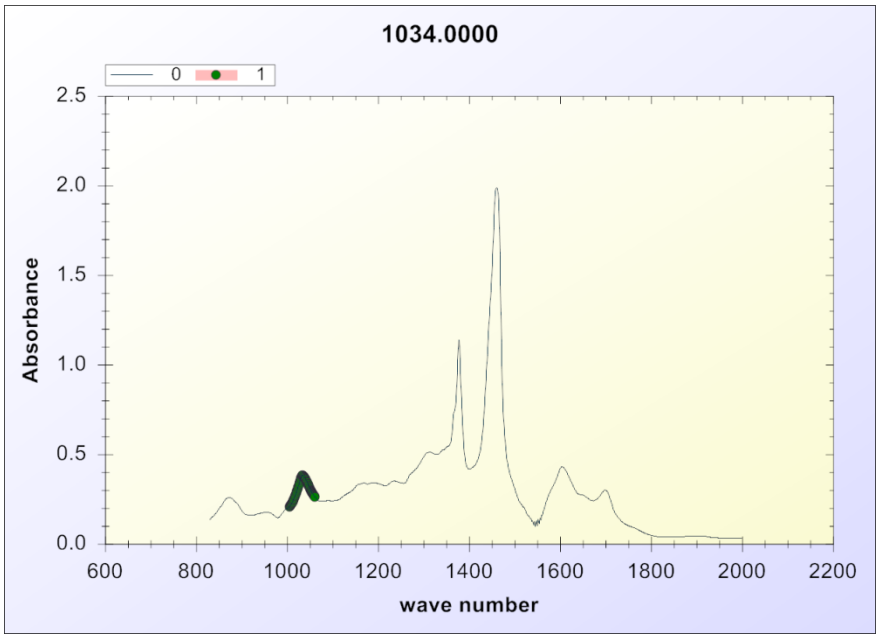

Figure 123. Screenshot. Group 1034.

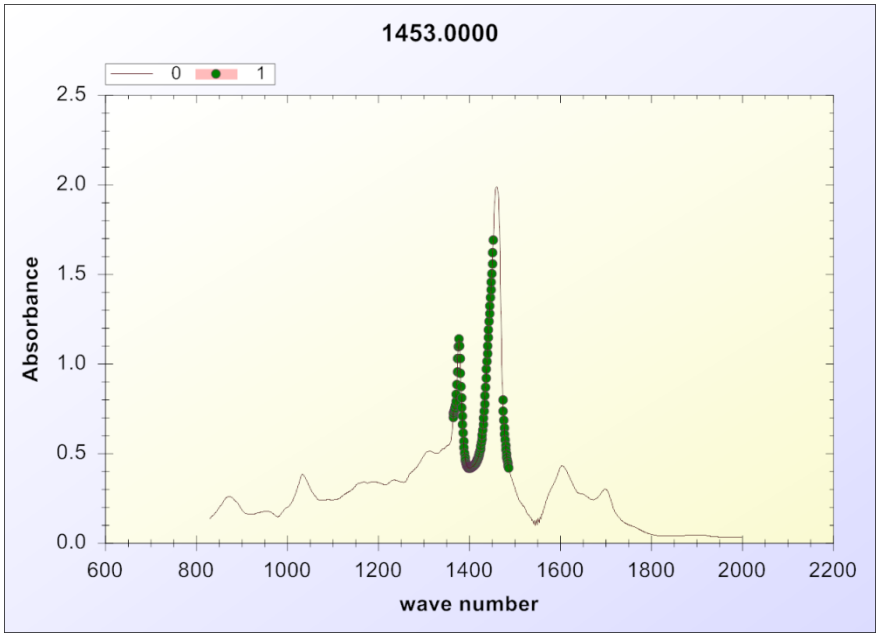

Figure 124. Screenshot. Group 1453.

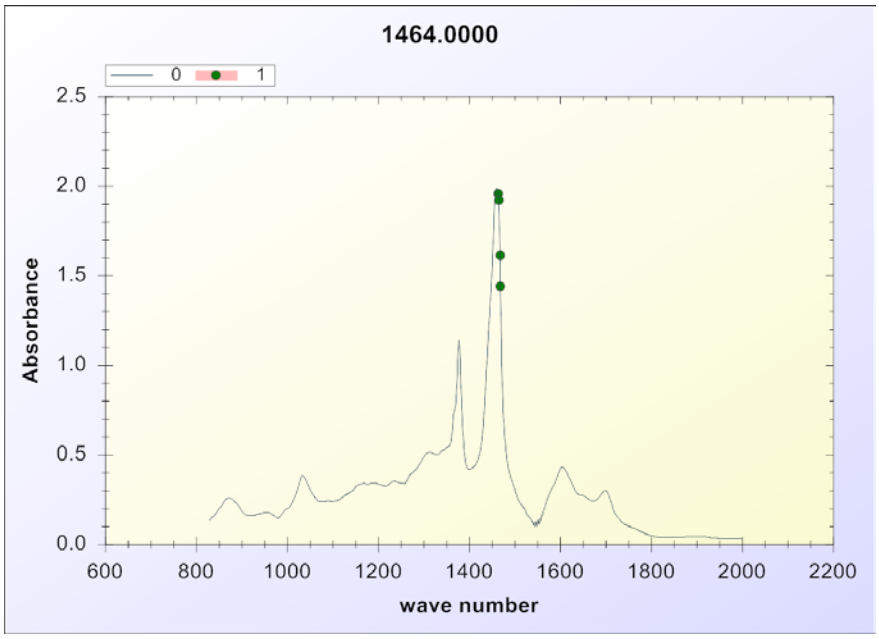

Figure 125. Screenshot. Group 1464.

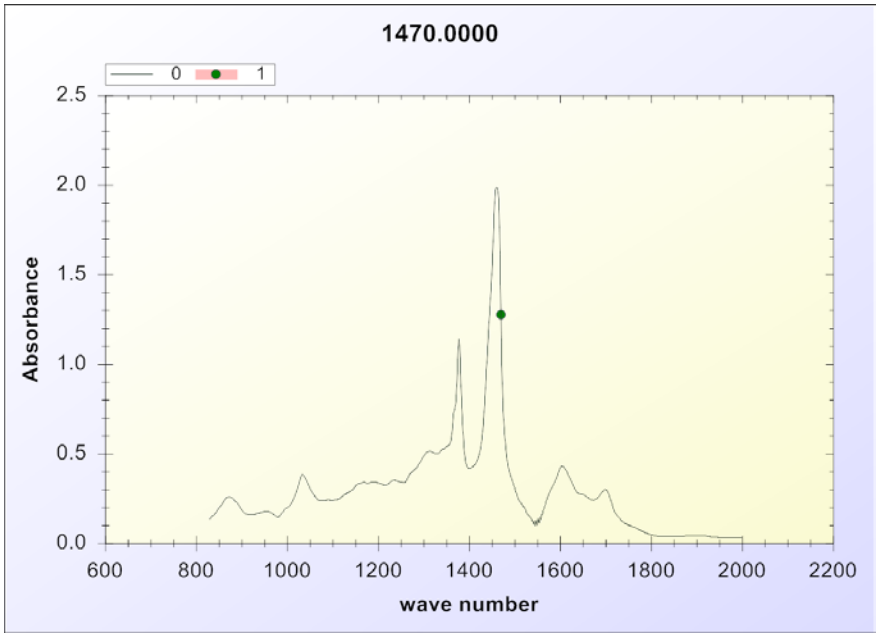

Figure 126. Screenshot. Group 1470.

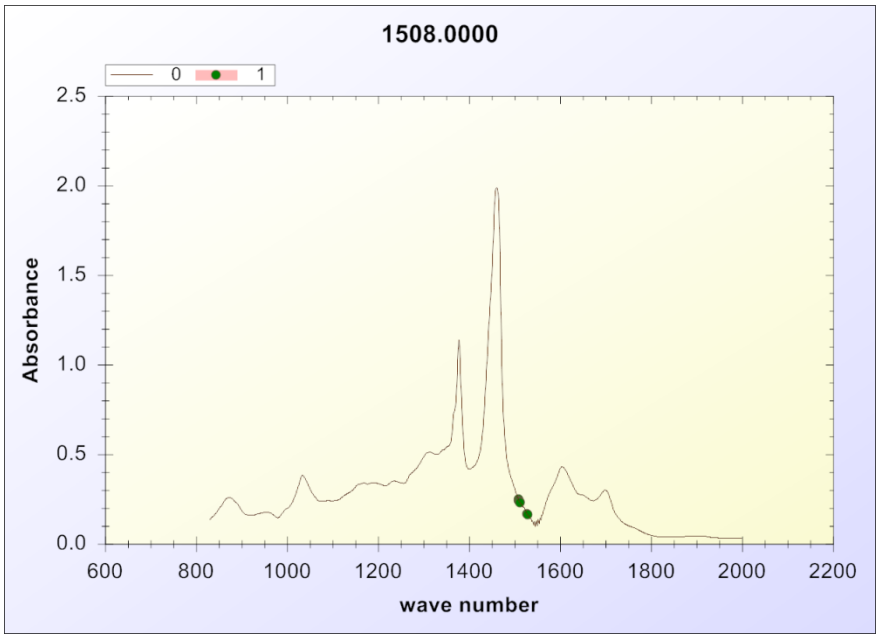

Figure 127. Screenshot. Group 1508.

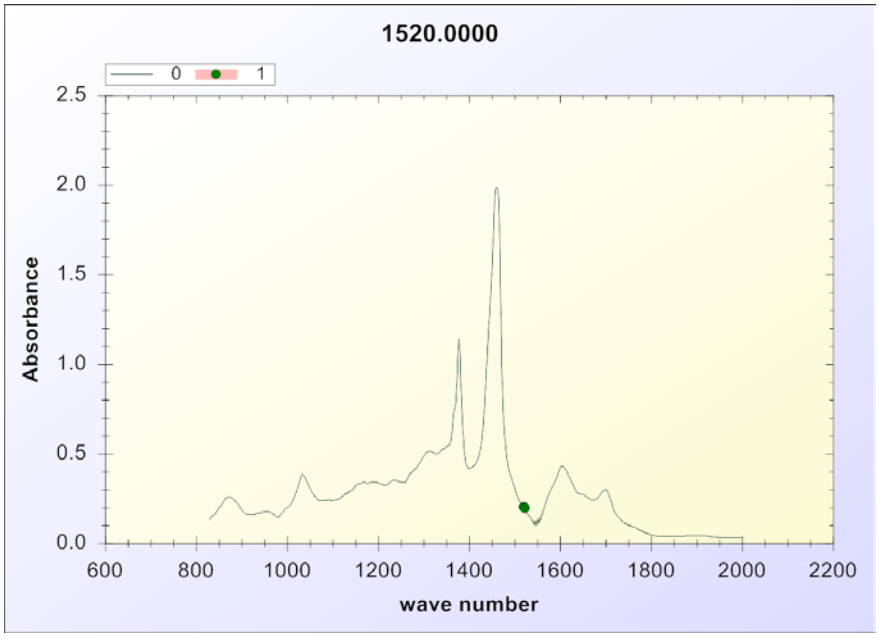

Figure 128. Screenshot. Group 1520.

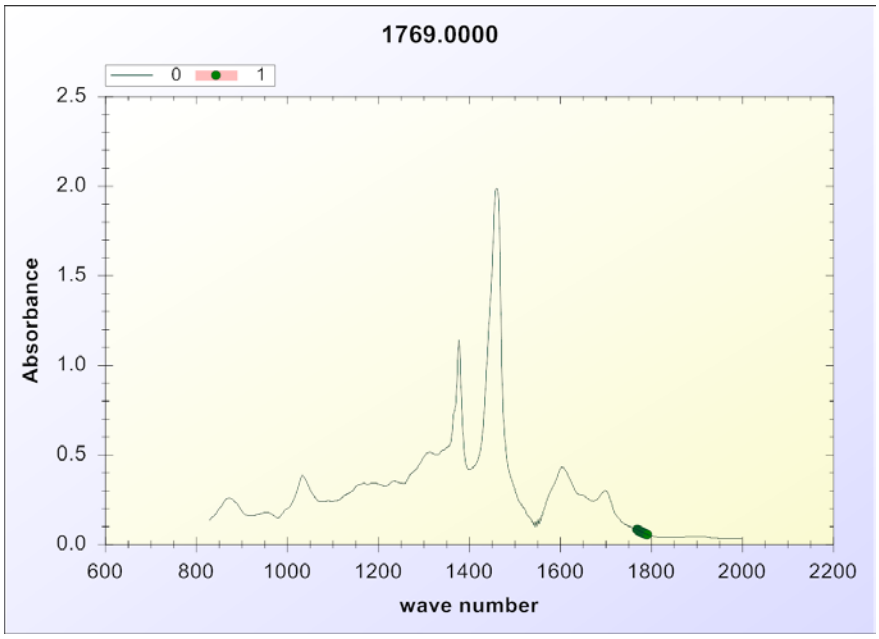

Figure 129. Screenshot. Group 1769.

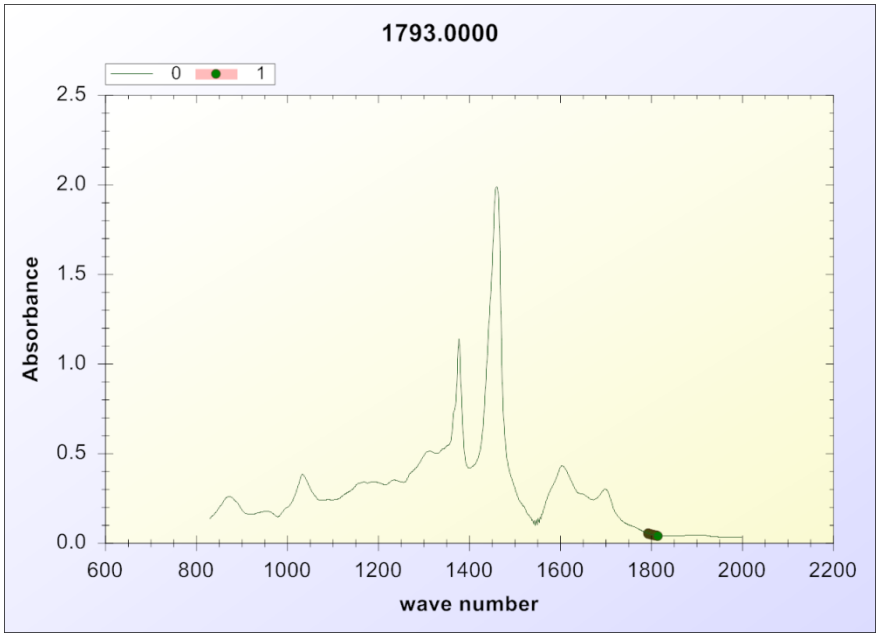

Figure 130. Screenshot. Group 1793.

Single binder correlations of IR measurements to crossover modulus and frequency are extremely good and quantitative with only four wave numbers, although not always the same wave numbers. Figure 131 shows a typical over fit plot for binder AAB-1. Obviously, a near perfect correlation (exceeding 0.995 correlation coefficient) can be found with only four wave numbers. This could be quite useful in pavement maintenance programs where an aging study is done in the laboratory to obtain the training set for the project binder, and then rheological changes monitored with very small samples using inexpensive infrared techniques instead of DSR measurements. These calibrations could be done on a binder by binder basis using ATR instead of the more difficult transmission IR used in this study as individual binders are correlated and Beer's law universality is not an issue. These fits are depicted in tables 40-63. A simple IR spectra can provide the master curve and all derivative metrics.

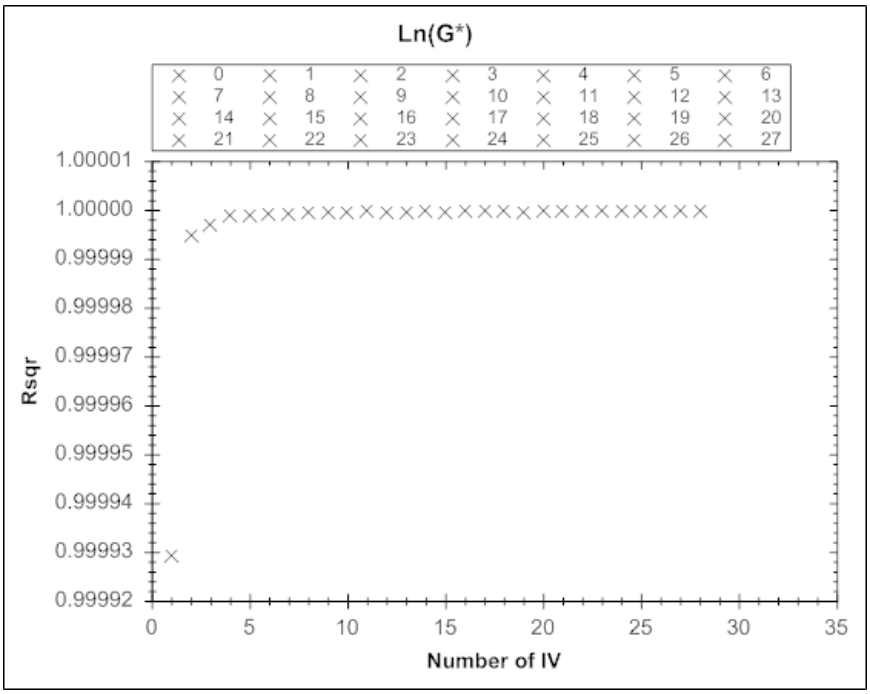

Figure 131. Screenshot. Binder AAB-1 over fit plot.

Table 40. Binder AAB-1 IR spectra fit to logarithm of crossover modulus.

Coefficient of determination = 0.9994				
Regression data				
IV x	Coefficient	Group no.	F	Good
x(0)	1.875E001			
x8	-2.601E000	1699.0000	00130.070	YES
x10	-4.989E000	1313.0000	00174.508	YES
x11	-2.633E000	1034.0000	00864.212	YES
x25	4.505E000	1558.0000	00148.905	YES

Table 41. Binder AAC-1 IR spectra fit to logarithm of crossover modulus.

Coefficient of determination = 0.9991				
Regression data				
IV x	Coefficient	Group no.	F	Good
x(0)	4.259E001			
x11	-5.289E000	1034.0000	00428.264	YES
x13	-1.412E001	1453.0000	00210.665	YES
x22	-6.645E-001	1520.0000	00084.048	YES
x24	-1.243E001	1560.0000	00248.786	YES

Table 42. Binder AAD-1 IR spectra fit to logarithm of crossover modulus.

Coefficient of determination = 0.9994				
Regression data				
IV x	Coefficient	Group no.	F	Good
x(0)	1.698E001			
x11	-3.761E000	1034.0000	07467.935	YES
x17	8.868E-001	1466.0000	00014.307	YES
x18	-1.182E000	1470.0000	00015.517	YES
x22	1.926E000	1520.0000	00226.268	YES

Table 43. Binder AAM-1 IR spectra fit to logarithm of crossover modulus.

Coefficient of determination = 0.9999				
Regression data				
IV x	Coefficient	Group no.	F	Good
x(0)	3.022E001			
x8	-4.846E000	1699.0000	26096.476	YES
x16	-3.683E000	1464.0000	00113.454	YES
x18	-5.498E000	1470.0000	00129.926	YES
x22	3.461E-001	1520.0000	00246.771	YES

Table 44. Binder ABD-1 IR spectra fit to logarithm of crossover modulus.

Coefficient of determination = 0.9993				
Regression data				
IV x	Coefficient	Group no.	F	Good
x(0)	2.583E001			
x8	-6.214E000	1699.0000	00487.713	YES
x11	6.615E000	1034.0000	01233.188	YES
x17	-4.113E000	1466.0000	00273.194	YES
x25	-5.247E000	1558.0000	00073.098	YES

Table 45. Binder ALF IR spectra fit to logarithm of crossover modulus.

Coefficient of determination = 0.9953				
Regression data				
IV x	Coefficient	Group no.	F	Good
x(0)	1.718E001			
x1	6.544E000	0833.0000	00042.843	YES
x8	-6.910E000	1699.0000	06165.841	YES
x13	3.669E000	1453.0000	00323.269	YES
x18	-5.250E000	1470.0000	00129.006	YES

Table 46. Binder ARC-1 IR spectra fit to logarithm of crossover modulus.

Coefficient of determination = 0.9996				
Regression data				
IV x	Coefficient	Group no.	F	Good
x(0)	1.239E001			
x8	2.500E000	1699.0000	01199.606	YES
x11	-5.604E000	1034.0000	06403.299	YES
x15	2.504E000	1461.0000	00077.446	YES
x22	2.221E000	1520.0000	00417.795	YES

Table 47. Binder ARC2 IR spectra fit to logarithm of crossover modulus.

Coefficient of determination = 0.9959				
Regression data				
IV x	Coefficient	Group no.	F	Good
x(0)	2.004E001			
x8	5.231E000	1699.0000	00203.184	YES
x11	-4.747E000	1034.0000	00369.945	YES
x17	-9.136E-001	1466.0000	00045.295	YES
x22	-7.566E000	1520.0000	01845.831	YES

Table 48. Binder AZ1-1 IR spectra fit to logarithm of crossover modulus.

Coefficient of determination = 0.9894				
Regression data				
IV x	Coefficient	Group no.	F	Good
x(0)	2.703E001			
x8	-3.190E000	1699.0000	00094.032	YES
x17	-5.003E000	1466.0000	00036.040	YES
x25	-9.940E000	1558.0000	00344.048	YES
x26	-9.590E000	1769.0000	00051.169	YES

Table 49. Binder MCR IR spectra fit to logarithm of crossover modulus.

Coefficient of determination = 0.9986				
Regression data				
IV x	Coefficient	Group no.	F	Good
x(0)	1.819E001			
x8	-5.392E000	1699.0000	03337.661	YES
x17	4.494E000	1466.0000	00544.711	YES
x18	-6.936E000	1470.0000	00638.981	YES
x25	-5.190E000	1558.0000	00460.135	YES

Table 50. Binder MN1-3 IR spectra fit to logarithm of crossover modulus.

Coefficient of determination = 0.9978				
Regression data				
IV x	Coefficient	Group no.	F	Good
x(0)	3.52E000			
x8	-9.110E000	1699.0000	00933.073	YES
x14	7.500E000	1460.0000	00127.460	YES
x22	6.587E000	1520.0000	00422.413	YES
x24	-1.173E001	1560.0000	00223.256	YES

Table 51. Binder MN-1-4 IR spectra fit to logarithm of crossover modulus.

Coefficient of determination = 0.9957				
Regression data				
IV x	Coefficient	Group no.	F	Good
x(0)	5.584E000			
x11	-9.434E000	1034.0000	01935.208	YES
x13	1.863E001	1453.0000	00256.699	YES
x18	-1.185E001	1470.0000	00111.308	YES
x22	-1.654E001	1520.0000	00319.674	YES

Table 52. Binder AAB-1 IR spectra fit to logarithm of crossover frequency.

Coefficient of determination = 0.9997				
Regression data				
IV x	Coefficient	Group no.	F	Good
x(0)	6.443E000			
x8	-9.932E000	1699.0000	00307.660	YES
x10	-7.671E000	1313.0000	00046.768	YES
x11	-1.228E001	1034.0000	02887.751	YES
x22	-4.899E000	1520.0000	00070.417	YES

Table 53. Binder AAC-1 IR spectra fit to logarithm of crossover frequency.

Coefficient of determination = 0.9962				
Regression data				
IV x	Coefficient	Group no.	F	Good
x(0)	7.11E001			
x8	-6.977E000	1699.0000	00223.872	YES
x11	-1.740E001	1034.0000	00400.384	YES
x13	-3.957E001	1453.0000	00163.200	YES
x22	-2.845E000	1520.0000	00158.617	YES

Table 54. Binder AAD-1 IR spectra fit to logarithm of crossover frequency.

Coefficient of determination = 0.9989				
Regression data				
IV x	Coefficient	Group no.	F	Good
x(0)	1.205E000			
x11	-1.781E001	1034.0000	01993.562	YES
x13	1.478E001	1453.0000	00064.977	YES
x18	-1.592E001	1470.0000	00084.582	YES
x22	-1.612E001	1520.0000	00223.593	YES

Table 55. Binder AAM-1 IR spectra fit to logarithm of crossover frequency.

Coefficient of determination = 1.0000				
Regression data				
IV x	Coefficient	Group no.	F	Good
x(0)	1.003E001			
x8	-1.675E001	1699.0000	05948.358	YES
x11	-9.096E000	1034.0000	00150.742	YES
x13	-1.913E000	1453.0000	00004.065	YES
x18	-6.003E000	1470.0000	00033.067	YES

Table 56. Binder ABD-1 IR spectra fit to logarithm of crossover frequency.

Coefficient of determination = 0.9998				
Regression data				
IV x	Coefficient	Group no.	F	Good
x(0)	1.501E000			
x8	-2.260E001	1699.0000	01368.645	YES
x11	8.640E000	1034.0000	00237.381	YES
x22	3.811E000	1520.0000	00060.874	YES
x25	-1.114E001	1558.0000	00073.654	YES

Table 57. Binder ALF IR spectra fit to logarithm of crossover frequency.

Coefficient of determination = 0.9996				
Regression data				
IV x	Coefficient	Group no.	F	Good
x(0)	-1.208E001			
x8	-1.757E001	1699.0000	05133.938	YES
x11	-1.012E001	1034.0000	01297.627	YES
x13	7.945E000	1453.0000	01888.302	YES
x22	8.133E000	1520.0000	00298.377	YES

Table 58. Binder ARC1 IR spectra fit to logarithm of crossover frequency.

Coefficient of determination = 0.9999				
Regression data				
IV x	Coefficient	Group no.	F	Good
x(0)	-1.961E001			
x8	3.547E000	1699.0000	00037.883	YES
x11	-2.077E001	1034.0000	06373.398	YES
x14	1.223E001	1460.0000	00137.869	YES
x25	-5.339E000	1558.0000	00016.784	YES

Table 59. Binder ARC2 IR spectra fit to logarithm of crossover frequency.

Coefficient of determination = 0.9981				
Regression data				
IV x	Coefficient	Group no.	F	Good
x(0)	2.8E001			
x8	-1.633E001	1699.0000	01001.046	YES
x18	-1.350E001	1470.0000	00237.534	YES
x22	-1.139E001	1520.0000	00216.444	YES
x24	-4.171E001	1560.0000	00660.850	YES

Table 60. Binder AZ1-1 IR spectra fit to logarithm of crossover frequency.

Coefficient of determination = 0.9964				
Regression data				
IV x	Coefficient	Group no.	F	Good
x(0)	-4.837E001			
x8	-2.477E001	1699.0000	00466.889	YES
x16	2.636E001	1464.0000	00085.934	YES
x25	-3.439E001	1558.0000	00385.388	YES
x26	-2.172E001	1769.0000	00028.911	YES

Table 61. Binder MCR IR spectra fit to logarithm of crossover frequency.

Coefficient of determination = 0.9989				
Regression data				
IV x	Coefficient	Group no.	F	Good
x(0)	-3.688E001			
x11	-1.687E001	1034.0000	01505.282	YES
x16	2.495E001	1464.0000	01547.040	YES
x21	-1.476E001	1513.0000	00462.946	YES
x25	-2.942E001	1558.0000	00802.813	YES

Table 62. Binder MN1-3 IR spectra fit to logarithm of crossover frequency.

Coefficient of determination = 0.9980				
Regression data				
IV x	Coefficient	Group no.	F	Good
x(0)	6.422E000			
x8	-2.085E001	1699.0000	00289.825	YES
x11	-1.249E001	1034.0000	00312.248	YES
x22	9.017E000	1520.0000	00445.701	YES
x24	-1.999E001	1560.0000	00074.850	YES

Table 63. Binder MN1-4 IR spectra fit to logarithm of crossover frequency.

Coefficient of determination = 0.9978				
Regression data				
IV x	Coefficient	Group no.	F	Good
x(0)	1.767E001			
x1	-4.855E001	0833.0000	00105.675	YES
x8	-1.565E001	1699.0000	00048.659	YES
x11	-1.765E001	1034.0000	00101.681	YES
x22	-2.892E001	1520.0000	00107.365	YES

CONCLUSIONS

INFRARED QUANTIFICATION

Peak Extraction

The mathematical separation of individual peaks from oxidized spectra is not currently possible without extensive study to constrain the parameter list. One possibility is a careful study of in-situ peak locations using model compounds. However, the study did provide an increased understanding of the complex nature of asphalt infrared spectra, and indicates the narrowness of fundamental peaks. The “peaks” generally described in the literature, i.e. carbonyl and sulfoxide, are actually a collection of responses of the functional group of interest attached to a range of molecular structures coexisting with responses from other functional groups that have responses in the same region. This situation makes subtraction, where possible, an attractive tool for simplifying the response to some extent and improving the correlation results. In addition, natural asphalts appear to contain very similar functional groups, in differing proportions, and produce the same responses in differing proportion when oxidized.

Approximate Methods Compared

1) The subtraction of zero time spectra provides improvements in the quality of the quantification of the net response no matter which method is used.
2) Total peak heights on subtracted spectra provides the best quantification and is simple to do and efficient when automated. There may be some exceptions if the product’s functional group attached molecule changes over time and the peak shifts and has a different extinction coefficient. In such a case, both wave numbers should be measured independently and combined according to the individual extinction coefficients, if known.
3) Peak areas using constant wave number end points provide essentially the same precision as peak heights with a bit more computation. There may be some advantage if the functional group of interest exists over a range of wave numbers, but net peak height on each wave number and the application of absorbtivity weighted averages is still preferred over a gross average.
4) Peak areas based upon emergent tangent end points should not be used.

CHEMOMETRIC METHODS-MULTIVARIABLE CORRELATIONS OF CHEMICAL CHANGE WITH RHEOLOGICAL CHANGES

These conclusions are based upon correlations of mid-infrared spectra against complex modulus at 60°C and 10 radians/s using legacy data from four binders aged over a range of temperatures (60, 80, and 100°C) and times (0 to 480 hours) in a 20 atmosphere air pressurized reactor. The samples were prepared in a standard PAV pan. These films are 1/8 inch thick (3175 microns) and probably exhibit some diffusion control at the higher temperatures. The user is cautioned that some of these conclusions do not apply to our findings at ambient pressure using 100 micron films.

Single Wave Number Studies

Regression scans of individual waves numbers, correlated against complex modulus at a fixed frequency and temperature, is useful in identifying areas of the spectra where approximate estimates of rheological change can be monitored with a single wave length. A knowledge of these areas could find practical application in simple aging indicating instruments using band pass filtering, and, of course, remote sensing where the entire spectra is not available, usually because of atmospheric water.

Multivariate Correlations of IR and Complex Modulus for Four Asphalts

The computational methods developed in the study can be applied to a wide range of measurement methods where large x:y data set responses are recorded for a single candidate dependant variable. With regard to asphalt oxidation changes and rheological changes because of oxidation, no more than 6 wave numbers are needed to get extremely good correlations and these same wave numbers correlate with complex, loss or storage modulus, with different coefficients, of course. All of the wave numbers of significance are thought to describe responses from functional groups containing heteroatoms, usually sulfur and oxygen, or carbon and oxygen. The implication here is that intermolecular force changes, leading to rheological changes, are likely mostly electrostatic in nature caused by partial charges induced by the heteroatom containing functional groups. Pi bond stacking may also play a role, although the use of carbon disulfide as the dilution solvent obscures the 1600 wave number best suited to examine this possibility. The use of carbon tetrachloride in the ambient pressure studies that followed this section of the study, indicates increased aromaticity as oxidation progresses. As few as two wave numbers, 1034 and 1693, generally associated with sulfoxide and carbonyl functional groups, respectively, provide excellent correlations.

DIFFUSION FILM THICKNESS STUDY

Asphalt oxidation is a heterogeneous reaction system. The rate observed is the combined effect of the reactants being delivered to the reaction site, and the rate as controlled by the reaction itself. The gaseous reactant, oxygen, is delivered to the bitumen via molecular diffusion. When studying reaction kinetics, it is desirable to use very small diffusion paths to insure the rate is controlled by the chemistry, and not the movement of oxygen into the sample. The rates of diffusion and oxidation both increase with temperature; however, the temperature effect for the chemical rate is larger than for molecular diffusion. Hence, a minimum diffusion path dimension for a given temperature is sufficiently thin for lower temperature conditions, but not for higher temperature conditions. Our tests indicate that a film thickness of 100 microns is sufficiently thin to insure the reaction rate is chemically controlled at temperatures below 70°C, but this thickness would be smaller at higher temperature. The role of pressure on the minimum film thickness needed to neglect diffusion effects was not studied in this work.

AMBIENT PRESSURE ASPHALT OXIDATION

A simple dual mechanism (Petersen 1998; Glaser et al. 2012) model successfully fits the oxidation of 34 asphalt binders originating from a wide variety of sources using only one adjustable parameter (reactive material) when the extent of oxidation is tracked using a sum of sulfoxide and carbonyl infrared responses. The successful use of two universal Arrhenius equations for 34 binders suggests that asphalt oxidation occurs by nearly identical chemical mechanisms for a wide range of petroleum based binders. These conclusions are based upon studies of mostly unmodified binders. Limited work indicates that the same model applies well to polymer modified binders. This result suggests that modified asphalt binders oxidize with essentially the same chemical mechanism with regard to the asphalt phase. The additives exist in such small amounts, typically, that their oxidation behavior in situ is difficult to observe with infrared methods. Since the Arrhenius parameters apply universally, material testing at several temperatures is not required. A simple test may be performed to characterize the oxidation kinetics for binders without doing expensive long term oxidation experiments, provided we can clearly demonstration the temperature and pressure ranges where corrections to pavement conditions are reliable. A limited study of the SARA fractions on oxidized samples suggests a strong relationship between reactive material and the initial amount of naphthene aromatics. It is thought that the reactive material is a component of the naphthene aromatics. The identification of that component, and direct determination of its amount, would likely improve the correlation.

PRESSURE DEPENDENCY

Fitting the oxidation kinetic model results from the ambient pressure study to infrared data collected from aging 4 SHRP asphalts in 20 atmospheres air at 60, 80 and 100°C suggests that the partial pressure oxygen exponent may not be source dependant as previously believed. The best fits of the 20 atmosphere data at an exponent of 1/3, however, subsequent studies using high pressure isothermal DSC suggest the value may be closer to ½.Will the same exponent work with many binder sources when carbonyl and sulfoxide are used in the measurement of extent of reaction? The answer to that question remains to be seen until additional work is done. However, determining a consistent pressure correction, contrary to the findings of previous investigators that monitored only carbonyl (Domke et al. 2000), would lead to a simple accelerated test whose results can be mapped to pavement pressure conditions reliably.

RAP BLEND OXIDATION

With knowledge of the reactive material for the pure materials in the blend, the oxidation behavior of a blend of RAP and virgin binder can be estimated using a simple mass fraction weighted average of the pure binder and RAP reactive material amounts. In other words, the oxidation rate behavior can be predicted for the blends with only knowledge of the amount of reactive material present in the blend (provided the blend is well mixed). In general, the predictions come quite close to the actual observations and suggest that the chemical kinetic model captures the primary effects in this system and that the reactive material curve fitting parameter represents a concentration of some chemical entity or entities.

ALF BINDER OXIDATION ANALYSIS

Oxidation studies of the binders employed at the ALF facility provide an excellent opportunity to compare oxidation behavior from an unmodified binder, a preoxidized binder, and several polymer and rubber modified binders using the same base binder. The polymer and rubber materials oxidize at essentially the same rates as the unmodified base, but the preoxidized binder oxidizes at a slower rate, easily explained by the reduction in reactive material occurring in the pretreatment step. The oxidation model presented here fits the observed behavior of these modified materials as well as the unmodified materials, probably because these materials are still predominately asphalt and the contribution to measured oxidation from the modifier is so small and perhaps so similar to the asphalt that its contribution cannot be clearly distinguished from the base binder oxidation with IR methods. This observation supports Herrington's conclusion (1998) that microstructure has little to no effect on the chemical oxidation rate. An alternative way of stating this is that mass transfer inside the asphalt film is not rate limiting, suggesting that small moieties control the process and that molecular mobility of the larger asphalt molecules is not controlling the rate of oxidation. However, the relationship of the extent of oxidation to rheologic change does appear to depend on microstructure.

ALF CORE OXIDATION ANALYSIS

The oxidation model presented here describes only the chemical rate with no mass transfer control. Consequently, it is not surprising that using the model, in differential form to predict the extent of oxidation in the pavement using estimated pavement temperatures produces extents of oxidation predictions higher than those actually measured. The observed value divided by the predicted value can be easily computed. This correction factor embodies all mass transfer limitations (permeation, diffusion, thermal breathing, precipitation flushing) and also the partial pressure of oxygen reductions with depth caused by consumption by the asphalt as the air works its way through the pavement. The correction factors steadily increase with depth, suggesting that pore oxygen depletion may be the major factor in reducing the rate in real pavement systems.

OXIDATION AND RHEOLOGICAL CHANGES

General Correlations

The relationship between the extent of oxidation and the master curve changes in DSR measurements is primarily limited to the crossover parameters for frequency and complex modulus. The logarithms of both the crossover frequency and crossover modulus vary linearly with the extent of oxidation as quantified with the sum of the carbonyl and sulfoxide responses. Binders have fits that appear to be source dependent. Very large differences are observed with pre-oxidized materials. There is some indication that the glassy modulus may change as well, but the changes are small and difficult to quantify based upon the precision of the techniques used in this study. The activation energy of the shift factor, analogous to the activation energy of viscous flow term in the Joback correlation (Joback and Reid 1987), does not appear to change

significantly as a binder oxidizes, and is also very similar from one binder source to another. The log of the changes in crossover parameter is linear with oxidation extent, similar to pre-exponential behavior in the functional group determination of viscosity outlined by Joback. However, the correlation slope appears to be binder source dependent, but this variation may be due the limitations of tracking oxidation with only two functional groups using infrared spectroscopy. Accounting for other oxidation products, or measuring elemental oxygen to track oxidation extent may reduce the variance observed. However, even with a source dependent log-linear behavior, the characteristics of binder oxidation could be quantified using only two aging conditions to produce samples, possibly RTFO and PAV materials These samples could then be subjected to IR spectroscopy and DSR testing to provide sufficient data to characterize the two parameters needed for a complete picture of master curve changes as oxidation proceeds. In very open pore pavement designs, the air may possibly be replenished faster than the oxygen is depleted by reaction. Under these conditions the effect of oxygen partial pressure on the reaction rate is insignificant and can be eliminated from the calculations. If such situations can be demonstrated to be common, then the IR spectroscopy could be eliminated and the chemical kinetics expression modified to directly reflect rheological changes. However, limited study with core samples from the ALF facility indicates that true predictability requires accounting for mass transfer effects. Limited work suggests that the reactive material, and the CA model parameters, may be related to the naphthene aromatic content in the SARA fractions. Only a small number of binders (7) were tested, and they show very good correlations of the time-zero naphthene aromatic content and the reactive material, crossover modulus and crossover frequency correlation slopes.

Chemometric Studies

A major focus of so-called chemometric methods has been to replace difficult and expensive testing (usually of physical properties) with more economically attractive determinations based upon chemical compositions. The usual procedure involves the calibration of the chemical analytical method against the property of interest. Consequently, “one off” measurements may not be suited to this approach, but routine measurements for quality control and maintenance purposes can often benefit from such an approach. The mid infrared region of the electromagnetic spectrum provides an information rich picture into the chemical nature of asphalt binders and is inexpensive to perform when compared to most other methods.

This study has produced a fundamentally based reaction kinetic model that works quite well over a large range of binder sources and also modified binders. However, for design, pavement monitoring and purchase specification, the mechanical properties of the binder (particularly the rheological properties) are needed. Using the Spectrelate software developed at WRI under this contract (FP 06), the possibility of estimating DSR master curves from mid infrared spectra was investigated. The results indicate that infrared measurements can, in some applications, be used to avoid expensive DSR tests.

1) Use of IR spectra to estimate master curves for oxidized unmodified binders (including air blown materials with no calibration step.

With no DSR calibration, semi-quantitative estimates of oxidized binder master curves can be obtained using a regression result containing 10 wave number measurements to get CA model crossover modulus and frequency values. The precision of this approach is approximately within 50% of the rheometer produced master curve in real measurement units (not log transformed).

2) Use of IR spectra to estimate master curves for oxidized unmodified binders (including air blown materials with calibration.

   Calibration of a particular binder source produces 4 wave number regression equations that match CA model parameter very precisely. Correlation coefficients for these fits typically exceed 0.995 and are within the precision of the DSR measurements. This approach would provide a significant cost savings in monitoring the extent of oxidation in pavements, and provide a rational data base for asset management.

RECOMMENDATIONS

INFRARED QUANTIFICATION

Peak Extraction

The precision of infrared measurements could be greatly enhanced over areas of interest in the spectra with a model compound study to determine peak locations for functional groups of interest.

Approximate Methods Compared

No further work recommended is this area apart from standardization of IR measurements for asphalt studies.

CHEMOMETRIC METHODS-MULTIVARIABLE CORRELATIONS OF CHEMICAL CHANGE WITH RHEOLOGICAL CHANGES

Single Wave Number Studies

No further work recommended here.

Multivariate Correlations of IR and Complex Modulus for Four Asphalts

Multivariate investigations of asphalt data sets have proven to be very helpful in understanding the most significant variables in oxidation, assisting in the development of fundamental models. These results indicate that chemometric methods may provide reliable alternatives to expensive mechanical testing and more difficult chemical testing.

DIFFUSION FILM THICKNESS STUDY

The determination of the minimum film thickness needed to eliminate diffusion concerns in kinetic studies of asphalts should be extended to higher temperatures and pressures to assess the degree to which these variables can be adjusted to develop binder oxidation kinetic results in a practical time frame.

AMBIENT PRESSURE ASPHALT OXIDATION AND RHEOLOGICAL CHANGE KINETIC STUDY

Oxidation studies should continue with more modified binders, and a more in depth investigation of the SARA fraction relationships to reactive material content and rheological change correlations. In addition, studies should be done at elevated temperatures and pressures to gauge

how to best accelerate the oxidation process for testing purposes and still provide kinetics for pavement performance model inputs. Studies of mass transfer properties of compacted mixes and pavements are also needed as the limited results from this study indicate a strong control on the oxidation rate because of mix permeability and binder diffusivity.

PRESSURE DEPENDENCY

Studies should be conducted to determine if the pressure dependency observed in the limited tests performed in this study can be confidently applied to a wide range of asphalt binders.

RAP BLEND OXIDATION

A very small number of binder and extracted RAP binders were studied in this work. Confident use of oxidation aging rate predictions based upon calculated blend reactive material content would require testing a larger set of binder/RAP combinations.

ALF BINDER OXIDATION ANALYSIS

Oxidation studies should continue with more modified binders.

ALF CORE OXIDATION ANALYSIS

Very precise temperature histories with depth of pavements of interest are needed to properly estimate the magnitude of rate reduction from mass transfer processes. In some pavement designs, the overall oxidation may be controlled by mass transfer alone, making an understanding of the pavement permeability and mastic diffusivity key to oxidation rate predictions.

OXIDATION AND RHEOLOGICAL CHANGES

The study of the relationships between extent of oxidation and rheological change should be extended to modified binders. The relationship between SARA fractions and oxidation should also be expanded.

Chemometric Studies

The use of infrared spectra to estimate master curves works extremely well with source dependent calibrations. The use of infrared alone (without calibration) to estimate master curves is at least semi-empirical when examining unmodified binders. It is thought that additional information regarding molecular weight may be sufficient to perform reliable rheologic determinations using easily obtainable chemical and physical data. This potential cost saving approach should be investigated with unmodified and modified binders as well.

ACKNOWLEDGMENTS

The authors gratefully acknowledge the Federal Highway Administration, U.S. Department of Transportation, for financial support of this project under contract no. DTFH61-07D-00005. Advice and discussion with Turner Fairbanks Research Facility, Expert Task Group and numerous discussions at a wide variety of profession meetings have contributed to this work.

The advice and mentoring from Dr. J. C. Petersen has been particularly helpful in understanding the chemistry of asphalt oxidation.

DISCLAIMER

REFERENCES

Bell, C. A., A. J. Wieder, and M. J. Fellin, 1994, SHRP-A-390, *Laboratory aging of asphalt-aggregate mixtures: Field validation*. Strategic Highway Research Program, National Research Council, Washington, DC.

Christensen, D. W., and D. A. Anderson, 1992, Interpretation of dynamic mechanical test data for paving grade asphalt cements. *J. Assoc. Asphalt Paving. Technol.*, 61: 67-116.

Coons, R. F., and P. H. Wright, 1967, An Investigation of the Hardening of Asphalt Recovered from Pavements of Various Ages. *Proc., Association of Asphalt Paving Technologists*, 37: 510-528.

Dempsey, B. J., 1970, A heat transfer model for evaluating frost action and temperature related effects in multilayered pavement system. *Highway Research Record*, 342: 39-56.

Domke, C. H., R. R. Davison, and C. J. Glover, 2000, Effect of Oxygen Pressure on Asphalt Oxidation Kinetics. *Ind. Eng. Chem. Res.*, 39: 592-598.

Dorrence, S. M., F. A. Barbour, and J. C. Petersen, 1974, Direct Evidence of Ketones in Oxidized Asphalts. *Analytical Chemistry*, 46: 2242-2244.

Epps, J., J. C. Petersen, T. W. Kennedy, D. A. Anderson, and R. Haas, 1986, Chemistry, Rheology, and Engineering Properties of Manganese-Treated Asphalts and Asphalt Mixtures. *Transportation Research Record*, 1096: 106–119.

Glaser, R. R., and J. L. Loveridge, 2012, Low Temperature Oxidation Kinetics of Asphalt Binders. *Preprints, Div. of Petroleum Chemistry, American Chemical Society*, 57 (1): 9-11.

Glaser, R. R., J. F. Schabron, T. F. Turner, J. P. Planche, S. L. Salmans, and J. L. Loveridge, 2013, Low Temperature Oxidation Kinetics of Asphalt Binders. Transportation Research Board, Session 596, pp. 13-2761 through 13-2776.

Gui, J., P. E. Phelan, K. E. Kaloush, and J. S. Golden, 2007, Impact of pavement thermophysical properties on surface temperature. *Journal of Materials in Civil Engineering*, 19: 683-690.

Han, R., X. Jin, and C. J. Glover, 2011, Modeling Pavement Temperature for Use in Binder Oxidation Models and Pavement Performance Prediction. *Journal of Materials in Civil Engineering*, 23 (4): 351-359.

Herb, W., R. Velasquez, H. Stefan, M. Marasteanu, and T. Clyne, 2009, Simulation and Characterization of Asphalt Pavement Temperatures. *Road Materials and Pavement Design*, 10 (1): 233 to 247.

Hermansson, A., 2000, Simulation model for calculating pavement temperatures, including maximum temperature. *Transportation Research Record*: *Journal of the Transportation Research Board*, 1699: 134-141.

Hermansson, A., 2004, Mathematical model for paved surface summer and winter temperature: comparison of calculated and measured temperatures. *Cold regions science and technology*, 40: 1-17.

Herrington, P. H., 1995, Thermal Decomposition of Asphalt Sulfoxides. *Fuel*, 74 (8): 1232-1235.

Herrington, P. R., 1998, Reaction of Bitumen in the Presence of a Constant Concentration of Oxygen. *Petroleum Science and Technology*, 16 (9, 10): 1061-1084.

Herrington, P. R., J. E. Patrick, and G. F. A. Ball, 1994, Oxidation of Roading Asphalts. *Industrial and Engineering Chemistry Research*, 33: 2801-2809.

Hubbard, P., and C. S. Reeve, 1913, The Effect of Exposure on Bitumens. *J. Ind. Eng. Chem*., 5 (15): 15-18.

Jennings, P. W., J. A. Pribanic, B. Fanconi, and D. L. VanderHart, 1993, SHRP-A-335, *Binder Characterization and Evaluation by Nuclear Magnetic Resonance Spectroscopy*. Strategic Highway Research Program, National Research Council, Washington, DC.

Joback, K. G., and R. C. Reid, 1987, Estimation of Pure-Component Properties from Group-Contributions. *Chem. Eng. Commun*., 57: 233-243.

King, G. N., 1993, Oxycyclics: Understanding Catalyzed Oxidation Mechanisms in Bitumen and Other Related Petroleum Products. *Fuel Science and Technology*, 11 (1): 201-238.

King, W. H., and L. W. Corbett, 1969, Relative Oxygen Absorption and Volatility Properties of Submicron Films of Asphalt Using the Quartzite Crystal Microbalance. *Analytical Chemistry*, 41: 580-583.

Knotnerus, J., 1972a, Bitumen Durability: Measurement by Oxygen Absorption. *Industrial and Engineering Chemistry*, 11: 411-422.

Knotnerus, J., 1972b, Oxygen Uptake by Bitumen Solutions as a Potential Measure of Bitumen Durability. *Preprints, Division of Petroleum Chemistry*, American Chemistry Society, 16 (1): D37-D59.

Lau, C. K., K. M. Lunsford, C. J. Glover, R. R. Davidson, and J. A. Bullin., 1992, Reaction Rates and Hardening Susceptibilities as Determined From Pressure Oxygen Vessel Aging of Asphalts. *Transportation Research Record*, 1342: 50-57.

Lee, D. Y., and R. J. Huang, 1973, Weathering of Asphalts as Characterized by Infrared Multiple Internal Reflectance Spectroscopy. *Applied Spectroscopy*, 27: 435.

Liu, M., K. M. Linsford, R. R. Davidson, C. J. Glover, and J. A. Bullin, 1996, The Kinetics of Carbonyl Formation in Asphalt. *Aiche Journal,* 42 (4): 1069-1076.

Lytton, R. L., D. E. Pugahl, C. H. Michalak, H. S. Liang, and B. J. Dempsey, 1989, An integrated model of the climatic effects on pavements, Report FHWA-RD-90-033 prepared for Texas Transportation Institute, College Station, TX.

Martin, K. L., R. R. Davidson, C. J. Glover, and J. A. Bullin, 1990, Asphalt Aging in Texas Roads and Test Section. *Transportation Research* Record, 1269: 9-19.

Mill, T., 1996, The Role of Hydrocarbons in Oxidative Aging in Asphalt. *Preprints, Division of Fuel Chemistry*, American Chemistry Society, 41 (4): 1245-1249.

Mill, T., and D. Tse, 1990, Oxidation and Photooxidation of Asphalts. *Preprints, Division of Petroleum Chemistry*, American Chemistry Society, 35 (3): 483-489.

Mushrush, G. W., 1992, Fuel Instability 1: Organo-Sulfur Hydroperoxide Reactions. *Fuel Science and Technology*, (10) 9: 1523-1560.

Nellenstyn, F. J., 1924, The Constitution of Asphalt. *Journal of the Institute of Petroleum Technologists,* 10: 311-325.

Nunn, S., and K. Nishikida, 2008, Advanced ATR Correction Algorithm, Application Note: 50581, Thermo Scientific. Accessed 5/6/2008. (https://www.thermo.com/eThermo/CMA/PDFs/Product/productPDF_57540.PDF)

Pelikán, P., M. Čeppan, and M. Lǐska, 1993, Resolution of Spectra, Chapter 2 in *Application of Numerical Methods in Molecular Spectroscopy*, S. D. Brown, ed., CRC Press, London.

Petersen, J. C., 1981, Oxidation of Sulfur Compounds in Petroleum Residues: Reactivity-Structural Relationships. *Preprints, Division of Petroleum Chemistry*, American Chemistry Society, 26 (4): 898-906.

Petersen, J. C.., 1986, Quantitative Functional Group Analysis of Asphalts Using Differential Infrared Spectrometry and Selective Chemical Reactions: theory and Application. *Transportation Research Record*, 1096: 1-11.

Petersen, J. C., 1998, A Dual Sequential Mechanism for the Oxidation of Asphalts. *Petroleum Science and Technology*, 16 (9, 10): 1023-1059.

Petersen, J. C., 2009, *A Review of the Fundamentals of Asphalt Oxidation. Transportation Research Circular E-C140.* Transportation Research Board, Washington, D.C.

Petersen, J. C., and R. Glaser, 2011, Asphalt Oxidation Mechanisms and the Role of Oxidation Products on Age Hardening Revisited. *Road Materials and Pavement Design,* 12 (4): 795-819.

Petersen, J. C., F. A. Barbour, and S. M. Dorrence, 1974, Catalysis of Asphalt Oxidation by Mineral Aggregate Surfaces and Asphalt Components. *Proc., Association of Asphalt Paving Technologists*, 43: 162-177.

Petersen, J. C., J. F. Branthaver, R. E. Robertson, P. M. Harnsberger, J. J. Duvall, and E. K. Ensley, 1993, Effects of Physicochemical Factors on Asphalt Oxidation Kinetics. *Transportation Research Record*, 1391: 1-10.

RITA, 2010, Asphalt Surface Aging Prediction (ASAP) System, Final Report prepared for Research and Innovative Technology Administration, Contract No. DTOS59-07-H-0006, by Western Research Institute, Innova Engineering, LLC, PLX, Inc., and SimWright. Accessed August 2013, http://ntl.bts.gov/lib/42000/42300/42380/FinalReport.pdf

Rostler, F. S., and R. M. White, 1959, Influence of Chemical Composition of Asphalts on Performance, Particularly Durability. *American Society for Testing Materials*, 277: 64-88.

Ruan, Y., R. R. Davison, and C. J. Glover, 2003, An Investigation of Asphalt Durability: Relationships Between Ductility and Rheological Properties for Unmodified Asphalts. *Petroleum Science and Technology*, 21 (1, 2): 231-254.

Rumney, T. N., and R. A. Jimenez, 1969, Pavement temperatures in the Southwest. *Highway Research Record*, 361: 1-13.

Solaimanian, M., and T. W. Kennedy, 1993, Predicting maximum pavement surface temperature using maximum air temperature and hourly solar radiation. *Transportation Research Record*: *Journal of the Transportation Research Board*, 1417: 1-11.

Sui, C., M. J. Farrar, W. H. Tuminello, and T. F. Turner, 2010, New Technique for Measuring Low-Temperature Properties of Asphalt Binders with Small Amounts of Material. *Transportation Research Record*, 2179: 23-28.

Thurston, R. R., and E. C. Knowles, 1936, Oxygen Absorption Tests on Asphalt Constituents. *J. Ind. Eng. Chem.*, 28 (1): 88-91.

Vallerga, B. A., R. M. White, and K. S. Rostler, 1970, *Changes in Fundamental Properties of Asphalts During Service in Pavements.* Final Report, Contract No. FH-11-6147. Office of Research and Development, U. S. Bureau of Roads, January 1970.

Van Gooswilligen, G., H. Berger, and F. Th. De Bats, 1985, Oxidation of Bitumens in Various Tests. *Proc., European Bitumen Conference* 1: 95-101.

Van Oort, W. P., 1956, Durability of Asphalt (Its Ageing in the Dark). *Ind. Eng. Chem.*, 48: 1196-1201.

Western Research Institute, 2005, “Fundamental Properties of Asphalts and Modified Asphalts II, Final Report, Volume II: New/Improved Test Methods,” prepared for Federal Highway Administration, Contract No. DTFH61-99C-00022, submitted for publication, November 2005.

Zou, J., R. Roque, and T. Byron, 2012, Effect of HMA ageing and potential healing on top-down cracking using HVS. *Road Materials and Pavement Design*, 13 (3): 518-533.